Doctoral theses at NTNU, 2016:5

Iryna Kulagina

Magnetization Dynamics and Spinsupercurrents in Superconductingand Multiferroic Systems

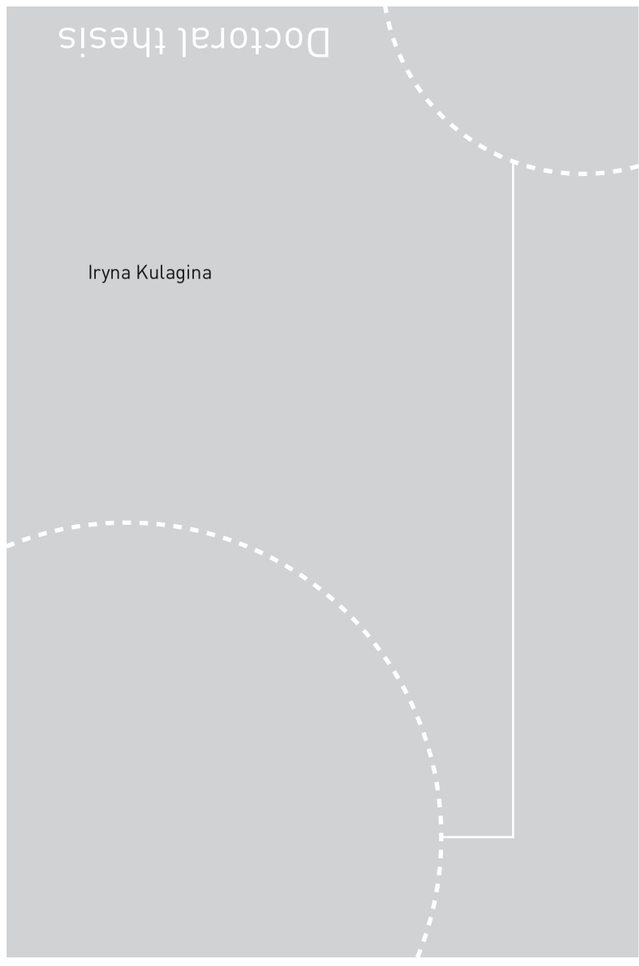

ISBN 978-82-326-1356-4 (printed ver.)
ISBN 978-82-326-1357-1 (electronic ver.)
ISSN 1503-8181

NTNU
Norwegian University of
Science and Technology

Doctoral theses at NTNU, 2016:5

NTNU
Norwegian University of
Science and Technology
Thesis for the Degree of
Philosophiae Doctor
Faculty of Natural Sciences and Technology
Department of Physics

NTNU

Iryna Kulagina

Magnetization Dynamics and Spinsupercurrents in Superconductingand Multiferroic Systems

Thesis for the Degree of Philosophiae Doctor

Trondheim, January 2016

Norwegian University of Science and Technology
Faculty of Natural Sciences and Technology
Department of Physics

NTNU
Norwegian University of
Science and Technology

NTNU
Norwegian University of Science and Technology

Thesis for the Degree of Philosophiae Doctor

Faculty of Natural Sciences and Technology
Department of Physics

ISBN 978-82-326-1356-4 (printed ver.)
ISBN 978-82-326-1357-1 (electronic ver.)
ISSN 1503-8181

Doctoral theses at NTNU, 2016:5

Printed by NTNU Grafisk senter

Abstract

This thesis presents the research findings from three articles which have been published or submitted for publication. In the first article, we study the magnetization dynamics and anomalous supercurrent that can arise in a textured magnetic Josephson junction. We show that supercurrent-induced magnetization switching is possible and that for special magnetic configurations, a supercurrent can flow even at zero phase difference. In the second article, we study domain wall motion induced by current and spin-waves in multiferroic systems. We demonstrate that it is possible to exert electric control over domain-wall motion in such systems and that one can create magnonic torques even on homogeneous magnetic order parameters. In the third article, we prove that it is possible to obtain a long-ranged triplet supercurrent when using only one single homogeneous magnetic layer, in contrast to previous works in the literature. This is made possible by depositing thin heavy normal metal layers at the superconducting interfaces which induce Rashba spin-orbit coupling. We show that the spin supercurrent arising in this way has several unusual properties, including that it does not decay spatially even in the presence of magnetic impurities and that its polarization direction can be tuned via the superconducting phase difference.

Preface

This thesis is submitted as part of the requirements for the degree Philosophiae Doctor at the Norwegian University of Science and Technology (NTNU). The thesis represents three years of work, of which courses equivalent to one year are included. My supervisor has been Professor Jacob Linder, and the research has been funded by the Norwegian Research Council, Grant No. 205591/F20 (FRINAT).

Iryna Kulagina
Trondheim, November 2015

List of publications

Paper I: **I. Kulagina** and J. Linder.
Spin supercurrent, magnetization dynamics, and ϕ-state in spin-textured Josephson junctions.
Physical Review B **90**, 054504 (2014)

Paper II: **I. Kulagina** and J. Linder.
Electric-field control over spin-wave and current induced domain wall motion and magnonic torques in multiferroics.
Submitted to Physical Review Letters (arXiv:1411.3327)

Paper III: S. Jacobsen, **I. Kulagina**, and J. Linder.
Controlling superconducting spin-flow with spin-flip immunity using a single homogeneous ferromagnetic layer.
Submitted to Physical Review Letters (arXiv:1510.02488)

Contents

Chapter 1

Introduction

Scientific progress has moved with giant steps in the last century in all aspects of human life, whether it is the automobile industry, cooking, or engineering. Electronic technology is certainly not an exception. It is not that long ago that the first computer, created in the middle of the 20th century, was so large that it occupied an entire room. By now, the size of the parts that make up the foundation for a computer are on the nanoscale. The volume of data that exists today, stored on harddrives all over the world, surpasses human imagination.

One of the possible routes that may lead to further development in the computational industry is the field of spintronics [1]. The key idea in this field is to use spin to complement the charge degree of freedom as an information carrier. The spin does not have to be provided by an electron: collective excitations such as spin waves can also transport spin, which has opened a subfield known as magnon spintronics [2]. Another approach which has attracted attention recently is to combine superconductors with magnetic materials and thus explore the concept of superconducting spintronics [3].

The main focus of this thesis is to consider how spintronics phenomena such as magnetization switching, domain wall motion, and spin currents can be en-

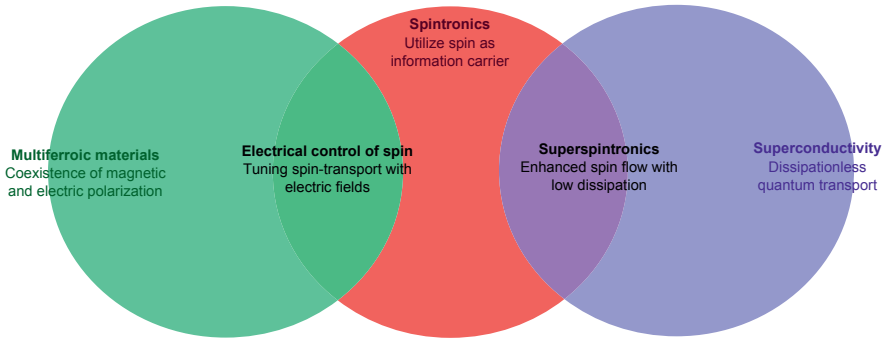

Figure 1.1: The motivation for looking at multiferroic and superconducting materials in the context of spintronics.

hanced by utilizing both multiferroic materials (chapter 3) and superconductors (chapter 2 and 4). Each chapter starts with a motivation for studying the particular system under consideration and a brief introduction to some of the key physical concepts and theoretical techniques that we have made use of. The research results that have been obtained then follow.

It is safe to say that both the road to actual technological implementation using magnon or superconducting spintronics still lies in the future, although not necessarily in the distant future. Nevertheless, history shows that fundamental physics research often establishes the foundation for groundbreaking technological applications. Famous examples of this includes laser technology and the giant magnetoresistance effect: the impact of their application was completely unanticipated at the time of their discovery and they were both born out of fundamental research.

Chapter 2

Magnetization dynamics, spin-supercurrent, and ϕ-junction in textured SFS junctions

2.1 Introduction

The synergistic effects of combining ferromagnetism and superconductivity, two seemingly disparate phenomena, have garnered much attention in recent years [3, 4, 5, 6]. Investigations regarding the mutual interplay between these condensed phases may be traced back to the early work of Ginzburg [7] and it is by now established that ferromagnetic order not necessarily acts detrimentally toward superconductivity - the two may even coexist in a series of uranium-based heavy fermion compounds such as UGe_2, UCoGe, and UIr [8, 9, 10]. Whereas such systems pose several challenges with regard to experimental investigations *e.g.* due to requirements of very high pressures in some cases, the combined influence of FM and SC order can be studied in a more controllable fashion by tailoring hybrid structures with the desired properties.

The physical mechanism behind the unlikely alliance of magnetic and superconducting order is symmetry breaking combined with the Pauli exclusion principle [11]. As long as the Cooper pair wavefunction respects the correct antisymmetry property under an exchange of the particle-coordinates for spin, space, and time, the Cooper pairs can in fact become spin-polarized. Such an effect takes place in F|S structures since both the explicit translation symmetry breaking due to the interface and the presence of a band-splitting exchange field creates Cooper pairs with different symmetry properties than in the bulk superconductor [12]. The consequence of same-spin electrons constituting a Cooper pair is that they become insensitive to the paramagnetic limitation of internal or external magnetic fields, allowing such correlations to survive distances up to hundreds of nanometer inside a ferromagnet [13], even in extreme cases such as half-metallic compounds [14, 15]. In such a scenario, the limiting factor of the

penetration depth is not determined by the strength of the magnetic exchange field, but by other pair-breaking events such as spin-flip and inelastic scattering [16]. Experiments have unambiguously observed such long-ranged superconducting correlations arising in F|S structures that feature magnetic textures of some sort: this includes multilayered magnetic structures [17, 18], domain wall or intrinsically textured ferromagnets [19, 20], and interfaces with spin-active scattering and/or disorder [21, 22]. A large amount of theoretical work has recently been devoted to the topic of spin-triplet correlations arising in S/F hybrid structures (see *e.g.* [23, 24, 25, 26, 27, 28, 29, 30, 31, 32, 33, 34, 35, 36, 37, 38, 39, 40, 41, 42, 43, 44, 45, 46, 47]).

The existence of long-ranged spin-polarized superconducting correlations raises an interesting question: is it possible to utilize this to obtain a superconducting analogue to central topics in spintronics such as domain wall motion and magnetization switching? It is well-known that resisitive (normal) spin-polarized currents play a central part in terms of obtaining magnetization dynamics in spintronics [1]. Spin-currents enable a transfer of angular momentum to the magnetic order parameter of a material via the effect of spin-transfer torque [48, 49]. Since spin-supercurrents also carry angular momentum, the same effect is possible in this context and a few previous works have investigated the possibility of magnetization dynamics in superconducting hybrid structures [51, 52, 63, 54, 55, 57, 56]. However, it remains unclear how the superconducting phase difference affects the dynamics via the Andreev bound-state spectrum. In this paper, we will consider three experimentally relevant types of F|S weak-link structures that all have in common that the region separating the superconductors is spin-textured. We will compute the spin-polarized supercurrent analytically, and demonstrate that its spin-torque can give rise to magnetization switching by solving the non-linear Landau-Lifshitz-Gilbert [58, 59] equation numerically. This constitutes a way to directly utilize the spin-polarized nature of the recently observed long-range triplet currents in order to dynamically alter magnetization textures. In addition to this, we will demonstrate that the magnetic structure in such Josephson junctions has a profound effect on the superconducting ground-state itself. Whereas it is known that superconductor|ferromagnet|superconductor (S|F|S) junctions normally have a ground-state phase difference of 0 or π, it was very recently demonstrated experimentally that it is possible to construct a φ-state junction where the ground-state phase takes on any value between 0 and π [60]. Such a φ-state was originally proposed to occur in SFS junctions in [61] and subsequently studied in several works [62, 63, 64, 65, 66, 67, 68, 69], offering the unique possibility to design phase batteries [70, 71] with an arbitrary phase-shift rather than only 0 or π which could be used to bias both classical and quantum circuits. We will compute the free-energy and belonging supercurrent-phase relation in inhomogeneous magnetic Josephson junctions and show that anomalous behavior arises in the form of a finite supercurrent even at zero phase difference. As will be shown, this is intimately linked with a chiral spin symmetry breaking and scattering at the interfaces of the structure and results in the possibility of a controllable φ-state by adjusting the magnetization vectors in the system.

Before presenting our research results, we will give a brief introduction to the theoretical framework and key physical effects that are present in the system under consideration.

2.2 Bogoliubov-de-Gennes equation

One way to treat heterostructures is by microscopic wavefunctions that are obtained from an effective Hamiltonian. This method can be applied to the equilibrium state in inhomogeneous systems for *e.g.* the ballistic regime (the clean limit), where one obtains spatially varying fields used to describe quantum transport in superconducting systems. Bogoliubov developed a mathematical formulation for this based on BCS theory. To describe excitations in a superconductor, he introduced the concept of mixtures of the particles and holes. Later these particle-hole excited states was called Bogoliubons. In this theory the standard momentum operators ($\boldsymbol{k}$-space) have been replaced by field operators (real-space). The solutions are given by an electron-like part and a hole-like part of the quasiparticles in combination with the gap equation.

The equation of motion in this technique is called the Bogoliubov-de-Gennes equation [72], which is based on the reduced Hartree-Fock mean-field Hamiltonian

$$H = \int d^3r \sum_{\sigma} \hat{\psi}^{\dagger}_{\sigma}(\boldsymbol{r}) \hat{H}_0(\boldsymbol{r}) \hat{\psi}_{\sigma}(\boldsymbol{r}) + \sum_{\sigma,\sigma'} \int d^3r d^3r' \Big(\Delta_{\sigma\sigma'}(\boldsymbol{r},\boldsymbol{r}') \hat{\psi}^{\dagger}_{\sigma}(\boldsymbol{r}) \hat{\psi}^{\dagger}_{\sigma'}(\boldsymbol{r}') + h.c \Big) \tag{2.1}$$

where the integration is taken over the entire volume of the system $\boldsymbol{r} = (x, y, z)$ and summation over spins $\sigma, \sigma' = \uparrow, \downarrow$. $\hat{\psi}^{\dagger}_{\sigma}(\boldsymbol{r})$ and $\hat{\psi}_{\sigma}(\boldsymbol{r})$ are the fermionic creation and annihilation operator. The first term corresponds to the usual kinetic energy $\hat{H}_0(\boldsymbol{r}) = \frac{\hat{\boldsymbol{p}}^2}{2m} - \mu(\boldsymbol{r})$, where $\mu(\boldsymbol{r}) = \mu - eV(\boldsymbol{r})$ and μ is the electrochemical potential, whereas the last two terms are responsible for pairing corresponding to the existence of the superconducting complex order parameter.

The pairing field Δ is determined self-consistently:

$$\Delta_{\sigma\sigma'}(\boldsymbol{r},\boldsymbol{r}') = -\frac{1}{2} \sum_{\delta,\delta'} V_{\sigma\sigma'\delta\delta} \left\langle \psi_{\delta}(\boldsymbol{r}') \psi_{\delta'}(\boldsymbol{r}) \right\rangle \tag{2.2}$$

The pairing exist only for $V_{\sigma\sigma'\delta\delta'} > 0$ and at temperature below the transition temperature $T < T_c$. Otherwise, $\Delta_{\alpha\beta} = 0$. The spin structure of $\Delta_{\sigma\sigma'}(\boldsymbol{r},\boldsymbol{r}')$ determines the type of the superconducting pairing. For singlet $\Delta_{\alpha\beta}(\boldsymbol{r},\boldsymbol{r}') = (i\sigma_y)_{\alpha\beta}\Delta(\boldsymbol{r},\boldsymbol{r}')$. In a uniform superconductor, the interaction depends only on the relative position of electrons and so $V(\boldsymbol{r},\boldsymbol{r}') = V(\rho)$, where $\rho = \boldsymbol{r} - \boldsymbol{r}'$. In order to transform quantities from coordinate space to momentum space, we will use a Fourier transformation.

The next important step in solving the Hamiltonian is diagonalization via the Bogoliubov-Valatin transformation [74]. The canonical transformation is:

$$\psi_\sigma(\boldsymbol{r}) = \sum_n [u_{n\sigma}(\boldsymbol{r})\gamma_n - \sigma v^*_{n\sigma}(\boldsymbol{r})\gamma^*_n] \tag{2.3}$$

with the condition $|u_{n\sigma}(\boldsymbol{r})|^2 + |v_{n\sigma}(\boldsymbol{r})|^2 = 1$, where γ_n and γ^*_n are new fermionic quasiparticle operators. The coefficients u and v can be found by solving the Bogoliubov-de-Gennes equations:

$$\varepsilon u_\sigma(\boldsymbol{r}) = H_0(\boldsymbol{r})u_\sigma(\boldsymbol{r}) + \int d^3r' \Delta_{\sigma\sigma'}(\boldsymbol{r},\boldsymbol{r}')v_{\sigma'}(\boldsymbol{r}') \tag{2.4}$$

$$\varepsilon v_\sigma(\boldsymbol{r}) = -H^*_0(\boldsymbol{r})v_\sigma(\boldsymbol{r}) + \int d^3r' \Delta^*_{\sigma\sigma'}(\boldsymbol{r},\boldsymbol{r}')u_{\sigma'}(\boldsymbol{r}') \tag{2.5}$$

For simplicity, we suppressed here the label n. There are four unknown functions $\{u_\uparrow(\boldsymbol{r}),\, u_\downarrow(\boldsymbol{r}),\, \nu_\uparrow(\boldsymbol{r}),\, \nu_\downarrow(\boldsymbol{r})\}$. For a singlet superconductor $u_\uparrow(u_\downarrow)$ couples only to $\nu_\downarrow(\nu_\uparrow)$, and only two equations are coupled. But in the general case, *e.g.* for a triplet superconductor, all four functions may couple to each other.

This system of equation has to be complemented by the self-consistency equation for $\Delta_{\sigma\sigma'}$ which can be rewritten as follows:

$$\Delta_{\sigma\sigma'}(\boldsymbol{r},\boldsymbol{r}') = \frac{1}{2}V_{\sigma\sigma'\delta\delta'}(\boldsymbol{r},\boldsymbol{r}')\sum_n [\delta' u_{n\delta}(\boldsymbol{r}')v^*_{n\delta'}(\boldsymbol{r})f(-\varepsilon_n) - \delta v^*_{n\delta}(\boldsymbol{r}')u_{n\delta'}(\boldsymbol{r})f(E_n)] \tag{2.6}$$

where the Fermi distribution function is $f(\varepsilon) = [\exp(\varepsilon/k_BT)+1]^{-1}$ with k_B being the Boltzmann constant.

After the Fourier transformation into momentum space the Bogoliubov-de-Gennes equations take the form:

$$(\xi_{\boldsymbol{k}} - \varepsilon_{\boldsymbol{k}})u_{\boldsymbol{k}\sigma} + \Delta_{\sigma\sigma'}(\boldsymbol{k})v_{\boldsymbol{k}\sigma'} = 0 \tag{2.7}$$

$$(\xi_{\boldsymbol{k}} + \varepsilon_{\boldsymbol{k}})v_{\boldsymbol{k}\sigma} + \Delta^*_{\sigma'\sigma}(-\boldsymbol{k})u_{\boldsymbol{k}\sigma'} = 0 \tag{2.8}$$

where $\xi_{\boldsymbol{k}} = \epsilon(\boldsymbol{k}) - \mu$ is the quasiparticle energy measured with respect to the chemical potential μ.

For a singlet superconductor

$$(\xi_{\boldsymbol{k}} - \varepsilon_{\boldsymbol{k}})u_{\boldsymbol{k}\uparrow} + \Delta(\boldsymbol{k})v_{\boldsymbol{k}\downarrow} = 0 \tag{2.9}$$

$$(\xi_{\boldsymbol{k}} + \varepsilon_{\boldsymbol{k}})v_{\boldsymbol{k}\downarrow} + \Delta^*(-\boldsymbol{k})u_{\boldsymbol{k}\uparrow} = 0 \tag{2.10}$$

and the energy spectrum $\varepsilon_{\boldsymbol{k}} = \sqrt{\xi^2_{\boldsymbol{k}} + |\Delta(\boldsymbol{k})^2|}$, and the coefficients u and v:

$$u^2_{\boldsymbol{k}} = \frac{\varepsilon_{\boldsymbol{k}} + \xi_{\boldsymbol{k}}}{2\varepsilon_{\boldsymbol{k}}} \tag{2.11}$$

$$\nu^2_{\boldsymbol{k}} = \frac{\varepsilon_{\boldsymbol{k}} - \xi_{\boldsymbol{k}}}{2\varepsilon_{\boldsymbol{k}}} \tag{2.12}$$

The solutions of the Bogoliubov-de-Gennes equations are interpreted as the excitations from the superconducting ground state.

The model of Blonder-Tinkham-Klapwijk [73] is a famous example of the application of the Bogoliubov-de Gennes equation. In this model, one solves the equation for an $S|N$ interface with arbitrary barrier potential. They considered all possible reflection and transmission processes at the interface (normal reflection, Andreev reflection, normal transmission, branch-crossing transmission) and calculated the energy dependent transport probabilities and current-voltage (I-V) characteristics.

In matrix form the Bogoliubov-de-Gennes Equations can be written as:

$$\begin{pmatrix} \hat{H}_0(\boldsymbol{r}) & \hat{\Delta}(\boldsymbol{r}) \\ -\hat{\Delta}^\dagger \boldsymbol{r}) & -\hat{H}_0{}^T(\boldsymbol{r}) \end{pmatrix} \Psi(\boldsymbol{r}) = \varepsilon \Psi(\boldsymbol{r}) \tag{2.13}$$

where $\hat{\Delta}(\boldsymbol{r}) = i\sigma_2 \Delta(\boldsymbol{r})$, $\psi(\boldsymbol{r}) = [u_\uparrow(\boldsymbol{r}), u_\downarrow(\boldsymbol{r}), v_\uparrow(\boldsymbol{r}), v_\downarrow(\boldsymbol{r}),]^T$ is a four-component spinor with wave function $u_\sigma(\boldsymbol{r})$ for electron and $v_\sigma(\boldsymbol{r})$ for hole degree of freedom, while the single-particle Hamiltonian is:

$$\hat{H}_0(\boldsymbol{r}) = \left[-\frac{\nabla^2}{2m} - \mu(\boldsymbol{r}) \right] \hat{1} \tag{2.14}$$

To describe the proximity effect in S/F structure, one can also use the Bogoliubov-de-Gennes equations. For such a system, the single-particle Hamiltonian includes the exchange field h:

$$\hat{H}_0(\boldsymbol{r}) = \left[-\frac{\nabla^2}{2m} - \mu(\boldsymbol{r}) \right] \hat{1} - h\boldsymbol{f}(\boldsymbol{r}) \cdot \boldsymbol{\sigma} \tag{2.15}$$

where the vector $\boldsymbol{f}(\boldsymbol{r})$ is proportional to the magnetization vector.
The diagonal form of the Hamiltonian can be written as:

$$H_{\text{eff}} = E_g + \sum_{\boldsymbol{k},\sigma} \varepsilon_{\boldsymbol{k}} \gamma^\dagger_{\boldsymbol{k}\sigma} \gamma_{\boldsymbol{k}\sigma} \tag{2.16}$$

The first term corresponds the ground state and the second term describes sum over excitations with momenta$\boldsymbol{k}$.
Using the framework sketched above, one may compute the allowed energy-levels that exist in the Josephson junctions. These Andreev levels ε will depend on the junction geometry, the $U(1)$ superconducting phase gradient, and the magnetization texture. With them in hand, the free energy of the all system $\mathcal{F}$ is obtained via:

$$\mathcal{F}(\gamma) = -\frac{1}{\beta} \sum_j \ln(1 + \mathrm{e}^{-\beta\varepsilon_j}) \tag{2.17}$$

where $f(\varepsilon)$ is Fermi-Dirac distribution function and $\beta = 1/k_B T$.

2.3 Supercurrent from free energy

The supercurrent is a thermodynamic quantity, so that its value can be obtained by the variational derivative of the free energy $\mathcal{F}$ of a Josephson junction with respect to the phase difference γ:

$$I = \frac{2e}{\hbar}\frac{d\mathcal{F}}{d\gamma} \tag{2.18}$$

This expression can be applied to any kind of Josephson junction.
Using the grand canonical partition function $Z = \mathrm{Tr}\left(e^{-\hat{H}\beta}\right)$ and the relation between the partition function and the free energy $F = -\frac{1}{\beta}\ln(Z)$, the explicit dependence of the supercurrent on the Andreev bound state energy will look like:

$$I = \frac{2e}{\hbar}\sum_j f(\varepsilon_j)\frac{\partial\varepsilon_j}{\partial\gamma} = -\frac{2e}{\hbar}\sum_i \tanh\frac{\beta\varepsilon_i}{2}\frac{\partial\varepsilon_j}{\partial\gamma} \tag{2.19}$$

In the last operation it was taken into account that $\varepsilon_j = \pm\varepsilon_i$ and $f(-\varepsilon_j) = 1 - f(\varepsilon_j)$ which is a property of the Fermi function. Only the discrete Andreev levels contribute to the Josephson current in the short-junction limit and for point-contacts [50].

The fact that the supercurrent can become spin-polarized due to the long-ranged triplet proximity effect and that it flows under equilibrium conditions directly implies that the exchange interaction between the ferromagnets should be altered by the superconducting phase difference γ. In fact, there is an interesting co-dependence between the phase difference γ and the non-collinearity of the magnetization vectors regarding the supercurrent $\mathcal{I}$ and the equilibrium magnetic torque τ as first noted by Waintal and Brouwer [51]. Considering for simplicity two monodomain ferromagnets with a relative angle θ between the magnetization vectors, it follows from $\mathcal{I} = \frac{2e}{\hbar}\frac{\partial\mathcal{F}}{\partial\gamma}$ and $\tau = \frac{\partial\mathcal{F}}{\partial\theta}$ that:

$$\frac{\partial\mathcal{I}}{\partial\theta} = \frac{2e}{\hbar}\frac{\partial\tau}{\partial\gamma}. \tag{2.20}$$

The above equation is simple, yet it conveys a powerful message: if the supercurrent is sensitive to the magnetization orientation, then the torque exerted on the magnetic order parameters is sensitive to the superconducting phase difference. This is the core principle which enables the supercurrent-induced magnetization dynamics in inhomogeneous S|F|S junctions.

2.4 Magnetization dynamics

2.4.1 Effective field

Having obtained the free energy of the system from the Andreev levels, one may also compute the effective field $\boldsymbol{H}_{\mathrm{eff}}$ that couples to the magnetic order

parameter by:

$$\boldsymbol{H}_{\text{eff}} = -\frac{1}{V}\frac{\delta \mathcal{F}}{\partial \boldsymbol{M}} \tag{2.21}$$

2.4.2 LLG

The effective field is used to describe the supercurrent-induced magnetization dynamics in the free layer (blue region in Fig. 2.1) by solving the Landau-Lifshitz-Gilbert equation :

$$\frac{\partial \boldsymbol{M}}{\partial t} = -\zeta \boldsymbol{M} \times \boldsymbol{H}_{\text{eff}} + \alpha \boldsymbol{M} \times \frac{\partial \boldsymbol{M}}{\partial t}, \tag{2.22}$$

where ζ is the gyromagnetic ratio and α is the Gilbert damping constant. As long as the effective field is not fully aligned with the magnetization, it will exert a torque on it which induces magnetization dynamics. We are considering a monodomain macrospin model for the soft ferromagnetic layer, such that there is no contribution from the spin stiffness term $\sim \frac{\partial^2 \boldsymbol{M}}{\partial y^2}$. However, we include the influence of magnetic anisotropy with additional terms $\pm K_j \boldsymbol{M}_j^2$, $j \in \{x, y, z\}$ in the free energy where K_j are the anistropy constants and the $\pm$ sign determines the easy and hard axes of magnetization.

2.5 Spin-active interface

An electron that approaches a tunneling boundary between a superconductor and a normal metal from the superconducting part can enter the normal metal or reflect. The probability of tunneling is $|t|^2$ and the probability of reflection is $|r|^2$. These two probabilities have the property $|r|^2 + |t|^2 = 1$, and are complex numbers such that $r = |r|e^{i\phi}$, $t = |t|e^{i\theta}$, where $|r|$ and $|t|$ are the amplitudes of the probability, and ϕ and θ are the phases. If instead of a normal metal we consider a ferromagnetic layer, the probabilities for electron with spin-up and spin-down will be different. This means that $|t_\uparrow| \neq |t_\downarrow|$, and $|\theta_\uparrow| \neq |\theta_\downarrow|$. From a mathematical point of view, due to the difference between phase of the scattering coefficients in the presence of such an interface, the triplet Cooper pairs with $S_z = 0$ are created in addition to the singlet ones: $(\uparrow\downarrow - \downarrow\uparrow)\cos(\phi_\uparrow - \phi_\downarrow) + i\,(\uparrow\downarrow + \downarrow\uparrow)\sin(\phi_\uparrow - \phi_\downarrow)$. The generation of triplet Cooper pairs in this way is known as spin-mixing [14].

We know that in a usual superconductor there are only singlet Cooper pairs which consist of two electrons with opposite spins. But in a ferromagnet there is an imbalance of the electrons with opposite spin. If the ferromagnet has 100% polarization, singlet Cooper pairs can not exist in such a material. Moreover, singlet Cooper pairs decay in a ferromagnetic layer because of the exchange field, which tries to align the spins of the electrons along itself. On the other hand, triplet Cooper pairs with parallel orientation of the spin, on the other hand, can penetrate into a ferromagnetic layer a large distance unlike the singlet Cooper pair. The decay of singlet Cooper pairs in a normal layer and triplet Cooper

pairs with $S_z = \pm 1$ (assuming the magnetization to point in the z-direction) in a ferromagnet is monotonic, whereas the decay of singlet Cooper pairs and triplets with $S_z = 0$ in the ferromagnetic is oscillating. In a S|FI|N structure, where FI is a thin ferromagnetic insulator, we can get both singlet and triplet Cooper pairs due to spin-mixing and all of these Cooper pairs will penetrate in the normal layer. They decay similarly since there is no exchange field in the normal metal which causes one spin orientation to be beneficial with respect to the opposite. If the layer of the ferromagnetic insulator is thin (order 1-2 nm), this type of structure is called S|N with spin-active interface.
The boundary condition for the wave function at a spin-active interface with spin-dependent potential is:

$$\partial_y \left[\Psi_F(y) - \Psi_{S_L}(y)\right]|_{y=0} = \tag{2.23}$$

$$2mU_0 \left[\hat{1} - \rho\cos(\phi)\left(\tau_0 \otimes \sigma_3\right) - \rho\sin(\phi)\hat{M}(\psi)\right]\Psi_{S_L}(0) \tag{2.24}$$

where $\otimes$ is the Cartesian product, U_0 is the nonmagnetic barrier potential and $\rho = |\boldsymbol{U}|/U_0$ presents the ration between magnetic $\boldsymbol{U} = (U_x, U_y, U_z)$ and nonmagnetic potential [41].

2.6 Conventional Josephson junction

In the case of a contact between a superconductor and a non-superconducting material one observes the proximity effect. This leads to interesting phenomena in Josephson junctions which are composed of two superconductors and a weak link between them. The weak link may be represented by any non-superconducting material, for example an insulator, a normal metal, a ferromagnet, or any combination of the materials.

The essence of the proximity effect lies in the fact that superconducting correlations can penetrate into a normal metal a distance equal to the normal coherence length, which in a ballistic metal is $\xi_N \sim \hbar v_F/k_B T$, where $k_B T$ is the characteristic energy of the thermal fluctuation, which destroys the Cooper pair coherence in the normal metal. In a dirty metal, we have [4] $\xi_N \sim \sqrt{\hbar D/k_B T}$, where D is the coefficient of diffusion. The induced superconducting order parameter in the normal metal near the SN-boundary can be described by the wave function $\Psi_N(x) = \Psi_{N0}\mathrm{e}^{-k_N x}$, where $k_N = 1/\xi_N$. This wave function is damped monotonically to the distance of the coherence length ξ_N. Due to overlap of the wave functions of the two superconductors in the middle layer of a Josephson junction, there is a mixing of the two condensates which establishes the possibility to have a supercurrent transfer between superconductors. This supercurrent typically depends on the phase difference $\phi = \phi_L - \phi_R$ of the two superconductors as:

$$I_S(\phi) = I_C \sin(\phi) \tag{2.25}$$

where I_C is the maximum current which called the critical current. This is the Josephson effect. In general, higher harmonics of the type $\sin(2\phi)$ can also

contribute to the current-phase relation, although the magnitude of such terms are typically much smaller than the first harmonic.

The physics of this effect in *e.g.* SNS junctions can be understood from the phenomenon of Andreev reflection. Quasiparticles in the middle layer with energy smaller than energy gap ($E < \Delta$) can not penetrate into superconductor since there are no available states there. Let us consider this process in detail. An incoming electron from a normal metal with $E < \Delta$ cannot enter the superconductor by itself. However, if it teams up with an electron with energy $-E$ at momentum $-k$, they can create a Cooper pair inside the superconductor. A Cooper pair appears in the superconductor at the same time as a hole is created in the normal metal, describing the missing electron at $-k$. The hole then propagates with group velocity away from the interface, and the net result of this process is a transfer of the charge from the normal metal to the superconductor, i.e. the flow of an electrical current. The same process exist for electrons with energy bigger than gap ($E > \Delta$), but with a strongly reduced probability for Andreev reflection since such electrons can also tunnel directly into the superconductor as quasiparticles. It should be noted that the Andreev reflected hole has oppositely directed group velocity and momentum.

A supercurrent can then appear in an SNS junction by transferring a Cooper pair from one superconductor to another via Andreev reflection. The amplitude of the Andreev reflection process depends on the phase difference, so that the supercurrent also depends on this.

The supercurrent typically has some general properties [76] which does not depend on the specific material used:

- 1) The supercurrent is a 2π periodic function. Any change of the phase difference with 2π will not influence the supercurrent.
- 2) In system without explicitly broken time-reversal symmetry, changing the direction of the supercurrent is equivalent to changing the sign of the phase difference, i.e. $I(\phi) = -I(-\phi)$.
- 3) In the case of zero phase difference, there is no supercurrent.
- 4) As consequence of the first and third properties, the supercurrent is zero at phase differences equal πn, where n is any integer.

We underline that there are exceptions, and we will indeed see that property 3) does not always hold. The free energy of the junction can be obtained by $\int_0^\phi I_S(\phi')d\phi'$, and has a standard form

$$E(\phi) \sim I_C(1 - \cos(\phi)) \tag{2.26}$$

The Josephson junction with a normal metal has the minimum energy at $\phi = 0$ when there is no supercurrent as $I_C > 0$. Such a junction is known as a $0-$junction.

2.7 Josephson junction with ferromagnet

In the case of a ferromagnet as the weak link, the behaviour of the superconducting wave function in the middle layer has a different character. This is due to the fact that besides thermal fluctuation there is also an exchange field that tries to destroy the Cooper pairs by aligning the spin of the electrons along the field. Singlet Cooper pairs consist of two electrons with opposite spins and momentum. In a ferromagnet, the energy of the electron with spin along exchange field is smaller than energy of the electron with opposite spin by $2h$ where h (sometimes denoted E_{ex}) is the exchange field. To compensate for this difference in energy, the electron with spin up increases its kinetic energy and the electron with spin down decreases its kinetic energy so the difference in exchange energy of two electrons will be compensated by adjusting the kinetic energy, so that both electrons can reside at the same energy level. As a consequence, the Cooper pair gains a non-zero total momentum $q \propto h$, and causes the superconducting proximity-induced order parameter to be proportional to e^{iqx}. Together with the usual damping of the order parameter, there now exists an oscillation of the order parameter in the ferromagnet. The average exchange energy in the ferromagnet is typically much bigger than the thermal energy, so the decay length in the ferromagnet is governed by $\xi_{F1} = \sqrt{\hbar D/E_{ex}}$.

Let the length-scale determining the oscillations of the order parameter be denoted ξ_{F2}. One can expect that for some thickness of ferromagnetic layer, for example $d_F \simeq \pi\xi_{F2}$ the sign of the order parameter will be different: the equilibrium phase difference will equal π without external field and current. This gives a phase shift in the ground state on π, as first observed in Ref. [75].
In summary, the wave function describing the leakage of superconducting correlations into a ferromagnet reads:

$$\Psi_F(x) = \Psi_{F0}\mathrm{e}^{-k_F x} = \Psi_{F0}\mathrm{e}^{-k_{F1}x}\mathrm{e}^{-ik_{F2}x} \tag{2.27}$$

where $k_F = k_{F1} + ik_{F2}$. The imaginary part defines the length of oscillation wave $2\pi\xi_{F2}$ of order parameter in ferromagnetic. In a π-junction, the critical current I_c depends on length and temperature of the ferromagnet, and can become negative. In this case, the minimum energy corresponds to the phase difference $\phi = \pi$.

2.8 ϕ-junction

Besides 0 and π junction there exists so-called $\phi-$ junctions, where the ground-state occurs for an arbitrary phase difference $\phi \in [0, \pi]$. One example of this is Josephson junctions with three noncollinear ferromagnet layers between superconductors. In particular, the spin chirality χ needs to be non-zero, $\chi = \boldsymbol{M}_1 \cdot (\boldsymbol{M}_2 \times \boldsymbol{M}_3)$. To understand the physics of this phenomena we consider Andreev reflection in $S|F_x|F_y|F_z|S$ junction, where the magnitude of the magnetization of all three layers are equal. For simplicity, we will not consider normal reflection at FS interface, because it influences only the amplitude

of the supercurrent and does not affect our argument below. For the case $E \ll h \ll E_F$, we can use that the wavevectors for spin up and down can be written $k_\pm \simeq k_F(1 \pm \frac{h}{2\mu})$. Consider an electron in the first ferromagnetic layer moving rightwards. At the second ferromagnetic layer the electron has a wave function $(1, -i, 0, 0)^T$. After moving through the second layer and reaching the $F_y|F_z$ interface, it acquires a phase $e^{ik_\pm L_2}$. In the third layer the spin of the electron rotates and in the end of this layer the wave function will look like $(e^{ik_+ L_3}, ie^{ik_- L_3}, 0, 0)^T e^{ik_\pm L_2}$. At the $F_z|S$ interface, the electron reflects as hole (Andreev reflection) with reversed spin. The wave function of the hole after such an Andreev reflection is $(0, 0, ie^{ik_- L_3}, e^{ik_+ L_3})^T e^{ik_+ L_2} \frac{v}{u} e^{i\phi/2}$ (we used approximation $k_\pm^S \simeq k_F$, where $k_\pm^S$ is the wave vector of the electronlike/holelike quasiparticle in superconductor). After that the hole moves left to the $S|F_x$ interface and in passing through each ferromagnet layer the spin of the hole rotates according to the orientation of the magnetization in the layer. It also acquires a corresponding phase $e^{ik_\pm L_i}$, where $i = 1, 2, 3$. At the $S|F_x$ the hole is again Andreev-reflected as electron and moves to the starting point. The wave function after the complete cycle looks like $(1, -i, 0, 0)^T (\frac{v}{u})^2 e^{i\phi} e^{i\psi}$, where ψ depends on *e.g.* the length of the system and the barrier strength. The total superconducting phase difference ϕ between the superconductors has thus been renormalized by $\phi \to \phi + \psi$.

2.9 Results

We will now proceed to present our research results from **Paper I**.

The ferromagnetic part of the junction depends on the specific model considered as shown in Fig. 2.1. We will treat three experimentally relevant model systems in order to illustrate the rich physics that arises due to the spin-polarized nature of the long-ranged superconducting correlations. In Fig. 2.1(a), we consider a multilayered ferromagnetic junction. As predicted by Ref. [24], the Josephson current in such a structure should have a long-ranged contribution that depends on the relative orientation of the magnetization vectors in each of the ferromagnetic layers. To treat a general scenario, we consider an arbitrary direction of the magnetization in the free layer and fix the orientation in the two hard magnetic layers to the z- and x-axis, respectively. The three layers $j \in \{1, 2, 3\}$ are characterized by their thickness L_j and exchange field h_j, and we will also consider the influence of interface resistance captured by an effective dimensionless parameter Z (see Appendix A). As we will calculate below, the rich physics including supercurrent-induced magnetization reversal and the appearance of a φ-ground state is intimately related to chiral symmetry breaking by the magnetization vectors $\boldsymbol{M}_j$, characterized by a finite value of the chirality vector:

$$\chi = \boldsymbol{M}_1 \cdot (\boldsymbol{M}_2 \times \boldsymbol{M}_3). \tag{2.28}$$

Next, we consider in Fig. 2.1(b) a free magnetic layer with low anisotropy where the interface region coupling to the superconductors is spin-active. Such

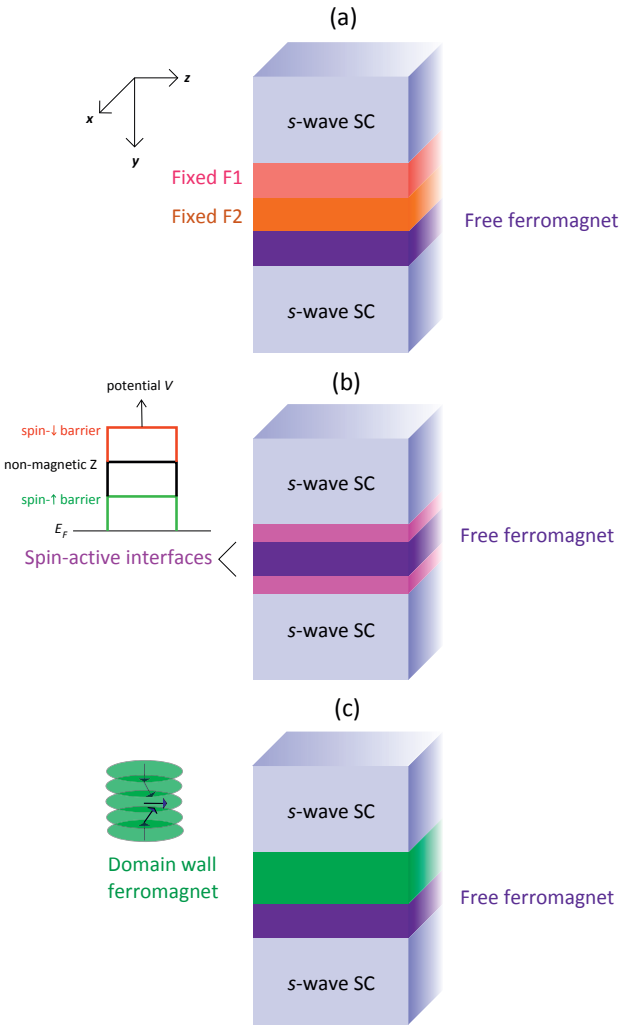

Figure 2.1: The three setups considered in this paper for magnetization dynamics induced by a spin-polarized supercurrent: (a) a trilayer S|F|S junction with non-collinear magnetization, (b) S|F|S junction with spin-active interfaces, and (c) S|DW|F|S junction where the supercurrent is polarized by a domain-wall.

interfaces are known to give rise to spin filtering, spin mixing, and spin flip scattering, all of which considerably alters the superconducting proximity effect. We consider a situation where the barrier moments lie in the $x-z$-plane and are parallel, perpendicular and antiparallel each other ($\phi_L = \phi_R = 0$; $\phi_L = 0$ and $\phi_R = \pi/2$; $\phi_L = 0$ and $\phi_R = \pi$). The spin-active interfaces are characterised by barriers

$$U = [\hat{1} - \rho\cos(\phi)(\tau_0 \otimes \sigma_3) - \rho\sin(\phi)(\tau_0 \otimes \sigma_1)], \tag{2.29}$$

One of our main results is that breaking chiral spin symmetry is not a sufficient condition to generate an anomalous zero-phase difference supercurrent. Instead, the scattering taking place at the interfaces separating the various regions will be shown to play a pivotal part in this. Finally, we include the effect of a domain wall by considering in Fig. 2.1(c) a setup where the ferromagnetic region consists of a domain wall and a free magnetic layer. The domain wall is taken to be of Bloch-type, thus rotating around the y-axis with a characteristic length scale of λ. This particular choice of domain wall is not essential to the resulting physics, and the results we obtain are qualitatively unchanged for other types of magnetization textures. The structure of the domain wall is described by a vector $\boldsymbol{f}$ proportional to the magnetization vector:

$$\boldsymbol{f}(y) = \begin{cases} [\sin(\frac{\pi y}{l_{\mathrm{dw}}}), 0, \cos(\frac{\pi y}{l_{\mathrm{dw}}})], & \text{if } 0 < y < l_{\mathrm{dw}}. \\ 0, & \text{otherwise.} \end{cases} \tag{2.30}$$

We start by considering the Andreev bound-state (ABS) spectrum, the system's free energy, the current-phase relation, and the ensuing magnetization dynamics via spin-supercurrents. We treat each of the three proposed systems in Fig. 2.1 separately. In each subsection, we start by considering the analytical expression for the ABS energy. Obtaining this quantity serves as the foundation for the computation of both the total free energy of the system and the equilibrium supercurrent, as given by Eq. (2.17) and Eq. (2.19). The technical procedure for doing so consists of three steps. First, we obtain the eigenstate wavefunctions that solve the BdG equations in each region. From these wavefunctions, the appropriate scattering states involving particle- and hole-like excitations are constructed with belonging probability coefficients. The energies ε that allow for a non-trivial solution of the scattering coefficients are obtained by matching the wavefunctions at each interface region using appropriate boundary conditions and setting up a system of linear equations of the type $\hat{A}\mathbf{x} = \mathbf{b}$ where $\mathbf{x}$ contains the scattering coefficients. Solving the characteristic equation $\det\hat{A} = 0$ allows one to identify the ABS solutions for ε. The boundary conditions require some special care for the systems under consideration in the present paper, i.e. they are modified from conventional boundary conditions both for setup (b) and (c) in Fig. 2.1.

2.9.1 Trilayered S|F|F|F|S structure

The magnetizations in the first two layers F_1 and F_2 are assumed to be fixed via strong anisotropy energies along the $\hat{z}$ and $\hat{x}$ directions, respectively. In F_3, we allow for an arbitrary magnetization direction in order to explore the effect of spin-supercurrent induced magnetization dynamics. This material should then consist of a much softer ferromagnet than F_1 and F_2. For a completely arbitrary parameter set, the analytical expression for the ABS-energy is overwhelming. However, physical insight can be obtained in experimentally relevant limiting cases. In the quasiclassical regime of a rather weak ferromagnet $h/\mu \ll 1$, one finds that:

$$\varepsilon_j = \Delta_0\sqrt{1 - \mathcal{A}\cos\gamma + \mathcal{B}Z^3(h_y/h)\sin\gamma - \mathcal{C} \pm \sqrt{\mathcal{D}(\gamma)}} \tag{2.31}$$

where the coefficients $\mathcal{A}, \mathcal{B}, \mathcal{C}$ are independent on the phase difference γ. Instead, they are functions of the junction parameters such as length L, barrier Z, and exchange field h. It should be noted that Eq. (2.31) is valid for arbitrary interface transparency Z. We provide some additional details for the coefficients in Eq. (2.31) in the Appendix A. The quantity $\mathcal{D}(\gamma)$ is a rather large expression which depends on γ; the essential property of this quantity is nevertheless that

$$\left.\frac{\partial \mathcal{D}(\gamma)}{\partial \gamma}\right|_{\gamma=0} \propto \mathcal{B}Z^3(h_y/h). \tag{2.32}$$

We prove now that it follows from the above properties of the Andreev-level that there will be a finite supercurrent at zero phase difference. This finding is then independent on the specific details of the coefficients introduced above.

The presence of an anomalous current is seen to be contigent on two factors: 1) the presence of scattering barriers and 2) $h_y \neq 0$ in the free F layer. The absence of either of these causes the supercurrent to revert to conventional behavior. We comment first on the role of the scattering barriers. In Eq. (2.31), it was assumed that the scattering barrier Z was the same for the interfaces between the ferromagnetic regions whereas the $S|F$ interface was taken to be completely transparent. By allowing for different barrier values, which will be the case in general since the value of Z depends on the specific materials connected, one finds that the term providing the anomalous current reads $\frac{1}{2}\mathcal{B}Z_1Z_2(Z_1+Z_2)h_y \sin\gamma$. Here, Z_1 is the barrier between the $F_1|F_2$ interface whereas Z_2 is the barrier between the $F_2|F_3$ interface. This demonstrates that in the short-junction regime where the Andreev bound-states carry the current, barriers at both ferromagnetic interfaces are required in order to produce the anomalous current: setting either Z_1 or Z_2 to zero cancels the $\sin\gamma$ term in Eq. (2.31). We will later establish a connection between this observation and the results for the domain wall junction to be considered in a section below.

Secondly, the fact that the anomalous supercurrent only appears when $h_y \neq 0$ means that the presence of an explicitly broken chiral spin symmetry the system is a necessary criterium. Interestingly, we find that direction of the current is actually controlled by the specific chirality, i.e. the sign of h_y. A consequence of this is that the magnetization direction then acts as a 0-π switch as it controls the direction of the supercurrent, which offers a novel way of exerting dynamical control over a superflow of spins. In a somewhat different multilayer setup where the magnetization vectors were all in-plane (and thus without any anomalous supercurrent), the direction of the magnetization rotation was also found to influence the sign of the supercurrent in Ref. [77]. The precise quantitative behaviour of our system depends also on the following parameters: the interface barrier, the magnetic anisotropy constant, and the length of ferromagnetic layers. For convenience, we introduce the normalized and dimensionless variables $\beta_i = \frac{k_F L_i h}{2\mu}$, where the index i denotes the ferromagnetic layer under consideration. Throughout this work, we set $k_F L = 2\pi n$, where n is integer. The presence of ferromagnetism introduces additional phase-shifts for the An-

dreev bound-states as they propagate through the system.

In Fig. 2.2, we plot the ABS-energy (a, d), the free energy (b, e) and the Josephson current (c, f) as function of the phase difference. We fixed $\beta_1 = \beta_2 = \pi/3$ and considered several values for β_3 and Z. The magnetization in the free layer has been set to $\mathbf{m} \parallel \hat{y}$ in order to demonstrate the appearance and consequences of the anomalous supercurrent. To give the reader a better idea about which values these correspond to in an experimental setup, we note that for a weakly polarized ferromagnet with $h/\mu = 0.02$ (exchange field of around 30 meV), $\beta = \pi/3$ corresponds to a length of 15 nm. In Fig. 2.2, we consider in (a-c) the effect of varying the width or exchange field of the free ferromagnetic layer, captured in the parameter β_3. We consider here a weakly transparent interface $Z = 2$. In (d-f), we instead fix β_3 and consider the influence of having different barrier potentials Z. The panels for the ABS-energies clearly display that the current is spin-polarized as their spin-degeneracy is completely removed in the present system. One important feature is that the effect of increasing Z on the spectrum is that the maxima and minima are shifted away from a phase difference $\gamma = 0$ and $\gamma = \pi$. The fact that the derivative of the ABS-energy with respect to γ does not vanish at these points implies that there will be a finite current even in the absence of any superconducting phase difference. This will be referred to as an *anomalous supercurrent*. We observe that there is no anomalous supercurrent when $Z = 0$, as seen also in Eq. (2.31).

The presence of an anomalous supercurrent is intimately related to an unusual property for the quantum ground-state of the system, which is illustrated in the plots for the free energy in Fig. 2.2 (b) and (e). The global minimum of F is seen to not necessarily occur at the conventional 0 and π states for the phase difference - in fact, for weakly transparent interfaces it deviates strongly from these values and occurs at an intermediate phase $\in [0, \pi]$. This is a manifestation of a so-called ϕ-junction. In the right column of Fig. 2.2, we plot the supercurrent-phase relation for various choices of the length and exchange field for the free ferromagnetic layer as well as different values of the interface transparency. When a ϕ-junction is realized, we have $I(\gamma = 0) \neq 0$ and an anomalous current is present. Its magnitude is strongly dependent on $\beta_3 \propto hL$ and Z, and is seen to reach up to 50% of the critical Josephson current (for $\beta_3 = \pi/4$ in the figure under consideration).

Having considered the equilibrium properties of the magnetically textured trilayer-Josephson junction, we now wish to address if magnetization dynamics will be generated when a spin-polarized supercurrent flowing through the system. In particular, we will consider if and how the presence of the aforementioned anomalous supercurrent alters the dynamics of the free ferromagnetic layer. To explore this, we solve the Landau-Lifshitz-Gilbert (LLG) equation numerically without any approximation for the ABS energies, i.e. valid for arbitrary parameter values. The main ingredient which makes this possible is the effective field, which contains both the contribution from anisotropy terms and the

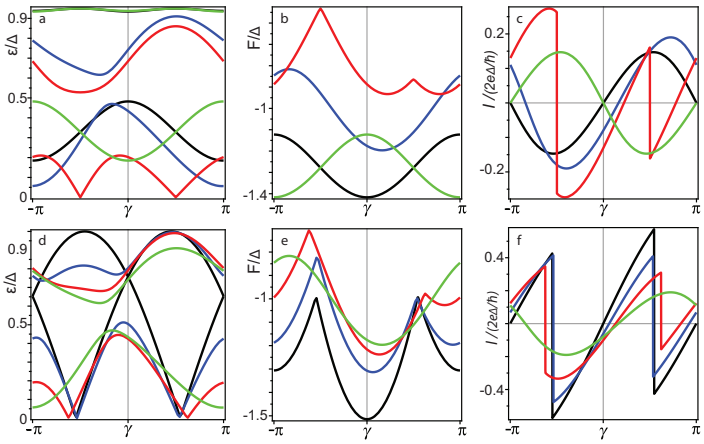

Figure 2.2: (a,d): Andreev bound-state energies as a function of superconducting phase difference γ. (b,e): free energy of the system as a function of γ and (c,f) supercurrent-phase relation for our trilayered S|F|F|F|S structure. In all plots, we have set $\beta_1 = \beta_2 = \pi/3$. In (a,b,c), we fix the barrier at $Z = 2$ and investigate the effect of different values of β_3 (proportional to both exchange field h and width L of the free ferromagnetic layer): $\beta_3 = 0$ (black), $15\pi/100$ (blue), $25\pi/100$ (red), $50\pi/100$ (green). For (d,e,f), we fix $\beta_3 = 15\pi/100$ and investigate the effect of a varying barrier potential: $Z = 0$ (black), 1 (blue), 1.5 (red), 2 (green).

.

ABS-energies. It may be written as:

$$\mathbf{H}_{\text{eff}} = \frac{2}{|M_0|}(K_e \boldsymbol{m}_i - K_h \boldsymbol{m}_j) - \frac{1}{V|M_0|}\frac{\partial \mathcal{F}}{\partial \boldsymbol{m}} \tag{2.33}$$

where $K_{e(h)}$ is the easy (hard) axis anisotropy constant while $\mathcal{F}$ is the contribution to the free energy from the ABS-energies [see Eq. (2.17)] and $i(j)$ can be x or y or z in accordance with in which direction is easy (hard) axis. We comment specifically on the regime of validity for our approach that consists of combining a scattering matrix approach in equilibrium with the time-dependent LLG-equation in Sec. 2.9.4. For now, we simply state that this framework is justified when the magnetization dynamics is sufficiently slow compared to the rate at which the system relaxes to an equilibrium state [79], and is commonly used in the literature. In our numerical simulations, we will set $\beta_1 = \beta_2 = \pi/3$, $\Delta = 10^{-22}$ J, $\mu_0 = 10^{-6}$ H/m, and $|M_0| = 10^5$ A/m. The Gilbert damping parameter is set to $\alpha = 0.02$.

Before discussing the obtained results, it should be noted that the time-dynamics of the magnetic order parameter in the free F layer depends on the relative magnitude of the anisotropy and ABS-energy terms in the effective field $\mathbf{H}_{\text{eff}}$. Depending on the parameters of the system, one of these will dominate or they will be of similar magnitude and compete. We will take the cross-sectional area of the junction to be $1\mu\text{m}\times 1\mu\text{m}$ and consider a width of 10 nm for the free

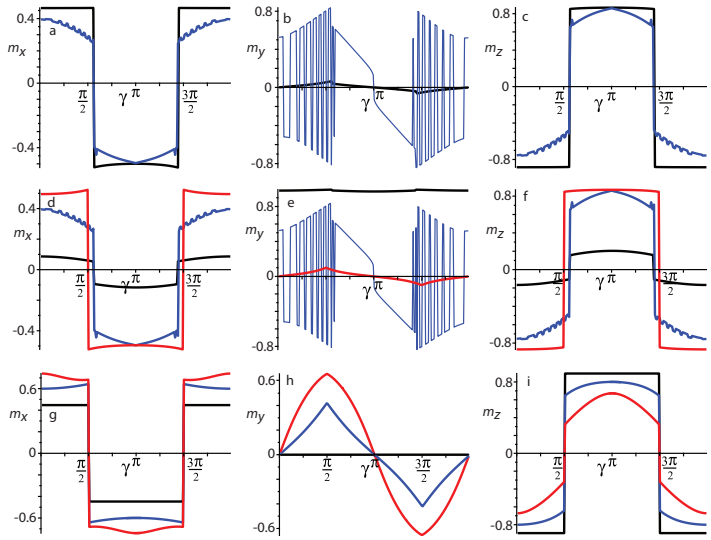

Figure 2.3: Stable magnetization state as a function of superconducting phase difference γ for $t \to \infty$ when $\mathbf{m}_3(t = 0) \parallel \hat{y}$ initially. The components of the magnetization are given in the left (m_x), middle (m_y), and right (m_z) columns. For all panels, we fix $\beta_1 = \beta_2 = \pi/3$. (a,b,c): We set $\beta_3 = 5\pi/100$, $Z = 0.5$, and consider different values of the anisotropy constant - $K = 10^4$ J/m^3 (black line), 10^5 (blue line). (d,e,f): We set $Z = 0.5$, $K = 10^5$, and consider different values of the β_3 parameter - $\beta_3 = \pi/100$ (black), $5\pi/100$ (blue), $25\pi/100$ (red). (g,h,i): We set $\beta_3 = 25\pi/100$, $K = 10^5$, and consider different values of the barrier transparency - $Z = 0$ (black), 1 (blue), 2 (red).

layer. With a lattice constant of $a = 0.1$ nm and estimating the number of transverse modes to $N/V = 10^{28}$ m^{-3}, we find that for $K \leq 10^3$ J/m^3 the ABS-term dominates whereas for $K \geq 10^5$ J/m^3 the anisotropy governs the dynamics. In order to limit the parameter space, we will consider only a high to moderate interface transparency ($Z \leq 2$) and a junction length of the free F layer satisfying $\beta_3 \leq 25\pi/100$. These values are representative for a set of experimentally attainable interface transparencies ranging from high to low as well as different values for the exchange field of the free ferromagnetic layer, ranging from weakly to moderately polarized. In each case, we solve the LLG-equation numerically and identify the stable state that arises when $t \to \infty$ and its dependence on the superconducting phase difference. The initial condition for the magnetization of the free layer is taken to be along its easy anisotropy axis. We discuss the experimental realization of this setup in more detail in Sec. 2.9.4.

Firstly, consider the case with anisotropy along the $\hat{y}$ direction shown in Fig. 2.3. We plot the stable state ($t \to \infty$) for each of the magnetization components and investigate the effect of varying the anisotropy strength K (top row), the combined effect of exchange field and width of the ferromagnetic layer $\beta_3 \propto hL$

(middle row), and the interface barrier transparency Z (bottom row). Several observations can be made. Whereas the qualitative behavior of the m_x (left column) and m_z (right column) components are equivalent, displaying a symmetry around $\gamma = \pi$, the m_y (middle column) component displays different behavior. For some parameter values, we observe very fast oscillations in terms of the value of the stable state as a function of the superconducting phase difference. Remarkably, this is a direct result of the presence of an anomalous supercurrent in the system. To see this, consider the LLG-equation for a stable, time-independent magnetization:

$$\mathbf{m} \times \mathbf{H}_{\text{eff}} = 0, \tag{2.34}$$

where $\mathbf{H}_{\text{eff}}$ contains a contribution from both the anisotropy and ABS-energies. From the definition of the effective field, one can show that the components of it satisfy:

$$\left(\mathbf{H}_{\text{eff}}\right)^i \propto \sum_k C(\varepsilon_k) \frac{\partial \varepsilon_k}{\partial h_i}. \tag{2.35}$$

Now, the partial derivative of the ABS-energy depends strongly on which component of the field one considers. For instance, one finds $\frac{\partial \varepsilon_k}{\partial h_y} \propto \sin\gamma$ (odd function of the phase difference) whereas $\frac{\partial \varepsilon_k}{\partial h_z}$ is mainly determined by $\cos\gamma$ (even function of the phase difference). In turn, these properties also determine the symmetries of $\left(\mathbf{H}_{\text{eff}}\right)_i$ with respect to γ. This observation is essential as it explains the qualitative behavior of the magnetization dynamics in Fig. 2.3. Let us write out the stable state condition componentwise where we explicitly separate the contribution from anisotropy and ABS-energies:

$$\begin{aligned} m_y H^z_{\text{ABS}} - m_z H^y_{\text{ABS}} - K m_y m_z &= 0, \\ m_x H^z_{\text{ABS}} - m_z H^x_{\text{ABS}} &= 0, \\ m_x H^y_{\text{ABS}} - m_y H^x_{\text{ABS}} + K m_x m_y &= 0. \end{aligned} \tag{2.36}$$

There are now three possible scenarios: 1) the anisotropy term dominates, 2) the ABS-energy term dominates, or 3) the contribution from both of these are comparable. When the anisotropy term dominates the effective field, one would expect that the magnetization does not deviate much from its original configuration (along the easy axis). This is seen in panel (e) for the black line. When the anisotropy term is small compared to H_{ABS}, we can neglect the terms $\propto K$ in Eq. (2.36) which allows us to conclude the following: since H^y_{ABS} is close to antisymmetric in γ whereas H^z_{ABS} is close to symmetric, the first and third line dictate that m_y must be close to antisymmetric in γ whereas m_x and m_z must be close to symmetric. This is again consistent with Fig. 2.3. Therefore, we may conclude that it is the appearance of the anomalous supercurrent (which is proportional to the $\sin\gamma$ term in the effective field) that is responsible for the qualitatively different behavior of m_y compared to the other components. Finally, the oscillatory behavior of m_y may be understood as a competition between the anisotropy and the ABS-contribution to the effective field. Whereas

dominating K permits a symmetric m_y with respect to the phase difference γ while dominating ABS-contribution gives an antisymmetric m_y, the two terms compete when they are of comparable magnitude and give rise to a stable-state for m_y which displays symmetry in a certain range of γ and otherwise antisymmetry. Having established the influence of the superconducting phase difference on the magnetization dynamics, the plots moreover show that magnetization switching is possible. For instance, panel (l) shows that depending on the phase difference γ, the stable magnetization state is almost fully aligned with either the $+\hat{z}$ or the $-\hat{z}$ direction.

Consider next the case where we change the initial magnetization configuration of the free ferromagnetic layer to be along the $\hat{x}$ or $\hat{z}$ directions. The results are shown in Fig. 2.4. The corresponding equation governing the stable-state now changes compared to Eq. (2.36) since the anisotropy contribution will now *always* appear in the second line. As a result, one concludes that regardless of the strength of the anisotropy and regardless of whether the initial configuration is along $\hat{x}$ or $\hat{z}$, the m_y component will always be close to antisymmetric in γ, as seen in Fig. 2.4.

Let us also comment specifically on the role played by the interface barrier potential Z and the parameter $\beta_3 \propto hL$ in terms of how they influence the magnetization dynamics. A common feature for both Fig. 2.3 and 2.4 is that the m_y-component grows with increasing barrier Z. This should be seen in conjunction with that the magnitude of the anomalous supercurrent also increases with Z (up to $Z \simeq 2$), as shown in Fig. 2.2. In effect, the anomalous supercurrent increases in magnitude with Z and is seen to have a feedback-effect on the magnetization in terms of enhancing the magnitude of m_y. With regard to the role of β_3, its main role is seen to oppose the effect of the anisotropy. As β_3 increases, the influence of the ABS-contribution to the effective field becomes more dominant as evidenced by the emergent antisymmetric m_y dependence on γ.

2.9.2 S|F|S junction with spin-active interface zones

We proceed to consider the structure shown in Fig. 2.1(b): an S|F|S junction where the interface are spin-active. More specifically, we allow (as before) for an arbitrary magnetization direction in the free ferromagnetic layer whereas the interface regions are modeled via Eq. (2.29) in the perpendicular configuration in order to allow for the possibility of spin chirality breaking with the interface moments and the bulk moment all pointing along different axes. In the quasiclassical regime of a sufficiently weak ferromagnet, we find the following analytical expression for the ABS-energy:

$$\varepsilon_j = \Delta_0 \sqrt{1 - \mathcal{A}\cos\gamma - \mathcal{B}(h_y/h)Z^2\rho_m^2\alpha\sin\gamma - \mathcal{C} \pm \sqrt{\mathcal{D}(\gamma)}} \tag{2.37}$$

where the coefficients $\mathcal{A}, \mathcal{B}, \mathcal{C}$ are independent on the phase difference γ. The quantity $\mathcal{D}(\gamma)$ is a rather large expression which depends on γ; the essential

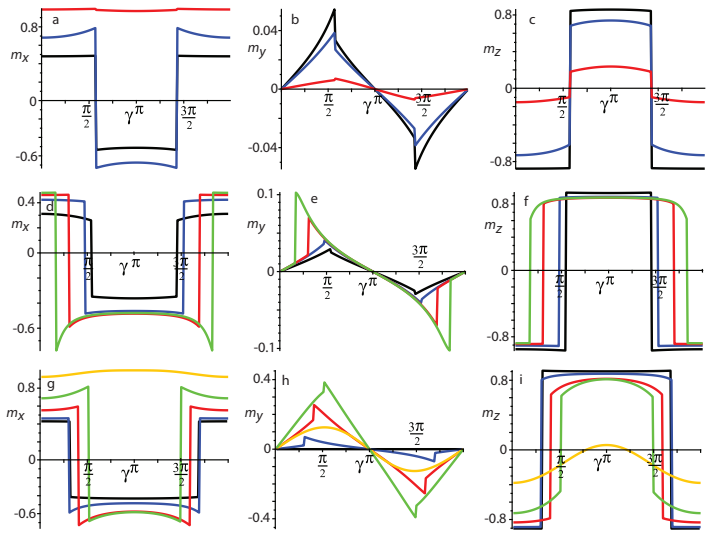

Figure 2.4: Stable magnetization state as a function of superconducting phase difference γ for $t \to \infty$ when $\mathbf{m}_3 \parallel \hat{y}$ initially. The components of the magnetization are given in the left (m_x), middle (m_y), and right (m_z) columns. For all panels, we fix $\beta_1 = \beta_2 = \pi/3$. (a,b,c): $\mathbf{m}_3(t=0) \parallel \hat{x}$ as initial condition with $\beta_3 = \pi/100$ and $Z = 0.5$. We consider several values of the anisotropy constant $K = 10^3\text{J/m}^3$ (black line), 10^4 (blue line) 10^5 (red line). (d,e,f): $\mathbf{m}_3(t=0) \parallel \hat{z}$ as initial condition with $Z = 0.5$ and $K = 10^4\text{J/m}^3$. We here consider different values of the β_3 parameter - $\beta_3 = \pi/100$ (black), $15\pi/100$ (blue), $25\pi/100$ (red). (g,h,i): $\mathbf{m}_3(t=0) \parallel \hat{z}$ as initial condition with $\beta_3 = 15\pi/100$ and $K = 10^4\text{J/m}^3$. We consider several choices for the barrier transparency $Z = 0$ (black), 0.5 (blue), 1 (red), 1.5 (green), 3 (yellow).

property of this quantity is nevertheless that

$$\left.\frac{\partial \mathcal{D}(\gamma)}{\partial \gamma}\right|_{\gamma=0} \propto \mathcal{B}(h_y/h) Z^2 \rho_m^2 \alpha. \tag{2.38}$$

Similarly to the trilayer structure the $\sin(\gamma)$ contribution is *only present* when $h_y \neq 0$ and is accompanied by an anomalous supercurrent. The effect increases with the strength of the interface barrier Z and its existence is actually contigent on a non-zero Z. Therefore, the same conclusion as for the trilayer structure holds here: chiral spin-symmetry breaking is not a sufficient criterion for the appearance of an anomalous supercurrent - it also requires scattering at the interfaces.

In Fig. 2.5, we provide a plot for the ABS-spectrum, free energy, and supercurrent-phase relation for the system with spin-active interfaces. In this structure, there is a new parameter compared to the trilayer case, namely the ratio between the magnetic and non-magnetic part of the barrier ρ_m. In what follows, we set $\rho_m = 0.5$. Considering first the ABS-spectrum, we see that the shift of the

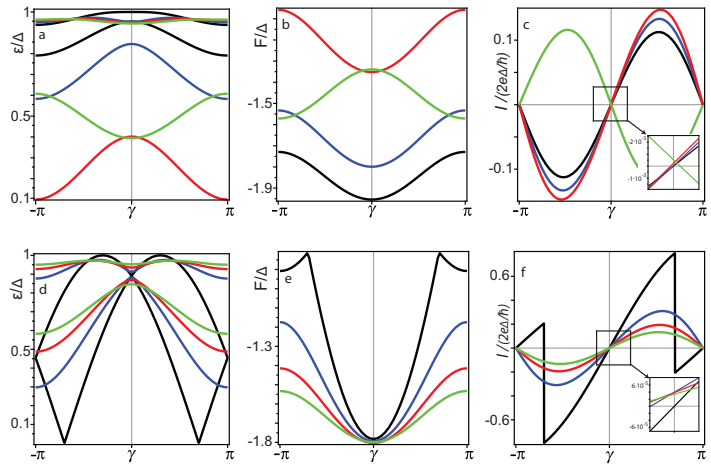

Figure 2.5: (a,d): Andreev bound-state energies as a function of superconducting phase difference γ. (b,e): free energy of the system as a function of γ and (c,f) supercurrent-phase relation for our spin-active SFS structure. In (a,b,c), we fix the barrier at $Z = 2$ and investigate the effect of different values of β (proportional to both exchange field h and width L of the free ferromagnetic layer): $\beta = 0$ (black), $15\pi/100$ (blue), $25\pi/100$ (red), $50\pi/100$ (green). For (d,e,f), we fix $\beta = 15\pi/100$ and investigate the effect of a varying barrier potential: $Z = 0$ (black), 1 (blue), 1.5 (red), 2 (green).

extremal values away from 0 and π are very small when the conditions for a non-zero anomalous supercurrent are present (finite Z and h_y). In fact, the free energy plots are very close to describing usual 0-π transitions. However, the zoom-in in the right column of Fig. 2.5 demonstrates that there is a small but finite value of the supercurrent at $\gamma = 0$, which is equivalent to saying that the junction is in a φ-state. Both the present and the trilayer system can then in principle act as phase batteries supplying whichever phase difference that may be desirable as its ground-state.

For the magnetization dynamics, we consider in this section only the case where the initial configuration is along the $\hat{y}$-axis since this gives the qualitatively most interesting behavior. Using the $\hat{x}$ and $\hat{z}$ directions as the free layer initial state provides similar results as in the previous section. One key difference is nevertheless that unlike the trilayer case, there is no magnetization dynamics whatsoever in the present scenario when $Z = 0$. The reason is that for perfectly transparent interfaces, the junction is equivalent to a homogeneous SFS junction and there is no spin-transfer torque due to misaligned magnetic moments. Moreover, we see that for all parameter choices we have $m_x(t \to \infty) = m_z(t \to \infty)$. This stems from the fact that the influence of both spin-active interfaces is equivalent in magnitude so that the induced x and z-components of the bulk magnetization take the same values. The qualitative behavior of the stable-state magnetization $m_y(t \to \infty)$ is determined by the relative contribution of

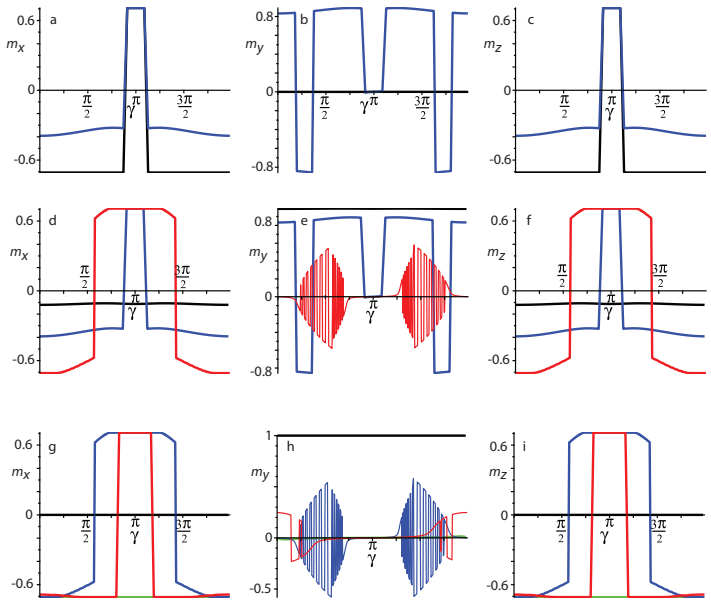

Figure 2.6: Stable magnetization state as a function of superconducting phase difference γ for $t \to \infty$ when $\mathbf{m}_3(t=0) \parallel \hat{y}$ initially. The components of the magnetization are given in the left (m_x), middle (m_y), and right (m_z) columns. In all panels, we fix $\rho_m = 0.5$. (a,b,c): We fix $\beta = 15\pi/100$, $Z = 0.5$, and consider several values of the anisotropy constant - $K = 10^4$ J/m^3 (black line), 10^5 (blue line). (d,e,f): We fix $Z = 0.5$, $K = 10^5$, and consider several values of the β parameter - $\beta = 5\pi/100$ (black), $15\pi/100$ (blue), $25\pi/100$ (red). (g,h,i): we fix $\beta = 25\pi/100$, $K = 10^5$, and consider several values of the interface transparency - $Z = 0$ (black), 0.5 (blue), 1 (red), 2 (green).

the anisotropy term and the ABS-energies, and a similar analysis as for the trilayer case holds here as well. With increasing $\beta \propto hL$, the influence of the anisotropy term decreases.

2.9.3 Domain wall S|F|S junction

The final structure under consideration in this work is one where the magnetic weak link connecting the superconductors consists of two layers: a magnetic domain wall ferromagnet and, as before, a free ferromagnetic layer. The domain wall is modeled via Eq. (2.30). In the quasiclassical regime $h \ll \mu$, we obtain the expression

$$\varepsilon_j = \Delta_0 \sqrt{1 - \mathcal{A}\cos\gamma - \mathcal{B} \pm \sqrt{(\mathcal{A}\cos\gamma)^2 + \mathcal{C}\cos\gamma + \mathcal{D}}} \tag{2.39}$$

where all coefficients A, B, C and D are independent of γ and instead depend on all the other parameters in the junction. In obtaining Eq. (2.39), we considered

the limit $\eta \ll 1$ and $\alpha_{\rm dw} \gg \eta$ where

$$\begin{aligned} \alpha_{\rm dw} &= h_{\rm dw}/2\mu, \\ \eta &= a^2/k_F^2,\ a = \pi/2l_{\rm dw}. \end{aligned} \tag{2.40}$$

To understand what this limit means physically, we note that it is equivalent to stating that the domain wall width $_{\rm dw}$ far exceeds a typical lattice spacing constant as it should. From this expression, it is clear that the ground-state energy will always occur at $\gamma = 0$ or $\gamma = \pi$, in contrast to the two previously analyzed configurations. The $\sin\gamma$ term responsible for the anomalous supercurrent and φ-junction is absent. For this reason, we do not include any results for the magnetization dynamics of this system. We instead show graphically in Fig. 2.7 the ABS-energies (a,d,g), the free energy of the system (b,e,h) and the supercurrent-phase relation (c,f,j) are all shown for various parameter choices. The fact that the anomalous supercurrent is absent is an important observation, because it demonstrates that chiral spin-symmetry breaking (or alternatively, non-coplanar magnetization vectors) alone is insufficient to induce such a term. In fact, the finding that the term causing a φ-junction is absent in the present case of a domain wall is consistent with our findings for the trilayer junction above. There, it was shown that if either interface barrier between the ferromagnetic layers was absent, the anomalous supercurrent vanishes. Such a scenario is similar to the present case, since two misaligned ferromagnetic regions without any interface scattering barrier can be thought of as a simplified domain wall.

2.9.4 Discussion

We discuss here some issues which are relevant for the approximations made in our model as well as how to realize experimentally the proposed setups. First of all, the variation of the magnetization dynamics on the superconducting phase difference can be probed in several ways. In our treatment, we have considered a phase-biased Josephson junction with a fixed superconducting phase rather than a fixed current bias. In the latter case, the superconducting phase would vary together with the magnetization dynamics since the supercurrent-phase relation is sensitive to the exact magnetization configuration. Instead, by phase-biasing the junction via a loop-geometry and a minute external field corresponding to a flux quantum (which has no effect on the magnetization dynamics), the current is allowed to vary as the magnetization dynamics takes place while the phase remains fixed. Another approach would be to study a phase-driven junction with a voltage-bias as done in *e.g.* [53, 55].

For the computation of the magnetization dynamics, we used as initial condition that the magnetization of the free layer was along the easy axis anisotropy. In general, however, the magnetization configuration that solves the static LLG equation in equilibrium is not necessarily with the free layer along the easy axis. This is due to the presence of the effective field stemming from the ABS-energies that exist in the junction. We have attempted to find a general analytical solution for the orientation of the free layer which solves $\mathbf{m} \times \mathbf{H}_{\rm eff} = 0$ when

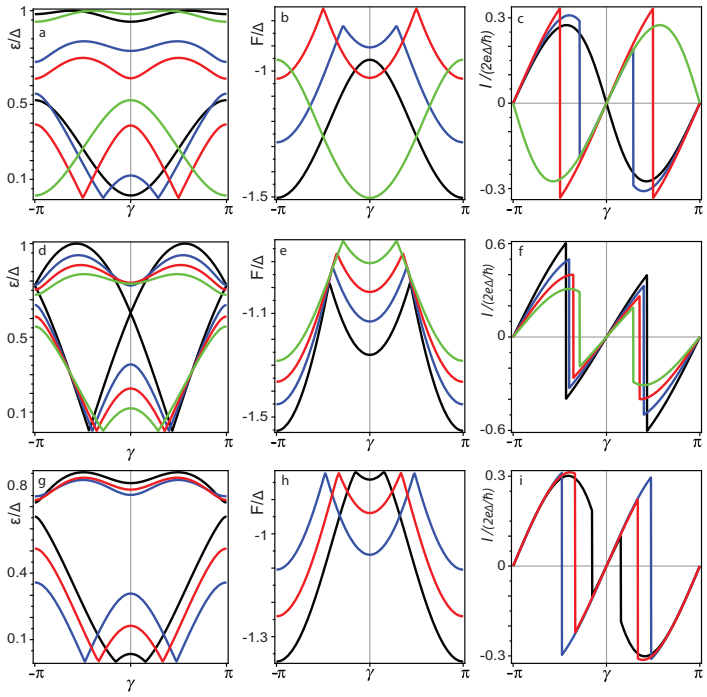

Figure 2.7: (Color online) (a,d,g): Andreev bound-state energies as a function of superconducting phase difference γ. (b,e,h): free energy of the system as a function of γ and (c,f,j): supercurrent-phase relation for our S/DW/F/S structure. In (a,b,c), we set $Z = 2$, $\eta = 10^{-4}$ and investigate the effect of different values of the β_2 parameter - $\beta_2 = 0$ (black), $15\pi/100$ (blue), $25\pi/100$ (red), $50\pi/100$ (green). In (d,e,f), we set $\beta_2 = 15\pi/100$, $\eta = 10^{-4}$ and investigate the effect of the magnitude of the barrier transparency - $Z = 0$ (black), 1 (blue), 1.5 (red), 2 (green). Finally, for (g,h,i) we set $Z = 2$, $\beta_2 = 15\pi/100$ and investigate the effect of the domain wall width - $\eta = 10^{-4}$ (black), 8×10^{-3} (blue), 5×10^{-3} (red)

including all terms in the free energy, but the resulting expressions were too cumbersome to be of any use. The initial condition used in the numerical simulations is nevertheless feasible to realize experimentally, simply by applying an external field along the anisotropy axis to artificially enhance it so that the free layer **m** is fixed along that direction. By then turning off the field, the resulting magnetization due to the Andreev-bound states and the change in superconducting phase difference may then be observed. It is important to underline that the supercurrent-induced magnetization dynamics studied in this paper is a non-equilibrium effect even when the SC phase difference is kept constant. The reason is that the system is initially prepared in a magnetization configuration which is not the ground-state of the system so that there is a finite torque acting on the free layer which eventually goes to zero as the system relaxes into a stable state for $t \to \infty$.

In the situation considered in the majority of previous literature on magnetic Josephson junctions, the magnetization is considered fixed and thus already being in its ground-state (*e.g.* due to strong anisotropy fixing). One then assumes that there is no feedback on the magnetization from the Josephson current, and so one only needs to minimize the superconducting part of the free energy with respect to the phase difference: the magnetic part is already assumed to be minimized. If one instead, as we have done, allows for the Andreev bound states and (thus supercurrent) to have a considerable influence on the free energy on equal footing as the anisotropy, the superconducting correlations will alter the favorable orientation of the magnetization. The free energy should then be minimized both with respect to the magnetization orientation and the superconducting phase difference.

Let us also comment specifically on our technical treatment of how the Andreev-bound state contribution to the free energy gives rise to an effective field that enters the LLG equation. By defining the effective field $\mathbf{H}_{\text{eff}}$ as the functional derivative of the magnetic order parameter evaluated at its instantaneous configuration requires that the magnetization dynamics is slow compared to relaxation processes in the system. In other words, the derived free energy may be treated as time-dependent if the system approximately equilibriates in pace with the change in magnetization. A lag between the magnetization dynamics $\mathbf{m}(t)$ and degrees of freedom that are coupled to it may be interpreted as a dissipation of energy and in turn captured by the Gilbert-damping parameter that we have accounted for [79]. For a driven superconducting phase where the phase difference is $\gamma(t) = \omega_J t + \gamma_0$, the above criterium is satisfied when $\omega_J \ll k_B T_c$ [53] so that the phase is treated as a time-dependent perturbation.

It is worthwhile to point out that the diffusive limit of transport is usually the experimentally most relevant one. Our motivation for performing the calculations in the ballistic regime was primarily for the sake of analytical transparency: using the BdG-equations, we have obtained analytical expression for the Andreev bound-state energies from which one could directly infer the required conditions of the appearance of the anomalous supercurrent. In the diffusive limit, one would have to use the quasiclassical Usadel equations. For the type of structures that we have considered with multilayers, an analytical solution might be possible but probably not in a particularly illuminating form. In fact, a previous work [24] that considered a trilayer $S|F|S$ junction using the quasiclassical formalism was unable to identify the appearance of the ϕ-state using an analytical approach, presumably due to all the simplifications that are required for this purpose. This suggests that a calculation in the full proximity effect regime, where only a numerical approach is viable, would be required in the diffusive limit in order to correctly obtain the predicted effects. Whereas this is certainly interesting, it lies outside the scope of our work. Having stated this, we think it is reasonable to expect that our results will be qualitatively valid for the diffusive limit as well for the following two reasons: *i)* the fundamental mechanism for the generation of an anomalous supercurrent and ϕ-state rely on the breaking of a chiral spin symmetry combined with the presence of interface

scattering. None of these effects pertain uniquely to the ballistic limit of transport, and hence one would expect that the same physics would transpire in the diffusive limit given the same conditions as in our paper. *ii)* In the regime of moderate to low interface transparency ($Z \geq 1$ in our paper), the supercurrent-phase relation is close to sinusoidal and the higher harmonics (which typically are much more pronounced in the ballistic limit) are suppressed. In this way, our system becomes more comparable to the diffusive case where it is known that the first harmonic is by far the most important contribution. Quantitatively, there may certainly be some differences between the diffusive and ballistic treatments, but we do not expect any dramatic alterations of the underlying physics for the reasons mentioned above.

Finally, in order for the magnetization vectors to be misaligned as *e.g.* in the trilayer case, it is necessary to reduce the exchange coupling between the layers. This can be achieved by inserting a normal metal spacer between the F regions. We have omitted this layer in our calculations since it would merely complicate the analytical expressions without introducing any new physics. It should be noted that spacer thicknesses as small as 4 nm are sufficient to experimentally allow for misaligned magnetization vectors in superconducting hybrid structures, as very recently reported in [80].

2.9.5 Conclusion

In conclusion, we have investigated the spin- and charge-transport in several models of magnetically textured Josephson junctions. We have made predictions for the ABS-energy spectrum, the free energy and its phase dependence, and the supercurrent-phase relation. Moreover, we have considered the magnetization dynamics induced by the presence of a triplet spin-supercurrent in these systems and computed how the stable-state magnetization $\mathbf{m}(t \to \infty)$ is controlled by the superconducting phase difference. A key finding is that the presence of an anomalous supercurrent $\propto \cos\gamma$, which results in a φ-state, strongly influences the resulting magnetization dynamics and gives rise to symmetry properties of the stable-state which may be understood by analyzing the resulting effective field $\mathbf{H}_{\text{eff}}$. Moreover, we demonstrated that chiral spin symmetry breaking is insufficient to generate such an anomalous supercurrent: the presence of scattering barriers separating different magnetic regions play an instrumental role in creating this effect. Our results may provide a basis for future investigations of how controllable magnetization dynamics can be obtained with spin-supercurrents that are tuned via the superconducting phase difference.

Chapter 3

Domain wall motion via current and spin-waves in multiferroics

Over the last decade, there has been a surge of interest in multiferroic materials [82, 83, 84] which displays simultaneously ferromagnetic, antiferromagnetic, ferroelectric, and/or ferroelastic order [85]. Besides the obvious allure of this multifunctionality from a practical viewpoint, such as usage for the purpose of magnetic random access memories [86, 87], the magnetoelectric cross-coupling between these orders is interesting from a fundamental physics perspective [58, 91, 92, 93, 94, 89, 88].

It is known that a wide variety of multiferroic materials host textured magnetic order parameter profiles [83] such as domain walls. Domain walls may be thought of as topological defects which interface different regions of a material and exhibit properties that differ from the ones in the homogeneous domains. Controlling the transport of magnetic domain wall structures is currently an active field of research [104] in spintronics as it offers an interesting way to transfer information in a non-volatile manner. In the context of multiferroics, inhomogeneous magnetic distributions $\boldsymbol{M}$ such as domain walls may induce an electric polarization $\boldsymbol{P}$ which opens up the possibility to influence magnetic domain walls via electric fields $\boldsymbol{E}$ [92]. Indeed, it has been experimentally shown that it is possible to manipulate magnetic domain wall structures via an external $\boldsymbol{E}$ field [95]. Magnetoelectric coupling has also been demonstrated to provide strain-controlled domain wall motion [96].

However, an analytical framework and understanding of how domain wall motion takes place in multiferroics when exposed to central driving forces in spintronics such as spin-polarized currents or spin-waves remains largely unexplored [98, 99]. In this chapter, we answer the question: how does magnetic domain walls in multiferroics respond to the spin-transfer torque induced by electric currents and spin-waves?

3.1 Ferromagnetism

3.1.1 Exchange interaction

The physical mechanism that is responsible for the alignment of electron spins is the exchange interaction. It can arise in different forms: the direct exchange interaction and superexchange where spins on a pair of magnetic ions interact via a third mediating ion. In all of these cases, the Coulomb interaction and Pauli principle are central. The Coulomb repulsion between two electrons can be reduced by increasing the distance between them via their spins aligning, since the Pauli principle then forbids the electrons to reside at the same position. The magnitude of the exchange interaction thus depends on the distance between the spins and their relative orientation of magnetic moments. We will work in approach of a continuous medium, where for homogeneous or weakly inhomogeneous (scale of inhomogeneity $\gg$ interatomic distance) magnetization can be considered as a continuous function of the spatial coordinates. For a cubic crystal structure of the ferromagnet, the free energy resulting from the exchange interaction is

$$F_{\text{exc}} = \int dr \Big\{ - J_0 \cdot \boldsymbol{m}^2 + J \Big[\Big(\frac{d\boldsymbol{m}}{dx} \Big)^2 + \Big(\frac{d\boldsymbol{m}}{dy} \Big)^2 + \Big(\frac{d\boldsymbol{m}}{dz} \Big)^2 \Big] \Big\} \tag{3.1}$$

where J_0 and J are the constants of homogeneous and inhomogeneous interaction respectively, while $\boldsymbol{m} = \boldsymbol{M}/M_0$, M_0 is the saturation magnetization. In the case of a ferromagnet, the exchange interaction favors a parallel alignment of spins. It is seen that the free energy is invariant with respect to a rotation of $\boldsymbol{m}$.

3.1.2 Anisotropy

As was stated above, the exchange interaction contributes to determining the dependence of the magnetic energy on the relative orientation of magnetic moments. At the same time there is also interaction between the magnetization and crystal lattice, which is called magnetocrystalline anisotropy. The origin of this interaction lies in the fact that orientations of the magnetization, which influences the atomic spin-orbit interaction, along different crystallographic axes are energetically unequal. This means that the orientation of magnetization M along one direction of crystal is energetically more profitable than along another. In the case of uniaxial crystal, the energy is minimal when the orientation of magnetization vector is along a symmetry axis of the crystal. The energetically profitable direction is called the easy axis, and the material can be magnetized in this direction to saturation at lower external magnetic fields. The direction in which the anisotropy energy is maximum, is called the hard axis.

But there are other sources of anisotropy besides magnetocrystalline anisotropy, such as are the sample shape and micro-scale texture. Shape anisotropy derives from the demagnetization field, which depends on the direction of magnetization in the sample relative its geometry. This is not intrinsic property and changes

when the geometry of the sample is changed. Induced anisotropy arises when an easy direction of magnetization is created by applied stress, or by depositing or annealing a disordered alloy in a magnetic field to create some atomic-scale texture.

A general expression for the anisotropy energy, regardless of its specific source, can be written as

$$F_{\text{an}} = \int \mathrm{d}\boldsymbol{r}(-\frac{K}{2}m_z^2 + \frac{K_\perp}{2}m_x^2) \tag{3.2}$$

where $K > 0$ and $K_\perp > 0$ are constants of anisotropy for easy and hard axis correspondingly. Later, we will use this effective anisotropy to determine magnetization dynamics.

3.1.3 Zeeman coupling

In the presence of the external magnetic field, the ferromagnet has also magnetostatic energy known as the Zeeman energy, which can be written in the form:

$$F_Z = -\int \mathrm{d}\boldsymbol{r}(\boldsymbol{M} \cdot \boldsymbol{B}_{\text{ext}}) \tag{3.3}$$

where $\boldsymbol{B}_{\text{ext}}$ is the external magnetic field.

3.1.4 Effective magnetic field

As seen, the total free energy of the ferromagnetic has different terms $F_{\text{tot}} = F_{\text{exc}} + F_{\text{an}} + F_Z$, and so the ferromagnet is influenced by an effective field $\boldsymbol{H}_{eff}$ which can be defined by derivative of the total free energy with respect to magnetization $\boldsymbol{M}$. Since the magnetic state of a ferromagnet is characterized not only by the magnetization $\boldsymbol{M}$, but also depends on the gradient of the magnetization, we must use the functional derivative. The effective field is formally defined as

$$\boldsymbol{H}_{\text{eff}} = -\frac{1}{M_0}\frac{\delta F}{\delta \boldsymbol{m}} \tag{3.4}$$

3.2 Magnetization dynamics and LLG-equation

Magnetization dynamics describes the time evolution of the magnetization M under the influence of external and internal torques. The first equation of motion of magnetization was introduced by Landau and Lifshitz [58, 90]. By this equation, one can describe the dynamical behavior of a magnetic order parameter, for example motion of domain walls or the nonlinear dynamics of various inhomogeneities. The Landau-Lifshitz equation is based on fundamental mechanical laws - the conservation of total angular momentum $\boldsymbol{J}$ and the fact that its time-derivative is equal to a torque:

$$\frac{d\boldsymbol{J}}{dt} = \boldsymbol{T} \tag{3.5}$$

The angular momentum of a volume unit of a ferromagnetic medium is proportional to the spin of electrons in that unit of volume which differ from magnetization vector by the coefficient of proportionality γ, the gyromagnetic ratio. A torque $\boldsymbol{T}$ acting on magnetic moment is caused by the effective field $\boldsymbol{H}_{\text{eff}}$, $\boldsymbol{T} = [\boldsymbol{M} \times \boldsymbol{H}_{\text{eff}}]$. One obtains the following equation of motion of for the magnetization

$$\frac{\partial \boldsymbol{M}}{\partial t} = -\gamma \boldsymbol{M} \times \boldsymbol{H}_{eff} \tag{3.6}$$

where $\gamma = g(e/2m_e) > 0$ is the gyromagnetic ratio which is proportional to ratio between the charge e and the mass m_e of the electron. The dynamics described by this equation is such that the magnitude of magnetization is conserved, as can be seen by taking the scalar product between the entire equation and $\boldsymbol{M}$. Without an external field, the system is in equilibrium. But when we apply an external force, such that $\boldsymbol{M} \times \boldsymbol{H}_{\text{eff}} \neq 0$, the effective field $\boldsymbol{H}_{\text{eff}}$ will induce a precession of local magnetization around direction of effective magnetic field. For the simplest models, this equation has an exact analytical solution.

In its present form, this equation cannot describe any relaxation of the system: a precession will persist indefinitely. In order to account for dissipation of energy, one instead describes the magnetization dynamics with the Landau-Lifshitz-Gilbert equation that has been proposed by Gilbert [59]:

$$\frac{\partial \boldsymbol{M}}{\partial t} = -\gamma \boldsymbol{M} \times \boldsymbol{H}_{\text{eff}} + \frac{\alpha}{M_s} \boldsymbol{M} \times \frac{\partial \boldsymbol{M}}{\partial t} \tag{3.7}$$

In this equation, a term α describes viscous damping which is proportional to the magnetization velocity.

3.2.1 LLG with current

We will in this work consider both the influence of spin-waves induced torques and current-induced torques, commencing with the latter. In this case, the standard phenomenological equation of motion used to describe the spin-transfer torque effect of an electric current is (in normalized form):

$$\frac{\partial \boldsymbol{m}}{\partial t} = -\boldsymbol{m} \times \boldsymbol{H}_{\text{eff}} + \alpha \boldsymbol{m} \times \frac{\partial \boldsymbol{m}}{\partial t} - u \frac{\partial \boldsymbol{m}}{\partial c} + \beta u \boldsymbol{m} \times \frac{\partial \boldsymbol{m}}{\partial c} \tag{3.8}$$

where α is the Gilbert damping constant, u is proportional to the current density, while β is the non-adiabatic term whose origin, although subject to some controversy, mostly is believed to be spin-relaxation processes that cause the itinerant electron spins constituting the current to not follow the domain wall profile fully adiabatically [103]. Although the magnetization is allowed to take any direction, we consider only variation along one spatial dimension (denoted c above) in order to provide analytical results.

3.2.2 LLG in spherical system

To investigate the texture of a domain wall it is convenient to use equations in a spherical system of coordinates. In the ferromagnet, the length of the magnetic

vector $\boldsymbol{M}$ is constant, so that the orientation of M can be characterized only by the azimuthal angle ϕ in the xy-plane and the polar vector θ. The vector $\boldsymbol{M}$ can be written as $\boldsymbol{M} = M_0(\sin(\theta)\cos(\phi), \sin(\theta)\sin(\phi), \cos(\theta))$. The effective field in the spherical coordinate system can be written

$$\boldsymbol{H}_{eff} = H_M \boldsymbol{n}_r + H_\theta \boldsymbol{n}_\theta + H_\phi \boldsymbol{n}_\phi \tag{3.9}$$

where $\boldsymbol{n}_r$, $\boldsymbol{n}_\theta$ and $\boldsymbol{n}_\phi$ are the unit vectors of spherical coordinate system, and

$$H_M = -\frac{\partial F}{\partial M_0}, H_\theta = -\frac{1}{M_0}\frac{\partial F}{\partial \theta}, H_\phi = -\frac{1}{M_0 \sin(\theta)}\frac{\partial F}{\partial \phi}, \tag{3.10}$$

3.3 Domain walls

The total magnetic moment of a ferromagnetic sample without an external magnetic field can become smaller when the magnetization distributes itself inhomogeneously in order to reduce the demagnetization field. The presence of a magnetic anisotropy leads to separation of magnetic domains which are homogeneously magnetized along one of the direction of easy axis. The separation between these domains are known as domain walls, areas where magnetic vector smoothly varies its orientation. Domain wall was investigated firstly by Bloch. The upper limit of the wall thickness is determined by the anisotropy energy. There is also a limit associated with the exchange interaction, which counteracts a sharp transition as such a twist in the magnetization is costly from an energetic point of view.

To obtain the equilibrium distribution of magnetization in a ferromagnet with a domain wall, one can consider the static case in which the equation

$$\boldsymbol{m} \times \boldsymbol{H}_{\text{eff}} = 0 \tag{3.11}$$

has to be satisfied. For the simplest case where we only take into account the free energy of the exchange field and the effective anisotropy such that the z-axis is the easy axis and the x-axis is the hard axis, with the assumption that ϕ is a constant, these equations have exact analytical solution:

$$\theta = 2\arctan\{\pm\exp[(c-\chi)/\delta]\} \tag{3.12}$$

$$\phi = \pm\frac{\pi}{2} \tag{3.13}$$

where $\delta = (A/K)^{1/2}$ is the width of the domain wall while χ defines of the position of the center of domain wall. In accordance with the geometry of sample and orientation of anisotropy, such a profile can describe three different types of domain wall: Bloch, Neel or head-to-head.

In a bulk ferromagnetic sample with uniaxial anisotropy the typical domain walls are Bloch walls, which are characterized by a rotation of the magnetization parallel to the domain wall plane. The magnetization in the domains is

parallel to the domain wall plane. In the case of a very large crystal, uncompensated surface charges are negligible too. Therefore, only the interplay between exchange interaction and magnetocrystalline anisotropy defines the domain wall shape.

In the case of thin film there is different distribution of the magnetization vector. In this case, the magnetocrystalline and shape anisotropy reorient the reoriente the easy axis to lie in the plane of film while the hard axis is directed along the normal to the surface. Neel derived in 1953 the domain wall transition in thin films. He demonstrated that in such structure, a domain wall type with an in-plane rotation of the magnetization has a lower energy than the Bloch wall. The magnetization in the Neel domain lies in plane of film parallel to the domain wall plane and rotation occurs in plane of film with output of magnetization from the plane of the domain wall. The width of Neel domain walls are typically bigger than Bloch domain wall.

In the description of Bloch and Neel walls one assumes infinitely extended structures. This allows one to neglect the contribution into free energy from the demagnetizing field . But in real structures, such as cylindrical nanowires, such approximations are not correct and the shape anisotropy contributes decisively to the total energy that lead to the easy axis lies along structure. It determines the magnetization direction in the domains along the wire. The resulting domain wall configurations are called head-to-head or tail-to-tail type. The magnetization in domain walls separated by head-to-head or tail-to-tail walls is perpendicular to the domain wall plane. In such structure the geometry parameters such as width and thickness of the wire also influence on the width of the domain wall.

3.4 Motion of domain walls

Domain wall motion is an important basic magnetization process in multidomain solids. Under the influence of an external input, such as an external magnetic field, domain walls move in a direction that lead to an increase of the volume of the domain oriented along the external field and, conversely, decreasing the volume of other domain with opposite magnetization. During this process the average magnetization increases. Another fundamental magnetization process is magnetization switching, where the magnetization changes orientation in a domain under an external driving force. This type of magnetization process was considered in chapter 2. Besides using magnetic fields, it is also possible to move domain walls by currents as will be discussed below.

3.4.1 Motion by external magnetic field

The free energy changes when an external magnetic field is applied to the system. The position of the domain wall, determined by the minimum of the free energy, thus changes. For a clean system, without impurity pinning centres, even small magnetic fields move the domain walls. The analytical model of

field-induced propagation process for simple 180^0 domain walls with easy axis was studied firstly by Walker and Schryer [78]. They found that velocity of the motion of the domain wall is proportional to the external magnetic field as $\mathbf{v} = (\gamma\delta/\alpha) \cdot \mathbf{H}$, where γ is the gyromagnetic ratio, δ is the width of the domain wall and α is the damping constant. The velocity depends linearly on the external field until the field reaches a certain critical value: the so-called Walker field $H_{Walk} = \frac{\alpha K_\perp}{m}$. Upon further increasing the field, a deformation of the domain wall takes place, and the domain wall does not move linearly more. This is known as Walker breakdown.

3.4.2 Motion by spin-polarized current

The current-induced wall propagation is based on the spin-transfer torque effect. As polarized itinerant electrons pass from one domain to another with opposite polarization, they transfer spin angular momentum to the localized magnetic moments. As the result, this torque rotates each of the localized moments which lead to motion of the domain wall in accordance with the conservation of angular momentum. In 2004, Zhang and Li [103] gave a comprehensive treatment of spin-transfer torque and included in addition to the adiabatic torque also the non-adiabatic torque. Adiabatic dynamics of the magnetization is slow compared to the dynamics of the conduction electrons. scattering with impurities and with electrons. While the non-adiabatic torque is solely responsible for the terminal domain wall velocity in regime below Walker breakdown, the adiabatic torque is the main contributor to the net wall velocity above Walker breakdown.

3.4.3 Motion via spin-waves

There exists a third method available to move a domain wall, namely by spin waves that pass through it. Interesting because of its potential applications to low dissipation solid-state data-storage and data-processing devices, magnonic domain wall motion is a relatively new field which has attracted increasing attention recently [2].

The elementary excitation of spins above the magnetic ground-state has a wave character and is called spin-waves. In the quasiclassical approximation, spin-waves are small deviation of spin from the z-axis (axis of equilibrium direction for the magnetization) arising due to the spin precession with a small amplitude. If a spin-wave is causing precession with a small amplitude around the equilibrium position, we can present the magnetization vector in the following form:

$$\boldsymbol{m} = \boldsymbol{e}_r + [m_\theta \boldsymbol{e}_\theta + m_\phi \boldsymbol{e}_\phi] e^{-i\omega t} \tag{3.14}$$

where $\boldsymbol{e}_r$ is unit vector along equilibrium direction, ω is the spin-wave frequency and m_θ and m_ϕ are small, $\sqrt{m_\theta^2 + m_\phi^2} \ll 1$. In order to obtain equations of motion for m_θ and m_ϕ we substitute this representation into the LLG equation. Taking into account that m_θ and m_ϕ are small, the equations of motion are

[101]:

$$-i\omega m_\theta = -2\gamma A m''_\phi - 2\gamma K m_\phi(2\sin^2\theta - 1) + i\omega\alpha m_\phi \quad (3.15)$$

$$-i\omega m_\phi = 2\gamma A m''_\theta + 2\gamma K m_\theta(2\sin^2\theta - 1) - i\omega\alpha m_\theta \quad (3.16)$$

Upon defining $\phi = m_\theta - im_\phi$, $\xi = \frac{z}{\Delta}$, and $q^2 = \frac{\omega}{K} - 1$, these equations can be rewritten as:

$$q^2\phi(\xi) = \left[-\frac{d^2}{d\xi^2} - 2\mathrm{sech}^2\xi\right]\phi(\xi). \quad (3.17)$$

Interestingly, this has the form of a Schrödinger equation with solutions of the form of a propagating wave:

$$\phi(\xi) = \rho\frac{\tanh\xi - iq}{-iq - 1}e^{iq\xi} \quad (3.18)$$

where ρ is the spin-wave amplitude. The asymptotic form of this solution are $\phi(\xi \to -\infty) = \rho e^{iq\xi}$ and $\phi(\xi \to +\infty) = -\rho\frac{1-iq}{1+iq}e^{iq\xi}$. We see that spin-wave propagates through the domain wall without any reflection and retains its amplitude. However, its phase (spin orientation) changes. A magnon, which is the quasiparticle name for a spin-wave, thus flips its spin as it propagates through the domain wall. According to conservation of angular momentum, the missing spin angular momentum must have been transferred to the domain wall and causes it to move. If the spin-wave propagates rightwards, the domain wall will move left to conserve angular momentum. One of the main motivations for considering magnon-induced domain wall motion is that unlike the current-induced case, there is no need to incorporate moving electrons and one thus avoids Joule heating. Magnon-induced domain wall motion therefore also works in magnetic insulators.

3.5 Multiferroics

In the previous part of this chapter, we described magnetic materials that have one order parameter - the magnetization $\boldsymbol{M}$. But there exists some materials which exhibit two or even three order parameters. These are so-called multiferroics. Besides magnetic order, it is also possible to obtain ferroelectricity where a material displays a spontaneous electric polarization, and ferroelastics which exhibit stress-switchable elastic strain. A multiferroic material is described by a complicated tensor susceptibility with components related to both magnetic and electric fields and can thus feature both a spontaneous magnetization and electric polarization.

The influence of an electric field on micromagnetic structure was predicted theoretically in a series of works [107, 108, 97]. These theoretical models took into account the so-called inhomogeneous magnetoelectric interaction that gives rise to electric polarization associated with magnetic inhomogeneities. The inhomogeneous magnetoelectric contribution into thermodynamic potential for the bulk crystal of ferrite garnets with cubic symmetry takes the following form:

$$f_{\mathrm{ME}} = -\gamma_0\boldsymbol{E}[\boldsymbol{M}\cdot(\nabla\cdot\boldsymbol{M}) - (\boldsymbol{M}\cdot\nabla)\cdot\boldsymbol{M}] \quad (3.19)$$

where $\boldsymbol{M}$ is magnetization vector, f_{ME} is the free energy density, ∇ is differential operator vector, $\boldsymbol{E}$ is the electric field, and γ is inhomogeneous magnetoelectric interaction constant. It is clear from this equation that f_{ME} respects both inversion and time-reversal symmetry since $\boldsymbol{E}$ changes sign under inversion $\boldsymbol{r} \to -\boldsymbol{r}$ whereas $\boldsymbol{M}$ remains invariant, while $\boldsymbol{E}$ remains constant under time reversal $t \to -t$ and $\boldsymbol{M}$ changes sign. The electric polarization induced by the magnetic inhomogeneity can be found in the following way for a cubic crystal [97]:

$$\boldsymbol{P} = \gamma[\boldsymbol{M}(\nabla \cdot \boldsymbol{M}) - (\boldsymbol{M} \cdot \nabla)\boldsymbol{M}]. \tag{3.20}$$

When considering a multiferroic material, we must thus include this cross-coupling term between the electrical and magnetic degrees of freedom in the free energy: $F_P = -\int \mathrm{d}\boldsymbol{r}\boldsymbol{E} \cdot \boldsymbol{P}$. The magnitude of the magnetoelectric coupling coefficient is denoted γ_0.

3.6 Results

We now present the research results from **Paper II**.

Based on the above description of the theory, the total free energy is then represented by $F = F_{\mathrm{exc}} + F_{\mathrm{an}} + F_Z + F_P$ and we make use of the Landau-Lifshitz-Gilbert equation (LLG) [58, 59] to investigate the dynamics of a domain wall in this multiferroic system. We will in this work consider both the influence of spin-waves induced torques and current-induced torques, commencing with the latter. In this case, the standard phenomenological equation of motion used to describe the spin-transfer torque effect of an electric current is (in normalized form):

$$\frac{\partial \boldsymbol{m}}{\partial t} = -\boldsymbol{m} \times \boldsymbol{H}_{\mathrm{eff}} + \alpha \boldsymbol{m} \times \frac{\partial \boldsymbol{m}}{\partial t} - u\frac{\partial \boldsymbol{m}}{\partial c} + \beta u \boldsymbol{m} \times \frac{\partial \boldsymbol{m}}{\partial c} \tag{3.21}$$

where α is the Gilbert damping constant, u is proportional to the current density, while β is the non-adiabatic term whose origin, although subject to some controversy, mostly is believed to be spin-relaxation processes that cause the itinerant electron spins constituting the current to not follow the domain wall profile fully adiabatically [103]. Although the magnetization is allowed to take any direction, we consider only variation along one spatial dimension (denoted c above) in order to provide analytical results. In what follows, we will consider time t in the unit of $(\gamma\mu_0 M_0)^{-1}$ where μ_0 is the vacuum permeability, γ is the gyromagnetic ratio, and use normalized length in the unit of $(J/M_0^2\mu_0)^{1/2}$. Finally, we express the current density parameter u in the unit of $\gamma\sqrt{J\mu_0}$, the free energy F and anisotropy constants K and $K_\perp$in the unit of $M_0^2\mu_0$, E in unit of $\gamma M_0\mu_0\sqrt{J\mu_0}$, and the magnetoelectric coupling constant γ_0 in the unit of $(\gamma M_0^2\mu_0)^{-1}$.

A key observation is that not all types of magnetic textures will provide a net magnetoelectric polarization $\boldsymbol{P}$: a net component of the magnetization along

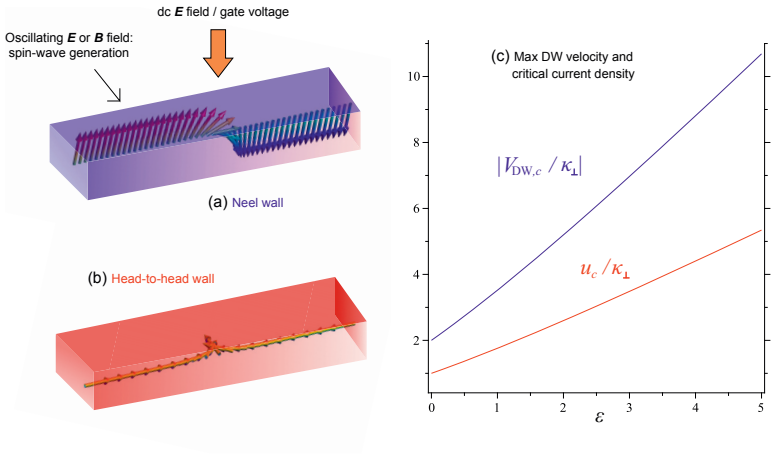

Figure 3.1: (Color online) Schematic setup considered in this work. We consider two types of domain walls in multiferroics which give rise to a net electric polarization due to the magnetoelectric effect: (a) Neel and (b) head-to-head domain walls. An ac $\boldsymbol{E}$ or $\boldsymbol{B}$ field is applied transversely to the structure in order to generate spin-waves locally, which then propagate through the system and interact with the domain wall. We also allow for the possibility of a dc $\boldsymbol{E}$ field (gate voltage) applied across the top and bottom of the structure. In (c), we show how the maximum domain wall velocity attainable before Walker breakdown $V_{\mathrm{DW},c}$ and the critical current density u_c scales with the applied normalized electric field ε. We have chosen parameters $\alpha = 0.01$ and $\beta = 0.02$.

the direction of spatial variation v is required, thus ruling out Bloch walls. For this reason, we will focus here on Neel (NDW) and head-to-head domain walls (HDW). To be concrete, we choose easy-axis of magnetic anisotropy along the z direction and the hard axis along x direction (see Fig. 3.1 for the schematic setup). Before we can explore the dynamics of multiferroic domain walls, one has to check whether an applied electric field alters the static domain wall profile itself. Some care must be exercised here, since we find that the validity of the usual Walker solution [78] for the domain wall profile depends on the orientation of the electric field relative the hard axis of anisotropy. For instance, the Walker profile is not valid for the NDW and HDW when the $\boldsymbol{E}$ field is applied along the hard-axis direction. Thus, we consider the electrical field as $\boldsymbol{E} = (0, 0, E_z)$ for NDW and $\boldsymbol{E} = (0, E_y, 0)$ for HDW. Due to our chocie for the coordinate axes, we can conventially write the normalized magnetization in the same way for both types of domain walls: $\boldsymbol{m} = (\sin(\theta)\cos(\phi), \sin(\theta)\sin(\phi), \sigma\cos(\theta))$, where $\theta(c) = 2\arctan[\exp^{(c-\chi)/\lambda}]$ where $c = y$ and $c = z$ for NDW and HDW correspondingly, λ is the DW width, χ is the position of the DW center, and the topological charge of the domain wall is σ. The azimuthal angle for the static Walker profile $\phi = \pm\pi/2$ for both our geometries and we assume that $K \gg K_\perp$ to justify the description of the domain wall as a solitonic object described only by the degrees of freedom associated with its center position and tilt angle [104]. The equation of motion for the center-coordinate $\chi(t)$ and the angle $\phi(t)$ is for

the NDW

$$\alpha\sigma\dot{\chi} + \lambda\dot{\phi} = -\sigma\beta u + \lambda B_z \text{ and } \sigma\dot{\chi} - \alpha\lambda\dot{\phi} = -\sigma u - \frac{1}{2}\lambda K_\perp \sin(2\phi) + \sigma\lambda\pi\gamma_0 E_y \cos(\phi). \tag{3.22}$$

For the HDW, we have

$$\alpha\sigma\dot{\chi} + \lambda\dot{\phi} = -\sigma\beta u,\ \sigma\dot{\chi} - \alpha\lambda\dot{\phi} = -\sigma u - \frac{1}{2}\lambda K_\perp \sin(2\phi) - \frac{B_y}{\pi}\cos(\phi) + 2\sigma\lambda\pi\gamma_0 E_z \cos(\phi). \tag{3.23}$$

The behaviour of the domain wall is different in two regimes which separated by the Walker breakdown, defined by $\partial_t\phi \neq 0$. In the regime where there is no Walker breakdown, the following equations must be satisfied for NDW $\frac{u}{\varkappa_\perp} = \sin(2\phi) + b_{\text{NDW}} - \epsilon\cos(\phi)$ and for HDW $\frac{u}{\varkappa_\perp} = \sin(2\phi) + (b_{\text{HDW}} + \epsilon)\cos(\phi)$ where $\varkappa_\perp = \frac{\sigma\alpha\lambda K_\perp}{2(\beta-\alpha)}$, $b = B/B_0$, $\epsilon = E/E_0$, $E_0 = \frac{\sigma K_\perp}{4\pi\gamma_0}$, $B_{0,\text{HDW}} = \frac{\pi\lambda K_\perp}{2}$, $B_{0,\text{NDW}} = \frac{\alpha K_\perp}{2}$ This allows us to determine a quantity of central practical importance, namely the critical current density u_c at which Walker breakdown takes place. We find:

$$u_{\text{HDW},c} = \varkappa_\perp[b + \sqrt{2}f(\epsilon)/32],\ u_{\text{NDW},c} = \sqrt{2}\varkappa_\perp f(\epsilon')/32, \quad f(x) = (3x + \sqrt{x^2+32})[16 - x^2 + x\sqrt{x^2+32}]^{1/2} \tag{3.24}$$

where $\epsilon^{'} = b + \epsilon$. From this, the maximum domain wall velocity $V_{\text{DW},c}$ that is attainable before deformation sets in is computed via $V_{\text{DW},c} = -\beta u_c/\alpha$. The corresponding angles ϕ corresponding to the constant tilt angle of the DW are $\phi_{WB} = -\arcsin(\frac{1}{8}(\epsilon - \sqrt{\epsilon^2+32}))$ and $\phi_{WB} = \pi - \arcsin(\frac{1}{8}(\epsilon^{'} - \sqrt{(\epsilon')^2+32}))$ for NDW and HDW, respectively. We here included the presence of a magnetic field for generality, and in the limit without any spin-transfer torque effect our expressions are consistent with Ref. [99]. Setting $B = 0$ in order to focus on the spin-transfer torque effect, it is seen from the above equations that the critical current in both the NDW and HDW case is the same and increases with E. This could be of practical importance since it offers a way to delay Walker breakdown induced by electric current, and increase the velocity of the domain wall transport, via a gate voltage. In Fig. 3.1 c, we plot the maximum domain wall velocity as a function of the applied electric field.

We now turn our attention to the question of how spin-waves interact dynamically with both homogeneous magnetization textures and domain wall structures in multiferroic materials. As it turns out, these two situations are inseparable and must be considered together. The reason for this is that we find that *spin-waves induce a torque even on a homogeneous magnetization due to the magnetoelectric coupling.* To illustrate this effect analytically, consider a thin-film ferromagnet with propagating magnons where the magnetization lies in-plane (say, xz-plane). Writing out the effective field explicitly, we then have:

$$\boldsymbol{H}_{\text{eff}} = J\partial_z^2\boldsymbol{m} + Km_x\hat{\boldsymbol{x}} + 2\gamma_0\partial_z m_z(E_x\hat{\boldsymbol{x}} + E_y\hat{\boldsymbol{y}}) - 2\gamma_0\hat{\boldsymbol{z}}(E_x\partial_z m_x + E_y\partial_z m_y). \tag{3.25}$$

To describe spin-wave propagation and its influence on the magnetic order parameter, we write the total normalized magnetization as $\boldsymbol{m} = (\sigma_0, \delta m_y + s_y, \delta m_z + s_z)$ where $\sigma_0 = \pm 1$ describes the equilibrium macrospin orientation, taking into account the possibility of ordering along both $\pm\hat{x}$ for the sake of generality. Moreover, δm_j and s_j describe the change in the magnetic order parameter and the spin-wave excitations, respectively, and are assumed to be small compared to σ_0 which allows for a perturbation treatment. With the above effective field, we insert $\boldsymbol{m}$ into the LLG equation and average over one spin-wave oscillation period. Discarding higher order terms, we are left with the following equations:

$$\begin{aligned} J\partial_z^2 m_z &= H_k m_z + \gamma_0 E_y \partial_z m_y + \gamma_0 \sigma_0 E_x \langle s_z \partial_z s_z \rangle, \\ J\partial_z m_y &= H_k m_y + \gamma_0 E_y \partial_z m_z + \gamma_0 \sigma_0 E_x \langle s_y \partial_z s_z \rangle. \end{aligned} \tag{3.26}$$

We also obtain a set of equations for the spin-wave amplitudes s_j to leading order:

$$\begin{aligned} \sigma_0 \partial_t s_y + \alpha \partial_t s_z &= \gamma J \partial_z^2 s_z - \gamma s_z H_k + \gamma\gamma_0 E_y \partial_z s_y, \\ \sigma_0 \partial_t s_z - \alpha \partial_t s_y &= -\gamma A \partial_z^2 s_y + \gamma s_y H_k - \gamma\gamma_0 E_y \partial_z s_z. \end{aligned} \tag{3.27}$$

The underlying assumption here is that the spin waves vary on a much shorter time scale than the magnetization texture, as is reasonable. Consider first the case with an electric field only along the $\hat{\mathbf{x}}$-direction of the film, such that $E_y = 0$. Remarkably, the above equations then become formally equivalent to the equations of motion for spin-waves and subsequent change in magnetization due to the torque from the spin-waves as occurring in both topological insulators [100] and ferromagnets with Dzyaloshinskii-Moryia interaction [102]. We may thus immediately conclude that there is a *spin-wave induced magnetoelectric torque* acting even homogeneous magnetization textures in multiferroic materials. This effect vanishes completely if one sets the magnetoelectric coupling γ_0 to zero. What is more, however, the present case appears to offer additional physics compared to the aforementioned scenarios: if we allow for an out-of-plane component for the electric field, $E_y \neq 0$, an extra term proportional to $\partial_z s_j$ and $\partial_z \delta m_j$ appear in Eqs. (3.26) and (3.27). This term influences the magnonic torque and offers an additional way to control it which differs from the influence of the in-plane electric field component. The influence of the new term $\propto E_y$ complicates the analytical solution, and so we choose to proceed via a numerical route in order to also investigate the influence of magnons on inhomogeneous spin-textures in multiferroics.

We are now in a position to determine how spin-waves interact with a domain wall texture, which thus also requires their interaction with the homogeneous part of the domains to be taken into account according to the above results. This is different from previous works on magnon-induced domain wall motion in ferromagnets [101], where no such homogeneous torque is present. We have thus solved the full LLG equation without any perturbative approximations where the initial profile at $t = 0$ consists of a magnetic domain wall center

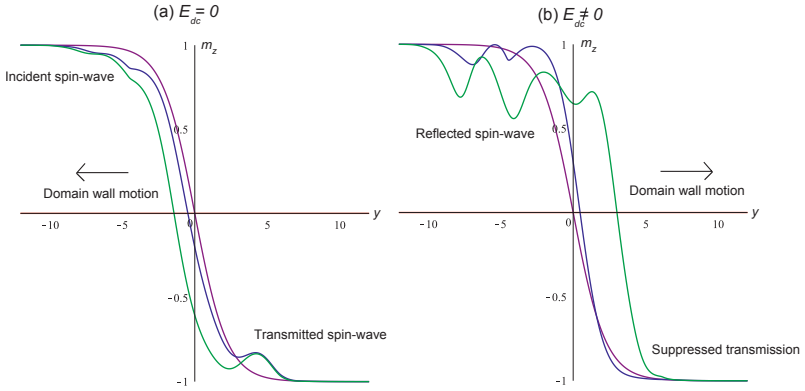

Figure 3.2: (Color online) Plot of spin-wave induced domain wall motion via a transverse AC electric field $E_{\rm ac}$. The normalized parameters used are $\omega = 0.75, K = 0.2, K_\perp = 0.01, E_{\rm ac}\gamma_0 = 5, \alpha = 0.01$. In (a), there is no gate voltage field $E_{\rm dc}$ and we present snapshots of the instantaneous domain wall profile at normalized times $t = 0$ (static profile, purple line), $t = 22$, and $t = 47$. In (b), we set $E_{\rm dc}\gamma_0 = 2$ and consider times $t = 0, 15, 21$.

around $z = 0$. Anti-reflection boundary conditions were implemented near the edges of the system in order to remove spin-wave backscattering, modelled by allowing the Gilbert damping α to rise rapidly very close to the edges. As a consistency check against previous works, we verified that spin-wave generation via an ac external magnetic field $\boldsymbol{B}(t)$, applied locally in a small region of one of the domains, induced motion in the opposite direction of the magnon flow.

Turning now to the present multiferroic system, we now demonstrate that the presence of the magnetoelectric coupling in the effective field offers a new result compared to previous work on spin-wave induced domain wall motion. Since a gradient in the magnetization couples to the electric field, one could envision that not only an ac magnetic field could drive spin-wave induced domain wall motion, but that the same could take place via an *ac electric field*. An important aspect of realizing such an effect is that the electric field would have to be applied in a region where there was a magnetization gradient, in effect not too deep inside the domains with fixed magnetization direction. To determine if electric-field induced domain wall motion via magnons is possible, we applied an ac electric field $\boldsymbol{E}(t)$ locally near the domain wall region and the result is shown in Fig. 3.2(a) (see figure caption for parameters used). As seen, the spin-waves emanating from this procedure indeed trigger domain wall motion and thus demonstrates the possibility to achiev electric control over magnon-induced magnetization texture transport. Remarkably, we find that even the direction of motion of the domain wall can be controlled by applying an additional constant gate-field: whereas the domain wall moves towards the spin-wave source without any such dc field, it moves away from the domain wall in its presence. This finding suggests that the magnetoelectric coupling alters the effective potential

felt by the spin-waves as they propagate through the domain wall, causing it to deviate from the reflectionless potential which is experienced by spin-waves in conventional ferromagnets with a belonging phase shift after passing through the wall [101]. In fact, the physical mechanism behind this effect is suggested by closer inspection of the curves in Fig. 3.2. When $E_{\rm dc} = 0$, the spin-waves pass through the domain wall and the wall moves toward the spin-wave source due to conservation of angular momentum. However, when $E_{\rm dc} \neq 0$, it is seen that no spin-waves emanate on the other side of the domain wall: instead, they are reflected and the domain wall moves *away* from the spin-wave source due to a transfer of linear momentum p. In this way, the direction of the domain wall motion is controllable by a gate voltage effect.

We have investigated the interaction between the spin-waves and the domain wall over a range of magnitudes for $E_{\rm dc}$ and find that it alters the amount of spin-wave reflection: Fig. 3.2(b) shows a scenario where the reflection is almost complete. An analytical description of this effect has proven elusive to us so far, due to the complicating factor of the spin-wave torque acting even on the homogeneous domains of the magnetization profile, although this is work in progress. We note that linear-momentum transfer of spin-waves to domain walls in ferromagnets have also been investigated in Ref. [105], and been shown to be possible at special resonance frequencies of the applied dc $\boldsymbol{B}$ field. In our treatment of the current-induced case, the dominant effect of the applied current is the spin-transfer torque effect described by the two last terms in the LLG equation and not the associated electric field along the structure which accompanies such a current, an approximation which should be better the higher conductivity the multiferroic is (in order to reduce the required voltage-drop, and thus field $\boldsymbol{E}$, that generates the current). Candidate materials for the effects predicted in this work include epitaxial iron garnet films, which when grown on (210) and (110) gadolinium-gallium garnet substrates generates a Neel component of the domain wall structure due to anisotropy and hence activates the magnetoelectric coupling [95]. We also note that very recently, domain wall motion via electric field was observed in a hybrid multiferroic consisting of ferromagnetic-ferroelectric heterostructure [106].

3.6.1 Conclusion

Concluding, we have here demonstrated that domain wall motion in multiferroic materials hosts a wealth of interesting effects which are distinct from conventional ferromagnets in terms of its response to spin-wave and current-induced torques, including the possibility to control the direction of the domain wall motion via a gate voltage, and hope that these findings may stimulate further investigations.

Chapter 4

Spin and charge supercurrents via spin-orbit coupling in S|F hybrids

4.1 Introduction

Current research in spintronics is attracting much attention, in large part due to the pivotal role that the quantum spin degree of freedom plays in an increasingly wide class of physical systems, ranging from ultracold atoms at the micro-Kelvin temperature scale to topological insulators at room-temperature. Spin transport in superconductors [109, 110, 111], which historically predated spin transport experiments in non-superconducting materials [112], have recently re-emerged as a potential avenue for enhancing and discovering new phenomena in spintronics. Recent results are encouraging, with experiments demonstrating not only infinite magnetoresistance [113], but also strongly enhanced quasiparticle spin lifetimes [114], spin relaxation lengths [115], spin Hall effects [116], and thermoelectric currents [117] compared with non-superconducting structures.

Creating and manipulating spin-flow is the central feature of superconducting spintronics [3, 6]. It is known that in the presence of magnetically inhomogeneous structures, such as multilayers or ferromagnets with intrinsic textures such as domain walls, spin-polarized Cooper pairs can emerge [13] which thus carry not only charge but also spin supercurrents [118, 28, 30, 119, 120]. Experimentally, it has been demonstrated [15, 21, 18, 17] that a dissipationless charge-current can flow through strong ferromagnets over distances far exceeding the penetration depth of conventional superconducting order into magnetic materials. This occurs precisely due to the creation of triplet Cooper pairs which are spin-polarized and thus insensitive to the pair-breaking effect of a magnetic Zeeman-field. In fact, triplet Cooper pairs were newly experimentally observed inside a conventional superconductor [121, 122]. In very recent developments, it has been shown that intrinsic spin-orbit coupling offers an alternative avenue for generating the long-range (LR) triplet component [123, 124]. In that case the appearance of the LR component depends on the relationship between

the spin-orbit coupling and the exchange field, with the LR triplet defined as having its spin aligned with the exchange field. This is in contrast to the short-ranged (SR) triplet component which has its spin perpendicular to the field, and is thus vulnerable to pair-breaking in the same way as conventional singlet Cooper pairs. As we will show below, these recent developments will have profound consequences for the generation of spin supercurrents in spintronics.

4.2 Quasiclassical theory

A powerful method to explore the physics of superconducting systems is to use Green functions. In general, the Green function representation is used in many areas of quantum mechanics. This method permits a formulation of the theory in a convenient form that provides a powerful tool to solve various problems in superconductivity. It can be used both for microscopic treatments and for quasiclassical treatments. Importantly, the Green function method can be used on systems with disorder and out-of-equilibrium. In its most general form, the Nambu-Gor'kov matrix Green function obeys the Gor'kov equations and is very complicated in general. Using the quasiclassical approximation leads to the Eilenberger equation [125] which can also be used in non-equilibrium situations. In the case where impurity scattering is the dominant energy scale in the problem (besides the Fermi energy), the Eilenberger equation reduce further to the Usadel equation [126]. Using the Keldysh technique, one can also describe dynamical (time-dependent) phenomena in the superconducting system.

4.2.1 Green function

In the theory of quantum many particle systems one uses the creation and annihilation operators, which create and annihilate particles at a time t and coordinate $\vec{r}$ with spin σ. With these operators one may define Green functions that are correlation functions playing the role of propagators. In the Keldysh formalism, the Green function is matrix:

$$\check{G} = \begin{pmatrix} \hat{G}^R & \hat{G}^K \\ 0 & \hat{G}^A \end{pmatrix} \tag{4.1}$$

and its elements are the retarded Green function:

$$\hat{G}^R_{\alpha\beta} = -i\theta(t_1 - t_2) \left\langle \left[\hat{\psi}_\alpha(\vec{r}_1, t_1), \hat{\psi}^\dagger_\beta(\vec{r}_2, t_2) \right]_+ \right\rangle, \tag{4.2}$$

advanced Green function:

$$\hat{G}^A_{\alpha\beta} = i\theta(t_2 - t_1) \left\langle \left[\hat{\psi}_\alpha(\vec{r}_1, t_1), \hat{\psi}^\dagger_\beta(\vec{r}_2, t_2) \right]_+ \right\rangle, \tag{4.3}$$

and Keldysh Green function:

$$\hat{G}^K_{\alpha\beta} = -i \left\langle \left[\hat{\psi}_\alpha(\vec{r}_1, t_1), \hat{\psi}^\dagger_\beta(\vec{r}_2, t_2) \right]_- \right\rangle \tag{4.4}$$

where $\langle ... \rangle$ denotes averaging with respect to quantum state of the system and $\theta(t_1 - t_2)$ is the Heaviside step function. By using these functions we can acquire information about transport in the system. The retarded Green function is a measure of the probability amplitude that an electron at a point r_1 at time t_1 will exist at a position r_2 at a later time t_2, where $t_2 > t_1$. The advanced Green function describes the opposite process. For a bulk homogeneous system, the Green functions depend only on the relative differences $t = t_1 - t_2$ and $\vec{r} = \vec{r}_1 - \vec{r}_2$. The anomalous Green functions are used to describe phenomena originating from superconductivity as it describes pair correlations that exist in the system. The expression for the anomalous Green functions read:

$$\hat{F}^R_{\alpha\beta} = -i\theta(t_1 - t_2) \left\langle \left[\hat{\psi}_\alpha(\vec{r}_1, t_1), \hat{\psi}_\beta(\vec{r}_2, t_2) \right]_+ \right\rangle \tag{4.5}$$

$$\hat{F}^A_{\alpha\beta} = i\theta(t_2 - t_1) \left\langle \left[\hat{\psi}_\alpha(\vec{r}_1, t_1), \hat{\psi}_\beta(\vec{r}_2, t_2) \right]_+ \right\rangle \tag{4.6}$$

$$\hat{F}^K_{\alpha\beta} = -i \left\langle \left[\hat{\psi}_\alpha(\vec{r}_1, t_1), \hat{\psi}_\beta(\vec{r}_2, t_2) \right]_- \right\rangle \tag{4.7}$$

4.2.2 Gorkov equation

The Green functions obey Gor'kovs equation of motion, which can be obtained from Heisenberg equation of motion for the field operators. The Gor'kov equation looks like:

$$\left\{ i\omega\hat{\boldsymbol{\tau}}_3 + \frac{\hbar}{2m}\frac{\partial^2}{d\boldsymbol{r}_1^2} + \mu + \widehat{\Delta}(\boldsymbol{r}_1) \right\} \widehat{G}(\boldsymbol{r}_1, \boldsymbol{r}_2) = \delta(\boldsymbol{r}_1 - \boldsymbol{r}_2)\,\hat{1} \tag{4.8}$$

This set of the equations must be completed with the self-consistency equation:

$$\Delta = -\frac{\lambda}{2} T \sum_\omega \mathrm{Tr}\,(\hat{\tau}_1 + i\hat{\tau}_2)\,\widehat{G} \tag{4.9}$$

where

$$\hat{\Delta} = \begin{pmatrix} 0 & \Delta \\ -\Delta^* & 0 \end{pmatrix} \tag{4.10}$$

$$\hat{G} = \begin{pmatrix} G & F \\ F^\dagger & -G \end{pmatrix} \tag{4.11}$$

and the solution of these equations must satisfy of the normalization condition:

$$G^2 + FF^\dagger = 1 \tag{4.12}$$

Although generally applicable, it is difficult to solve this set of equations exactly. For this reason, it is useful to make some simplifying assumptions which we describe below.

4.2.3 Eilenberger equation

The solution of the Gor'kov equation oscillates as a function of the relative coordinate $r_1 - r_2$ on scale of the Fermi wavelength λ_F. The characteristic lengths of a ballistic superconductor are $\xi_0 = \hbar v_F/\Delta$ and $\xi_T = \hbar v_F/2\pi T$, which are much larger that the Fermi wavelength λ_F. Quasiclassical equations can be obtained based on a gradient expansion of the Gor'kov equation using this small parameter λ_F. Integrating out the fast oscillations of the Gor'kov function, one obtains the quasiclassical Green function (see *e.g.* [127, 128, 6] for a review). This satisfies the equation:

$$\boldsymbol{v}_F \partial_R \hat{g} + [\omega\hat{\tau}_3 + \hat{\Delta} - \frac{1}{\tau}\langle\hat{g}\rangle, \hat{g}] = 0 \tag{4.13}$$

where τ is the impurity scattering time. The normalization conditions obeyed by the functions f and g are:

$$g^2(\boldsymbol{R}, \boldsymbol{n}) + f^\dagger(\boldsymbol{R}, \boldsymbol{n}) f(\boldsymbol{R}, \boldsymbol{n}) = 1 \tag{4.14}$$

$$f^\dagger(\boldsymbol{R}, \boldsymbol{n}) = f(\boldsymbol{R}, -\boldsymbol{n}), \tag{4.15}$$

where $\boldsymbol{n}$ is a unit vector in the direction of motion.

4.2.4 Usadel equation

In systems with strong elastic impurity scattering the motion of the quasiparticles is diffusive, and as result the direction of the momentum of the quasiparticles becomes random, but while retaining its magnitude p_F. It then becomes necessary to average the properties of the system over the direction of momentum. The system with the strong impurity scattering is system in which the impurity scattering rate $1/\tau$ is larger than any energy of the system (E, h, Δ) except the Fermi level. We may then expand the quasiclassical Green function to first order in momentum in spherical harmonics

$$\hat{g} = \hat{g}_s + \hat{\boldsymbol{p}}\hat{\boldsymbol{g}}_p \tag{4.16}$$

where $\hat{\boldsymbol{p}}$ is the unit vector in the direction of $\boldsymbol{p}$, and $\hat{g}_s$ and $\hat{\boldsymbol{g}}_p$ are independent of the direction of $\boldsymbol{p}$ Since the system properties should be close to isotropic in the diffusive limit, we may safely assume that $\hat{g}_p \ll \hat{g}_s$. One then arrives at the Usadel equation:

$$[\hat{\tau}^3 E + \hat{\Delta}, \hat{g}_s] - iD\partial_{\boldsymbol{R}}\hat{g}_s\partial_{\boldsymbol{R}}\hat{g}_s = 0 \tag{4.17}$$

The Usadel equation is a suitable starting point for addressing dirty superconducting systems. We have

$$\hat{g}_s = \begin{pmatrix} g_s^R & g_s^K \\ 0 & g_s^A \end{pmatrix} \tag{4.18}$$

The Usadel equation then gives separate equations for g_s^R and g_s^A, which describe the equilibrium properties of the system, and one kinetic equation for g_s^K which describes non-equilibrium properties (equation for the distribution function).

4.3 Spin-orbit coupling

In some crystal structures, there is no inversion centre present. This leads to a coupling between spin σ and momentum $\boldsymbol{p}$ of the electron known as anti-symmetric spin-orbit coupling. The simplest way to consider it is linearized interaction, that gives satisfactory results when comparing with the mesoscopic behaviour of many materials of interest.

To understand how the broken inversion symmetry influences the Hamiltonian, consider the electron which resides in an orbital around the nucleus. From the electron's viewpoint, it is the nucleus that moves around the electron, so the electron will experience a net magnetic field generated by the charged, moving nucleus. This occurs since a time-varying electric field induces a magnetic field according to Maxwell's equations. The net result is a coupling between the electric field generated by the gradient of the electric potential, $\nabla V(\boldsymbol{r}) = \hat{n}E_0$, where $\hat{n}$ is the unit vector along the gradient and E_0 is a constant, and the spin and momentum of the electron. Taking into account all aforesaid the single-particle Hamiltonian for this type of interaction in systems lacking inversion symmetry can be written in the form:

$$H = -\frac{\alpha'}{m} \cdot \boldsymbol{p} \cdot \boldsymbol{A} \tag{4.19}$$

where $\boldsymbol{p}$ is momentum of the electron, α' characterizes the strength of the SO coupling, and $\boldsymbol{A} = \hat{n} \times \vec{\sigma}$ is called spin-orbit field. $\boldsymbol{A}$ is an SU(2) vector field, i.e. has vector form in real space and 2×2 matrix form in spin space. In the general case, the spin-orbit coupling field $\boldsymbol{A}$ looks like:

$$\begin{aligned} \boldsymbol{A} =& \boldsymbol{i}\left(\alpha_x\sigma_x + \beta_x\sigma_y + \gamma_x\sigma_z\right) + \\ & \boldsymbol{j}\left(\alpha_y\sigma_x + \beta_y\sigma_y + \gamma_y\sigma_z\right) + \boldsymbol{k}\left(\alpha_z\sigma_x + \beta_z\sigma_y + \gamma_z\sigma_z\right) \end{aligned} \tag{4.20}$$

The α-coefficients are determined by the geometry of the system under consideration, for instance along which direction inversion symmetry is broken. Formally, we see that this type of spin-orbit (SO) coupling couples to momentum just like a magnetic vector potential. Therefore, to use spin-orbit coupling in equations and boundary conditions, we need only (to lowest order) replace partial derivatives by their gauge covariant counterparts:

$$\bigtriangledown\left(\bullet\right) \rightarrow \widetilde{\bigtriangledown} \equiv \bigtriangledown\left(\bullet\right) - i\left[\widehat{A}, \bullet\right] \tag{4.21}$$

where $\widehat{A} = \mathrm{diag}\left(\boldsymbol{A}, -\boldsymbol{A}^*\right)$ is 4×4 matrix in spin-Nambu space.

4.3.1 Rashba coupling

One example of this type of spin-orbit coupling is the so-called Rashba interaction. Such a coupling is characteristic for samples with structural inversion asymmetry which generally is present at interfaces, *e.g.* in thin-films or nanowires. For example, consider a thin film in the yz-plane. The direction of

broken inversion symmetry is then the x-axis. The Rashba coupling takes the form:

$$H_R = \alpha \left(p_z \sigma_y - p_y \sigma_z \right) \tag{4.22}$$

where α is the Rashba coefficient.

4.3.2 Dresselhaus coupling

Another example of antisymmetric (linear in momentum) spin-orbit coupling is Dresselhaus coupling, which is present in system with a noncentrosymmetric crystal structure such as GaAs. System with such crystal structure are characterised by a bulk inversion asymmetry. The Hamiltonian for such a system can take the form:

$$H_D = \beta \left(-p_y \sigma_y + p_z \sigma_z \right) \tag{4.23}$$

where β is Dresselhaus coefficient. We will in what follows mostly focus on the pure Rashba case, which can be achieved by depositing heavy thin normal metals near interfaces.

4.4 Boundary conditions

In order to obtain a solution for a partial differential equation we must use boundary conditions or initial conditions. Initial conditions defines unknown function at a given time. This type of condition is typically utilized when describing the behaviour of a non-stationary process. Boundary condition defines the sought function on boundaries of the investigated area. Because we consider only stationary processes in our system, we will use boundary conditions. We consider a system consisting of two known Green functions at the outer left and right layer (superconductors) and then seek the solution of the quasiclassical Green function in the layers sandwiched in between the outer ones.

4.4.1 Continuous boundary condition

The simplest boundary condition is the continuous one, which is to say that the interface is fully transparent so that the wave function and its derivatives are continuous at interface between two layers. Because our unknown function is a Green function, being the product of two field operators, the Green function and its derivative must also be continuous across the interface.

4.4.2 Kuprianov-Lukichev boundary condition

When the transmission probability is not unity due to an effective barrier potential in the region connecting two layers, as is certainly more realistic than the case considered in the previous subsection, more complicated boundary condition must be used. The most general boundary condition for systems with arbitrary interface transparency is Nazarov boundary condition [129]:

$$\frac{\gamma_1 d_1}{2} g_1 \partial_z g_1 |_{z=z_0} = \frac{[g_1, g_2]}{4 + T\left(\{g_1, g_2\} - 2\right)} |_{z=z_0} \tag{4.24}$$

In tunneling limit $T \to 0$, this boundary condition reduces to Kuprianov-Lukichev boundary condition [130]

$$\hat{g}_1 \nabla_z \hat{g}_1 = 2\zeta L \left[\hat{g}_1, \hat{g}_2\right] |_{z=z_0} \tag{4.25}$$

where ζ is a measure of the ratio of barrier resistance and bulk resistance of the material (see next subsection).

4.4.3 Spin-active interfaces

The boundary conditions used so far assume that there is no difference between electrons with spin-up and spin-down. But magnetic interface boundary condition was also derived by Millis [131]. The boundary condition for a spin-active interface in the tunnelling limit for a weakly polarized magnet takes the form:

$$2\zeta_l L_l \check{g}_l \partial_z \check{g}_l|_{z=z_0} = [\check{g}_l, \check{g}_r] + G_{MR}\left[\check{g}_l, \left\{\hat{A}, \check{g}_r\right\}\right] + iG_\phi^l \left[\check{g}_l, \hat{A}\right] |_{z=z_0} \tag{4.26}$$

$$2\zeta_r L_r \check{g}_r \partial_z \check{g}_r|_{z=z_0} = [\check{g}_l, \check{g}_r] + G_{MR}\left[\check{g}_r, \left\{\hat{A}, \check{g}_l\right\}\right] + iG_\phi^r \left[\check{g}_r, \hat{A}\right] |_{z=z_0} \tag{4.27}$$

Here, $\check{g}_l$ and $\check{g}_r$ are the Green functions on the left and right side spin-active interface. We see that first terms of the boundary condition in right hand side of equation are simply the Kuprianov-Lukichev boundary condition, which we considered before. The last two terms represent the influence of the magnetic interface on the spin-up and spin-down electrons: G_{MR} is a magnetoresistance term expressing that the transmission probability is different for the two spin species, while G_ϕ represents so-called spin-dependent phase shifts (discussed in chapter 2). The parameters in the boundary condition are: $L_{l/r}$ is length of the left/right layer, $\zeta_{l/r} = \frac{R_B}{R_{l/r}}$ represents the resistance of the interface, $R_{l/r}$ is the bulk resistance of the left/right materials, R_B is normal state resistance of the interface. $G_{MR} = \sum_n T_n P_n / \sum_2 2T_n$ and $G_\phi^{l/r} = -\sum_n d\phi_n^{l/r} / \sum_n T_n$, where T_n is transmission probability for channel n, P_n is spin polarization of transmission probability. We assume that $P_n \sim P \ll 1$, consequently $G_{MR} = P/2 \ll 0.5$. $d\phi_n^{l/r}$ is the spin-mixing angle and $G_\phi^{l/r}$ can take, in principle, arbitrary values. Finally, A is the interface matrix

$$\hat{A} = \begin{pmatrix} \boldsymbol{m}\cdot\boldsymbol{\sigma} & 0 \\ 0 & \boldsymbol{m}\cdot\boldsymbol{\sigma}^* \end{pmatrix} \tag{4.28}$$

where $\boldsymbol{m}$ is unit vector along magnetization of the ferromagnetic layer, σ is Pauli matrix vector in spin space [132, 133, 134].

4.5 Parametrization of the Green function

In order to facilitate the calculation, the Greeen function may be appropriately parametrized. Using the internal symmetries between elements of the Green function matrix in addition to its normalization property, we can strongly reduce the amount of independent variables. In quasiclassical theory of the superconductivity, the two most used parametrizations are the θ-parametrization and the Ricatti parametrization.

4.5.1 θ-parametrization

This parametrization is particularly suitable for *e.g.* a bulk superconductor. Restricting our attention for now to equilibrium, it is sufficient to consider the retarded Green function $\hat{g}^R$. In this particular case of a BCS superconductor, one has:

$$\hat{g}^R = \begin{pmatrix} g(X,E) & 0 & 0 & f(x,E) \\ 0 & g(x,E) & -f(x,E) & 0 \\ 0 & -f^*(X,-E) & -g^*(X,-E) & 0 \\ f^*(X,-E) & 0 & 0 & -g^*(X,-E) \end{pmatrix}. \tag{4.29}$$

The normalization condition then gives, for instance:

$$g(X,E)\cdot g(X,E) + f(X,E)\cdot f^*(X,-E) = 1 \tag{4.30}$$

One can introduce following parametrization:

$$g^R(X,E) = \cosh\theta(X,E) \tag{4.31}$$
$$f^R(X,E) = \sinh\theta(X,E)e^{i\chi(X,E)} \tag{4.32}$$

where the functions $\theta(X,E)$ and $\chi(X,E)$ are complex and have these symmetry properties:

$$\theta^*(X,-E) = -\theta(X,E) \tag{4.33}$$
$$\chi^*(X,-E) = \chi(X,E) \tag{4.34}$$

By substituting this parametrization into the equation for a bulk Green function, one finds

$$\theta_{BCS} = \arctan\left(\frac{|\Delta|}{\epsilon}\right) \tag{4.35}$$

where Δ is gap of the superconductor. Moreover, χ is superconducting phase.

4.5.2 Ricatti parametrization

The θ-parametrization has several-disadvantages: it becomes quite cumbersome in the presence of equal spin pairing correlations and it is numerically unstable in some parameter regimes. Instead, one may utilize the Ricatti parametrization [135] where one writes the Green function in the form:

$$\hat{g}^R = \begin{pmatrix} \underline{N}(1+\gamma\tilde{\gamma}) & 2\underline{N}\gamma \\ -2\tilde{\underline{N}}\tilde{\gamma} & -\tilde{\underline{N}}(1+\tilde{\gamma}\gamma) \end{pmatrix} \tag{4.36}$$

where normalization is guaranteed via the 2×2 normalization matrices: $\underline{N} = (\underline{1}-\underline{\gamma\tilde{\gamma}})^{-1}$ and $\tilde{\underline{N}} = (\underline{1}-\underline{\tilde{\gamma}\gamma})^{-1}$ and $\tilde{\gamma}$ - tilde conjugation means complex conjugation $i\to -i$ and a sign change of the quasiparticle energy $\varepsilon\to-\varepsilon$.

The new unknown function γ is a 2×2 matrix and is single-valued and bounded, making it much more numerically attractive than the θ-parametrization.

4.6 Ricatti-parametrized Usadel equation with spin-orbit coupling

We commented previously that the Usadel equation for a layer including spin-orbit coupling can be obtained by substituting:

$$\nabla(\bullet) \rightarrow \tilde{\nabla}(\bullet) \equiv \nabla(\bullet) - i\left[\check{A}, \bullet\right]. \tag{4.37}$$

Inserting the Ricatti parametrization, one obtains the following equation of motion:

$$\begin{aligned} D_F(\partial_k^2\gamma + 2(\partial_k\gamma)\tilde{N}\tilde{\gamma}(\partial_k\gamma)) &= -2i\varepsilon\gamma \\ &+ D_F\left[\underline{A}\underline{A}\gamma - \gamma\underline{A^*}\underline{A^*} + 2(\underline{A}\gamma + \gamma\underline{A^*})\tilde{N}(\underline{A^*} + \tilde{\gamma}\underline{A}\gamma)\right] \\ &+ 2iD_F\left[(\partial_k\gamma)\tilde{N}\left(\underline{A_k^*} + \tilde{\gamma}\underline{A_k}\gamma\right) + \left(\underline{A_k} + \gamma\underline{A_k^*}\tilde{\gamma}\right)N(\partial_k\gamma)\right] \end{aligned} \tag{4.38}$$

where k is direction in Cartesian coordinates along structure and $\underline{A} = (A_x, A_y, A_z)$. In a ferromagnetic layer, the Usadel equation in Ricatti parametrized form reads:

$$D_F\left(\partial_k^2\gamma + 2(\partial_k\gamma)\tilde{N}\tilde{\gamma}(\partial_k\gamma)\right) = -2i\varepsilon\gamma \tag{4.39}$$

$$-ih(\underline{\sigma}\gamma - \gamma\underline{\sigma^*}) \tag{4.40}$$

where $\underline{h} = (h_x, h_y, h_z)$ is the ferromagnetic exchange field along an arbitrary direction. $\underline{\sigma} = (\sigma_x, \sigma_y, \sigma_z)$ is the Pauli vector of the usual Pauli matrices.

The Kupriyanov-Lukichev boundary condition expressed via the Ricatti-matrices $\{\gamma, \tilde{\gamma}\}$ at an interface between a superconductor on the left side and a SO coupled layer on the right side becomes:

$$\partial_k\gamma_{SO} = \frac{1}{L_{SO}\zeta_{SO}}(1 - \gamma_{SO}\tilde{\gamma}_{S_L})N_{S_L}(\gamma_{SO} - \gamma_{S_L}) \tag{4.41}$$

$$+oA_k\gamma_{SO} + i\gamma_{SO}A_k^* \tag{4.42}$$

where γ_{S_L} is the Green function of the bulk left superconductor in Ricatti parametrization

$$\gamma_{S_L} = \frac{i\sigma_y \sinh(\theta)}{1 + \cosh(\theta)} e^{i\chi_L} \tag{4.43}$$

with $\theta = \operatorname{arctanh}(|\Delta|/\varepsilon)$ and

$$\tilde{\gamma}_{S_L} = -\frac{i\sigma_y \sinh(\theta)}{1 + \cosh(\theta)} e^{-i\chi_L}. \tag{4.44}$$

A boundary between a ferromagnet on the left side and a superconductor on the right side, taking into account the spin-dependent properties of the interface, has the form:

$$\partial_k \gamma_F = \frac{1}{L_F \zeta_F}[(1 - \gamma_F \tilde{\gamma_{S_R}})\, N_{S_R}\,(\gamma_{S_R} - \gamma_F) + \left(-G_{MR}\gamma_F c\,(\boldsymbol{m}\sigma^* + \boldsymbol{m}\sigma) + \frac{1}{2} i G_\phi \gamma_F\,(\boldsymbol{m}\sigma^* - \boldsymbol{m}\sigma)\right)] \tag{4.45}$$

where $c = \cosh(\theta)$. The Usadel equation and the boundary condition for $\tilde{\gamma}$ can be written easily by changing $i \to -i$ and $\varepsilon \to -\varepsilon$, and also $\gamma \to \tilde{\gamma}$, $\tilde{\gamma} \to \gamma$ in the equations above.

4.7 Weak proximity effect

The normal Green function is related to the propagation of single electrons in space and time. The anomalous Green function describes the propagation of the Cooper pairs, so in non-superconducting isolated material this anomalous Green function is equal to zero. If, however, the non-superconducting material is connected to a superconductor the proximity effect ensures that Cooper pairs will penetrate into the non-superconducting material, inducing a non-zero value of the anomalous Green function. Its magnitude depends upon, among other things, the strength of the barrier potential between the superconductor and the normal layer.

It is easier to make analytical progress with the Usadel equation if one assumes that the proximity effect is weak, which amounts to stating that the value of the anomalous Green function components are small, $|f| \ll 1$. This occurs for instance if the transmission probability between the layers is very low. Moreover, the inverse proximity effect (the weakening of the superconducting correlations inside the superconductor) can be neglected in this case, so that we can use the bulk Green function in the S layer.

In the weak proximity effect regime, one thus assumes that $|\gamma|_{ij} \ll 1$ and the Green function in the non-superconducting region takes the much simplified form:

$$\hat{g}^R \simeq \begin{pmatrix} \underline{1} & \underline{f} \\ -\underline{\tilde{f}} & -\underline{1} \end{pmatrix} \tag{4.46}$$

We have in effect neglected all terms of second order in γ and $\tilde{\gamma}$ in the Usadel equation.

4.8 Charge current

One of the interesting physical quantities in superconducting proximity structures is the presence of the supercurrent in the junction without voltage drop, thus an equilibrium effect. In the representation of the quasiclassical Green

functions, the charge-supercurrent is given by the general expression:

$$I_Q = \frac{N_0 eDA}{4} \int_{-\infty}^{\infty} d\varepsilon \mathrm{Tr}\left\{\hat{\rho}_3 \left[\check{g}\left(\partial_k \check{g}\right)\right]^K\right\} \tag{4.47}$$

where N_0 is the density of states at the Fermi level in the normal state, A is the cross section area, $\mathrm{Tr}\left\{\hat{B}\right\}$ is the trace of the matrix $\hat{B}$, and K means the Keldysh part of the matrix. We know that in equilibrium the Keldysh Green function can be represented by the retarded and advanced Green function:

$$\hat{g}^K = \left(\hat{g}^R - \hat{g}^A\right) \tanh\left(\frac{\beta\varepsilon}{2}\right) \tag{4.48}$$

There also exists a relation between the advanced and retarded Green function:

$$\hat{g}^A = -\left(\hat{\rho}_3 \hat{g}^R \hat{\rho}_3\right)^\dagger \tag{4.49}$$

One then obtains the following form of the supercurrent

$$\begin{aligned} I \sim \int_{-\infty}^{\infty} d\varepsilon [2\tanh(\frac{\beta\varepsilon}{2})\{f_s(\varepsilon)\partial f_s^*(-\varepsilon) - f_s(-\varepsilon)\partial f_s^*(\varepsilon) \\ -\boldsymbol{f}(\varepsilon)\partial \boldsymbol{f}^*(-\varepsilon) + \boldsymbol{f}(-\varepsilon)\partial \boldsymbol{f}^*(\varepsilon) + h.c.\}]. \end{aligned} \tag{4.50}$$

Taking into account symmetry properties of the Green function and Ricatti parametrization:

$$\begin{aligned} I \sim \int_{0}^{\infty} d\varepsilon [\tanh\left(\frac{\beta\varepsilon}{2}\right) \Re\{f_s(\varepsilon)\partial f_s^*(-\varepsilon) - f_s(-\varepsilon)\partial f_s^*(\varepsilon) - \\ \boldsymbol{f}(\varepsilon)\partial \boldsymbol{f}^*(-\varepsilon) + \boldsymbol{f}(-\varepsilon)\partial \boldsymbol{f}^*(\varepsilon)\}] \end{aligned} \tag{4.51}$$

where f_s is the singlet anomalous Green function:

$$f_s = \frac{f_{\uparrow\downarrow} - f_{\downarrow\uparrow}}{2} \tag{4.52}$$

and $\boldsymbol{f}$ is the vector of the triplet anomalous Green function:

$$\boldsymbol{f} = \left(\frac{f_{\downarrow\downarrow} - f_{\uparrow\uparrow}}{2}, -i\frac{f_{\downarrow\downarrow} + f_{\uparrow\uparrow}}{2}, \frac{f_{\uparrow\downarrow} - f_{\downarrow\uparrow}}{2}\right) \tag{4.53}$$

4.8.1 Long-range and short-range current

The penetration depth of superconducting correlations in a ferromagnetic layer is typically $\sim \xi = \sqrt{\frac{D}{\varepsilon + |\boldsymbol{h}|}}$, where $\boldsymbol{h}$ is exchange field of the layer. For a normal metal $\boldsymbol{h} = 0$, and for small ε the anomalous Green function will penetrate a long distance, limited in practice by inelastic scattering. It is actually possible for superconducting correlations to extend an equally long distant as in the S|N

case in a ferromagnet. This happens if one creates triplet correlations where both electrons have their spins aligned with the magnetization direction. If the magnetization points along the z-axis, the $f_{\uparrow\uparrow}$ and $f_{\downarrow\downarrow}$ pairs are then long-ranged.

Generalizing, the components of $\boldsymbol{f}$ parallel with the exchange field are short-ranged, and components that are perpendicular to the exchange field are called long-range components. As for the supercurrent, we know that charge current has a contribution from all the anomalous Green function components, both singlet and triplets, and so the supercurrent can also become long-ranged if components $\boldsymbol{f} \perp \boldsymbol{h}$ exist.

4.9 Spin-current

If triplet Cooper pairs, carrying spin, are present there can also exist a net superflow of spin besides the charge current. Singlet Cooper pairs have zero total spin and cannot contribute to spin transport. One may derive an expression for the spin supercurrent in quasiclassical theory. The polarization component of the spin supercurrent along the unit vector $\boldsymbol{n}$ reads:

$$I_s(\boldsymbol{n}) = \int_{-\infty}^{\infty} d\varepsilon \mathrm{Tr}\left\{\hat{\rho}_3 \hat{R}(\boldsymbol{n})\left(\check{g}\partial\check{g}\right)^K\right\} \tag{4.54}$$

where matrix $\hat{R}$ defines the direction of the polarization current:

$$\hat{R} = n_x \begin{pmatrix} \sigma_x & 0 \\ 0 & \sigma_x \end{pmatrix} + n_y \begin{pmatrix} \sigma_y & 0 \\ 0 & \sigma_y^* \end{pmatrix} + n_z \begin{pmatrix} \sigma_z & 0 \\ 0 & \sigma_z \end{pmatrix}. \tag{4.55}$$

One can also write out explicitly the polarization components of the spin supercurrent in the weak proximity effect [136]:

$$I_s^x \propto \int_0^{\infty} d\varepsilon \tanh(\frac{\beta\varepsilon}{2}) 2\Re[\{-(f_{\uparrow\uparrow}+f_{\downarrow\downarrow})\partial(\tilde{f}_{\uparrow\downarrow}+\tilde{f}_{\downarrow\uparrow}) - (f_{\uparrow\downarrow}+f_{\downarrow\uparrow})\partial(\tilde{f}_{\uparrow\uparrow}+\tilde{f}_{\downarrow\downarrow})\} - \{\tilde{...}\}] \tag{4.56}$$

$$I_s^y \propto \int_0^{\infty} d\varepsilon \tanh(\frac{\beta\varepsilon}{2}) 2\Im[\{(f_{\uparrow\uparrow}-f_{\downarrow\downarrow})\partial(\tilde{f}_{\uparrow\downarrow}+\tilde{f}_{\downarrow\uparrow}) - (f_{\uparrow\downarrow}+f_{\downarrow\uparrow})\partial(\tilde{f}_{\uparrow\uparrow}-\tilde{f}_{\downarrow\downarrow})\} + \{\tilde{...}\}] \tag{4.57}$$

$$I_s^z \propto \int_0^{\infty} d\varepsilon \tanh(\frac{\beta\varepsilon}{2}) 4\Re[\{-f_{\uparrow\uparrow}\partial\tilde{f}_{\uparrow\uparrow} + f_{\downarrow\downarrow}\partial\tilde{f}_{\downarrow\downarrow}) - \{\tilde{...}\}] \tag{4.58}$$

It is seen that all of these equations are independent on the singlet anomalous Green function f_s, as is physically reasonable.

4.10 Results

We now present the research results from **Paper III**.

To date, structures with magnetic inhomogeneities such as multiple magnetic layers have been required to create long-ranged spin-supercurrents [15, 21, 18, 17]. This can be experimentally challenging for several reasons, primarily because it is far from trivial to exert control over the individual layers of magnetically inhomogeneous structures, and can be complicated yet further if the magnetic layer has intrinsic texture (such as the spiral order in Ho). Here we will show that it is possible to create a spin-polarized supercurrent using just *one single homogeneous magnetic element*, which eliminates the experimental complexities and heralds a new era for harnessing the dissipationless spin-flow of superconductors in spintronics. In addition to this reduction of complexity in producing a spin supercurrent, we show that this spin supercurrent does not decay even in the presence of spin-flip processes, *e.g.* via magnetic impurities or spin-orbit impurity scattering. This spin-flip immunity is fundamentally different from spin currents in non-superconducting structures which remain polarized for the duration of the spin relaxation time. Finally, we show that the spin polarization components of the supercurrent respond qualitatively differently to a change in the superconducting phase difference ϕ. The surprising consequence of this is that the dissipationless charge flow and spin flow can be tuned separately. In particular, both the magnitude and the polarization direction of the spin flow is controlled via the superconducting phase, offering an entirely new way to control spin transport.

Consider the thin-film heterostructure depicted in Fig. 4.1, which shows a Josephson junction of conventional s-wave superconductive sources with normal and ferromagnetic elements typically utilized in proximity effect experiments.

We will now show that a long-ranged spin supercurrent is sustained in the junction even when only a single homogeneous ferromagnet is used. The key to achieving this is to deposit a very thin layer of a heavy normal metal such as gold or platinum at the superconducting interfaces. Recent experiments in the context of magnetization switching have shown that such interfaces will produce strong Rashba spin-orbit coupling due to the high atomic number of the metal and the interfacially broken inversion symmetry [139]. The magnetic element consists of a ferromagnetic alloy which has both an in- and out-of-plane component, achievable by using *e.g.* PdNi or CuNi, which can both feature out-of-plane magnetocrystalline anisotropy in thin-films [137, 138]. It is clear, therefore, that no magnetic inhomogeneities are required, and the ferromagnet does not need to feature any intrinsic spin-orbit coupling. This is in contrast to previous works that have considered long-ranged currents in either magnetically textured junctions (see *e.g.* Refs. [24, 118, 140]) or intrinsically spin-orbit coupled ferromagnets [123, 141, 142], where spin is not a conserved quantity, with several magnetic layers [124]. In our setup, only a single homogeneous

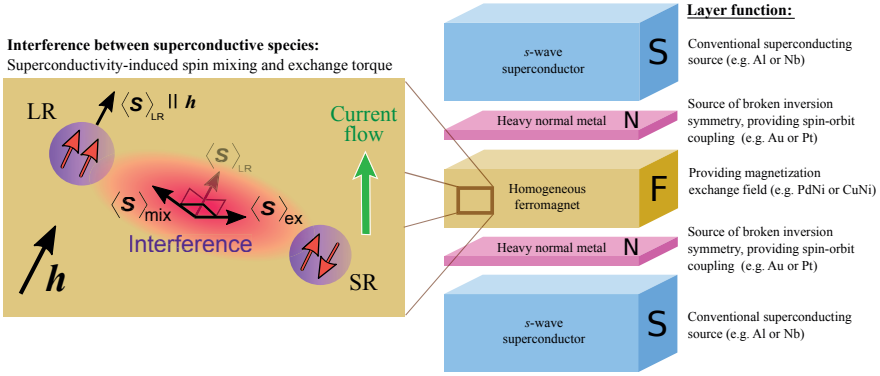

Figure 4.1: Schematic illustration of the thin-film superconducting junction within which a spin supercurrent is generated, which does not decay even in the presence of spin-flip scattering. There are two experimentally feasible ways to construct the thin-film such that the spin supercurrent appears. In the case where only Rashba spin-orbit coupling is present in the heavy-metal layers, the homogeneous ferromagnet is chosen to have out-of-plane magnetocrystalline anisotropy, such as the commonly available PdNi or CuNi [137, 138]. In combination with the shape-anisotropy of the thin-film geometry, the exchange field within the ferromagnet will then have both an in-plane and out-of-plane component. If both Rashba and Dresselhaus spin-orbit coupling is present in the normal layers, *e.g.* by using a two-dimensional electron gas such as GaAs, the ferromagnet only needs an in-plane component. In both cases, this induces an interference effect between the long-ranged and short-ranged Cooper pairs, which results in a spin mixing term and an exchange torque, which acts on the magnetization and is present even in the absence of a charge current.

ferromagnet is required because the heavy normal metals supply the spin-orbit coupling, significantly reducing the previously required level of junction complexity in order to host a spin supercurrent. Furthermore, as an alternative experimental scenario, it is possible to use a ferromagnet with a purely in-plane exchange field by employing normal layers that contain both Rashba and Dresselhaus coupling. Examples include crystals that lack an inversion structure and two-dimensional electron gases such as gallium arsenide. In this case, the singlet-triplet conversion is greatly enhanced [143, 144], resulting in stronger supercurrents (see Fig. 4.2).

The spin-supercurrent $\boldsymbol{I}_S$ may be computed via the quasiclassical Green function $\check{g}$ according to the formula [28]:

$$\boldsymbol{I}_S = I_{S_0} \int_{-\infty}^{\infty} \mathrm{d}\varepsilon \mathrm{Tr}\{\hat{\rho}_3 \hat{\boldsymbol{\tau}} (\check{g}\partial_z \check{g})^K\}. \tag{4.59}$$

Here, we have defined $\hat{\boldsymbol{\tau}} = \mathrm{diag}(\boldsymbol{m}\cdot\boldsymbol{\sigma}, \boldsymbol{m}\cdot\boldsymbol{\sigma}^*)$, where $\boldsymbol{m}$ is the desired polarization-direction of the spin supercurrent and $\boldsymbol{\sigma}$ is the vector of Pauli matrices, ε denotes the quasiparticle energy and K the Keldysh component of the Green function. $I_{S_0} = N_0 \hbar D A \Delta / 8 L_F$, where N_0 is the normal-state density of states at the Fermi level, D the diffusion constant and A the interfacial contact area. The integral in Eq. (4.59) is dimensionless since the energies have been normalized to the bulk superconducting gap Δ and lengths normalized to the ferromagnet length L_F. The matrix $\hat{\rho}_3 = \mathrm{diag}(1, 1, -1, -1)$. To find the Keldysh component we use the equilibrium relation

$$(\check{g}\partial_z \check{g})^K = [\hat{g}^R \partial_z \hat{g}^R + (\hat{\rho}_3 \hat{g}^R \partial_z \hat{g}^R \hat{\rho}_3)^\dagger] \tanh(\beta\varepsilon/2), \tag{4.60}$$

where R and A denote the retarded and advanced components of $\check{g}$ respectively and $\beta = 1/k_B T$ is the inverse temperature with k_B being the Boltzmann constant. We find $\hat{g}^R$ by solving the Usadel equation for the system shown in Fig. 4.1 both analytically in the weak proximity effect and numerically in the full proximity effect regime using the NOTUR supercomputer cluster (Kongull); see Appendix B for further details. We can then compute the spin supercurrent from Eq. (4.59), and the charge supercurrent $\boldsymbol{I}_Q$ can be obtained from the same formula by removing $\hat{\boldsymbol{\tau}}$ from the trace and taking $I_{S_0} \to 2I_{S_0} e/\hbar = I_{Q_0}$, where e is the electronic charge.

The critical charge supercurrent $\boldsymbol{I}_Q^C$, obtained at a phase-difference[150] $\phi = \pi/2$, is shown in Fig. 4.2a, demonstrating that it becomes long-ranged even if there is no magnetic inhomogeneity and only a single ferromagnet is used. The physical mechanism behind this effect is that the spin-orbit coupling present in the thin, heavy normal metal layers rotates the triplet Cooper pairs due to an anisotropic spin relaxation [124]. The spin-orbit coupling is described by α and β, being respectively the Rashba and Dresselhaus coefficients. These are normalised to the superconducting gap Δ and length of normal metal L_N in such a way that with a niobium superconductor of gap $\Delta \approx 3$ meV, $\alpha = 0.5/L_N$

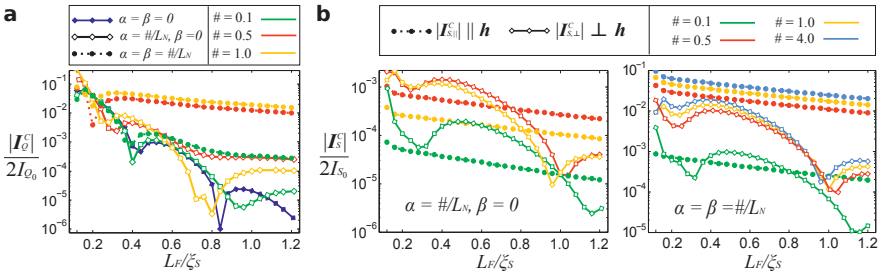

Figure 4.2: The magnitude of the critical charge current $\boldsymbol{I}_Q^C$ (**a**) and the components of the critical spin current $\boldsymbol{I}_S^C$ (**b**) in the ferromagnet as a function of the length of the layer L_F is shown on a logarithmic scale. In the presence of spin-orbit coupling, the current becomes long-ranged as it makes a transition from an exponential decay with superimposed oscillations to a much slower decay with respect to L_F. For long ferromagnetic junctions, it is clear that the charge current is almost entirely due to the long-range component. Including both Rashba and Dresselhaus coupling results in a substantial enhancement of the critical charge currents compared with pure Rashba coupling. We assume bulk superconductivity in the superconductors, an exchange field $\boldsymbol{h} = 50\Delta(0, \cos\theta, \sin\theta)$ with $\theta = 0.3\pi$, and a normal metal layer length of $L_N/\xi_S = 0.08$. The spin-orbit coupling parameters are normalised to the superconducting gap and length of normal metal in such a way that with a niobium superconductor with gap $\Delta \approx 3$ meV and coherence length $\xi_S = 25$ nm, $\alpha = 0.5/L_N$ corresponds to Rashba coupling of the order 3×10^{-12} eV m.

corresponds to a Rashba parameter of the order 3×10^{-12} eV m. It is clear from Fig. 4.2a that the critical current decays rapidly in the absence of spin-orbit coupling ($\alpha = \beta = 0$), and that this decay is strongly suppressed by the inclusion of spin-orbit coupling (note the log scale).

To model the ferromagnet, we assumed an exchange field $\boldsymbol{h} = h(0, \cos\theta, \sin\theta)$, with a strength $h/\Delta = 50$ and a canting of $\theta = 0.3\pi$ between the in- and out-of-plane components. The supercurrent exists for any orientation of the exchange field $\theta \in (0, \pi/2)$ and we will later discuss the precise dependence on the canting angle θ. We choose $\tilde{G}_{MR} = 0.2$ for the normalized interfacial magnetoresistance term and $\tilde{G}_\theta = 1$ for the interfacial scattering phase shift on both sides [134]. In this case, and with a typical superconducting coherence length of $\xi_S = 25$ nm, the LR component dominates for ferromagnets of length L_F greater than ~ 10 nm, causing the critical current $\boldsymbol{I}_Q^C$ to decay slowly despite the presence of an exchange field $h \gg \Delta$, remaining orders of magnitude larger than the SR component for increasingly long ferromagnets. In this scheme, the associated current densities for a sample length $L_F \sim 10$ nm will be of the order $|\boldsymbol{j}_Q^C| \sim 10^3$ A/cm^2 without spin-orbit coupling, and 1-2 orders higher with its inclusion (see Appendix B for details). This corresponds well with charge current densities measured in the experiment of Ref. [145], which also used a CuNi alloy as the ferromagnet. For stronger exchange fields, the LR component will

dominate for even shorter junctions, but the overall current magnitude will be suppressed. The supercurrent carried by the LR Cooper pairs can be significantly enhanced by including Dresselhaus coupling, as can be seen from the dotted line in Fig. 4.2a, in which case the achievable critical charge current is much greater than with Rashba coupling alone.

We now turn to the spin supercurrent. Without spin-orbit coupling, no spin-current flows in the junction since there exists no mechanism for converting from the SR to the LR component. In order to demonstrate the physical origin of the dissipationless spin current and its different polarization components, it is useful to first decompose the triplet correlations in the system into their long-ranged and short-ranged contribution: $\boldsymbol{f} = \boldsymbol{f}_{\rm LR} + \boldsymbol{f}_{\rm SR}$. To take an explicit example, consider the case with pure Rashba coupling and an exchange field $\boldsymbol{h} = (0, h_y, h_z)$. In that case, we may write the general expressions:

$$\begin{aligned} \boldsymbol{f}_{\rm LR} &= (f_x, -fh_z/h, fh_y/h), \\ \boldsymbol{f}_{\rm SR} &= (0, f'h_y, f'h_z)/h, \end{aligned} \tag{4.61}$$

so that $\boldsymbol{f}_{\rm LR} \cdot \boldsymbol{h} = 0$ when $\boldsymbol{f}_{\rm SR} \parallel \boldsymbol{h}$. Now, the spin expectation vector of a triplet Cooper pair is obtained by $\langle \boldsymbol{S} \rangle = i\boldsymbol{f} \times \boldsymbol{f}^*$. Inserting the long-ranged state $\boldsymbol{f}_{\rm LR}$, one obtains $\langle \boldsymbol{S} \rangle_{\rm LR} = 2{\rm Im}\{f^* f_x\}(h_y \hat{\boldsymbol{y}} + h_z \hat{\boldsymbol{z}})/h$. This means that the spin of the LR Cooper pairs points along the exchange field, as expected. Similarly, one finds that $\langle \boldsymbol{S} \rangle_{\rm SR} = 0$ for the SR Cooper pairs. However, there exists an additional contribution. The spin expectation vector of the total proximity-induced superconducting state may be written

$$\begin{aligned} \langle \boldsymbol{S} \rangle_{\rm tot} &= ß(\boldsymbol{f}_{\rm LR} + \boldsymbol{f}_{\rm SR}) \times (\boldsymbol{f}^*_{\rm LR} + \boldsymbol{f}^*_{\rm SR}) \\ &= \langle \boldsymbol{S} \rangle_{\rm LR} + \langle \boldsymbol{S} \rangle_{\rm SR} + (ß\boldsymbol{f}_{\rm LR} \times \boldsymbol{f}^*_{\rm SR} + {\rm h.c.}). \end{aligned} \tag{4.62}$$

It follows that there exists a novel *interference term* $\langle \boldsymbol{S} \rangle_{\rm int} = ß\boldsymbol{f}_{\rm LR} \times \boldsymbol{f}^*_{\rm SR} + {\rm h.c.}$ between the LR and SR Cooper pairs, which upon insertion of $\boldsymbol{f}_{\rm LR}$ and $\boldsymbol{f}_{\rm SR}$ is found to contain two terms, $\langle \boldsymbol{S} \rangle_{\rm int} = \langle \boldsymbol{S} \rangle_{\rm ex} + \langle \boldsymbol{S} \rangle_{\rm mix}$, where

$$\langle \boldsymbol{S} \rangle_{\rm ex} = 2{\rm Im}\{(f')^* f\}\hat{\boldsymbol{x}}, \tag{4.63}$$

$$\langle \boldsymbol{S} \rangle_{\rm mix} = 2{\rm Im}\{(f')^* f_x\}(\hat{\boldsymbol{y}} h_z - \hat{\boldsymbol{z}} h_y)/h. \tag{4.64}$$

The *exchange* term $\langle \boldsymbol{S} \rangle_{\rm ex}$ of Eq. (4.63) is independent of the direction of the field $\boldsymbol{h}$. In contrast, the second term changes its spin-polarization direction as $\boldsymbol{h}$ is altered. We will explain the physical meaning of each of these terms in the section below. Before doing so, we briefly discuss how the spin-polarization of the critical current depends on the length of the ferromagnet. This is shown for the critical spin supercurrent in Fig. 4.2b, displaying both the component parallel with the exchange field $\boldsymbol{I}^C_{S,\parallel} \parallel \boldsymbol{h}$ and the magnitude of the perpendicular components, $|\boldsymbol{I}^C_{S,\perp}| = (\boldsymbol{I}^2_{S,\rm ex} + \boldsymbol{I}^2_{S,\rm mix})^{1/2}$. It is clear that the polarization of the spin supercurrent along the magnetization direction has a qualitatively different behavior with the length of the system compared with the polarization perpendicular to the exchange field, which oscillates within its typical exponential decay. The reason for this is that the perpendicular component appears due

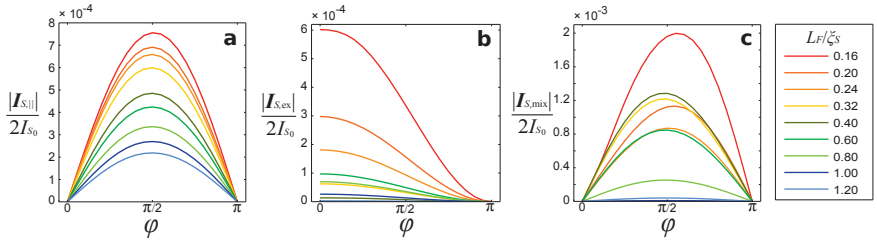

Figure 4.3: The dependence of the spin supercurrent on the phase difference ϕ between the superconductors of the junction illustrated in Fig. 4.1 is shown. The component parallel to the exchange field $\boldsymbol{h} = h(0, \cos\theta, \sin\theta)$ is given in **a**, the component perpendicular to the field polarized in the x-direction in **b** and the perpendicular component along $(0, \sin(\theta), -\cos(\theta))$ in **c**. The spin-orbit coupling is chosen to be of pure Rashba type with $\alpha = 0.5/L_N$, and the parameters used are otherwise the same as in Fig. **4.2**. Results with both Rashba and Dresselhaus coupling are qualitatively similar, with consistently higher current magnitudes.

to the interference between the LR and SR Cooper pairs, and thus is limited by the penetration depth of the short-ranged superconducting correlations. Note that there is a non-monotonic relationship between the maximal supercurrents and the magnitude of the spin-orbit coupling, in the same way as there exists a non-monotonic relation between the density of states and spin-orbit coupling in a ferromagnet [143].

By analyzing the dependence of the spin supercurrent on the phase difference between the superconductors, it becomes clear that there is another fundamental difference between the parallel and perpendicular components. We will prove that *(i)* there exists a superconductivity-mediated exchange interaction in the system, even in the absence of any charge supercurrent and magnetic inhomogeneities, which acts with a torque on the magnetic order parameter and that *(ii)* both the magnitude and polarization direction of the spin supercurrent can be tuned via the superconducting phase difference.

The phase-dependence of the component of the spin supercurrent parallel to the exchange field, $\boldsymbol{I}_{S,\parallel}$, is plotted in Fig. 4.3a, and shows the expected first-order sinusoidal dependence on the phase difference ϕ. This is physically reasonable since this component of the spin supercurrent is carried exclusively by the LR Cooper pairs which are polarized along the exchange field. When considering the perpendicular components of the spin supercurrent, however, the analysis in the preceding section showed that there exists two contributions $\boldsymbol{I}_{S,\mathrm{ex}}$ and $\boldsymbol{I}_{S,\mathrm{mix}}$ that originate from a novel interference between the LR and SR Cooper pairs. In order to unveil the physical meaning of these terms, we plot the variation of these with ϕ in Figs. 4.3b and *c*. It is seen that these polarization components exhibit a fundamentally different response to the superconducting phase difference: $\boldsymbol{I}_{S,\mathrm{ex}}$ is invariant under time-reversal $\phi \to (-\phi)$ and finite even

in the absence of any phase difference $\phi = 0$ where no net charge current flows, whereas $\boldsymbol{I}_{S,\mathrm{mix}}$ is antisymmetric under time-reversal. In effect, there exists a pure spin supercurrent flow without any charge current contamination in the system, even in the *absence* of any magnetic inhomogeneities or half-metallicity. Based on these observations, we offer the following interpretation of our findings. The polarization component of the spin supercurrent $\parallel \boldsymbol{h}$ is understood simply as the polarization of the LR Cooper pairs that carry the long-ranged charge current and thus obeys the same type of current-phase relation as the charge current itself, vanishing both at $\phi = 0$ and $\phi = \pi$. The interference between the SR and LR Cooper pairs now provides the spin supercurrent components with distinct physical origins. The term $\boldsymbol{I}_{S,\mathrm{mix}}$ represents the spin polarization that arises due to interference between LR and SR pairs carrying charge current, and is thus qualitatively similar to the charge current itself, with a $\sin\phi$ profile. In contrast, the term $\boldsymbol{I}_{S,\mathrm{ex}}$ represents something more exotic: *it is a superconductivity-induced exchange torque acting on the magnetization, which is present even in the absence of any charge current.* From its numerical evaluation, we find that it may be written as $|\boldsymbol{I}_{S,\mathrm{ex}}| = \mathcal{J}_1 + \mathcal{J}_2 \cos\phi$, with the constants $\{\mathcal{J}_1, \mathcal{J}_2\}$ depending on system-specific details such as the strength of the exchange field h, the length of the ferromagnet L_F and the strength of spin-orbit coupling α. This means that the exchange spin supercurrent is invariant under $\phi \to (-\phi)$ and that it has a term that is independent of the superconducting phase difference. The physical origin of this term is the following. Due to the proximity effect, both LR and SR superconducting correlations are induced in the ferromagnet in the presence of the inversion-symmetry breaking normal metal layers. The interference between these correlations create, according to Eq. (4.63), a net spin moment. Since this moment is misaligned with $\boldsymbol{h}$, it acts with a torque on the magnetic order parameter $\boldsymbol{h}$, attempting to rotate it so that the net torque vanishes. The presence of magnetic anisotropy in the system could be expected to attempt to counteract this torque. Importantly, this effect is present even without any net charge flow ($\phi = 0$) and exists with just a single, homogeneous ferromagnet. This is evident by comparing Figs. 4.3b and *c*, where the different polarization components of the spin supercurrent are plotted against the superconducting phase difference. This result shows that the magnitude and polarization direction of a dissipationless spin current can both be tuned exclusively via the superconducting phase difference, which is a surprising finding that offers a new way to control spin flow. The superconducting phase difference may itself be set in the conventional way via current-bias, or by applying an external magnetic flux in a loop-geometry[146]. We underline that this superconductivity-mediated exchange interaction is very different from exchange interactions in *e.g.* conventional spin-valves with two ferromagnets, where a deviation from the parallel or antiparallel configuration produces a net equilibrium spin current that tries to align the magnetizations via a spin-torque [147, 148, 149]. In contrast, here such a torque exists even with a single, homogeneous ferromagnet due to a unique interference effect between long-ranged and short-ranged triplet Cooper pairs.

It is clear from Fig. 4.3 that the maximal spin-current polarized along the ex-

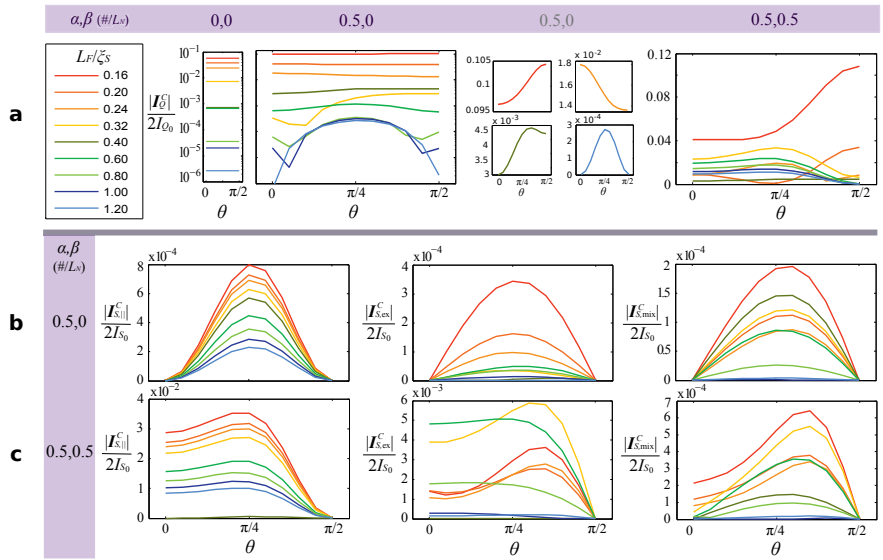

Figure 4.4: The effect of the canting angle θ between the in- and out-of-plane components of the exchange field $\boldsymbol{h} = 50\Delta(0, \cos\theta, \sin\theta)$ is shown for the charge current in **a**, and for the spin-current components in **b** and **c**. Without spin-orbit coupling, the charge current does not depend on the magnetization orientation, and there is zero spin-current. With Rashba spin-orbit coupling we see a significant enhancement in the charge current, with a canting profile stabilising towards a sinusoidal maximum at $\theta = \pi/4$ for increasingly large ferromagnets as the long-ranged triplet component become dominant. The parallel component of the spin-current monotonically decreases with ferromagnet length, while the perpendicular components are sensitive to the 0-π transition in the ground state. The inclusion of Dresselhaus spin-orbit coupling yields a dramatic increase in both charge- and spin-current, and it is evident that purely in-plane magnetization ($\theta = 0$) is sufficient to generate the long-range component.

change field is achieved around $\phi = \pi/2$, corresponding well with the definition of the critical spin current[150], taken to be the spin polarization of the critical charge current. These simulations were run for a canting angle of $\theta = 0.3\pi$, and since this angle is in large part determined by material and geometry constraints it is instructive to consider the effect of the canting angle on the results. This is shown in Fig. 4.4, and demonstrates that the long-ranged component of the charge current favours a canting angle of $\theta = \pi/4$, visible at longer sample lengths. It is also clear that the inclusion of both Rashba and Dresselhaus spin-orbit coupling allows the long-ranged component to be generated with a purely in-plane exchange field [123, 124].

Upon analysing the spin supercurrent in the above structure, one discovers an additional feature which pertains uniquely to currents generated by superconductors. Unlike conventional spin-polarized currents, we find that a spin *super*current does not decay due to either spin-orbit impurity scattering or spin-flip scattering caused by magnetic impurities. This result has immediate implications for the usage of superconductors in spintronics, since it means that spin-flow created in this way is preserved even in regions with strong spin-flip scattering. We emphasize that this stands in complete contrast to conventional spin-currents, which have a decay length dictated by the amount of spin-flip scattering present.

Here we provide a general proof that the spin supercurrent is conserved both in normal metal and ferromagnetic systems, even in the presence of spin-orbit impurity scattering and isotropic spin-flip scattering from magnetic impurities. Using the relation between the Keldysh, retarded and advanced components of the Green function which holds at equilibrium (Eq. (4.60)), the Usadel equation may be written

$$D\partial_z \mathrm{Tr}\{\hat{\rho}_3\hat{\tau}_j\hat{g}^R\partial_z\hat{g}^R\} + ß\mathrm{Tr}\{\hat{\rho}_3\hat{\tau}_j[\hat{\Sigma},\hat{g}^R]\} = 0, \tag{4.65}$$

where we have defined $\hat{\Sigma} = \varepsilon\hat{\rho}_3 + \hat{M} - \hat{\sigma}_{\mathrm{so}} - \hat{\sigma}_{\mathrm{sf}}$, and $\hat{\tau}_j$ denotes the polarization-direction of interest. $\hat{M} = \mathrm{diag}(\boldsymbol{h}\cdot\boldsymbol{\sigma}, (\boldsymbol{h}\cdot\boldsymbol{\sigma})^*)$, where $\boldsymbol{h}$ is the magnetization exchange field, whereas the spin-orbit and magnetic impurity spin-flip self-energies have been included via the terms $\hat{\sigma}_{\mathrm{so}}$ and $\hat{\sigma}_{\mathrm{sf}}$ (see Appendix B for details). For any matrix $\hat{X}$ one has $\mathrm{Tr}\{\hat{X}^\dagger\} = (\mathrm{Tr}\{\hat{X}\})^*$, from which it follows that if $\mathrm{Tr}\{\hat{\rho}_3\hat{\tau}_j[\hat{\Sigma},\hat{g}^R]\} = 0$, then the spin supercurrent will be conserved. By inserting the most general expression for the quasiclassical retarded Green function $\hat{g}^R$, direct evaluation shows that the above trace is always zero in the absence of an exchange field despite the presence of spin-flip scattering. In the presence of an exchange field, the same holds for the spin supercurrent $\boldsymbol{I}_{S,\|}$ polarized along the magnetization and remains true even if the exchange field is spatially inhomogeneous. It is remarkable that a spin supercurrent, controllable via the superconducting phase difference, has no decay even if both spin-orbit and magnetic impurities are present in the sample.

4.10.1 Conclusions

In conclusion, we have shown three major results: (i) a long-ranged spin supercurrent can be created without any magnetic inhomogeneities, (ii) the spin polarization components of the current can be tuned separately via the superconducting phase difference, and (iii) spin supercurrents created in this way do not decay even in the presence of spin-flip scattering, i.e. they display spin-flip immunity. We have proposed that this may be observed experimentally in a Josephson junction consisting of conventional s-wave superconductors (*e.g.* Al or Nb) with very thin layers of a heavy normal metal (*e.g.* Pt or Au) and a single homogeneous ferromagnet with magnetocrystalline out-of-plane anisotropy (*e.g.* PdNi or CuNi). We would like to note that no "exotic" materials, such as unconventional superconductors or noncentrosymmetric ferromagnets, are required – the effects predicted in this work appear by combining conventional superconductors and metals, which should make experimental verification of our results readily achievable. Our results confirm the significant and immediate advantage that superconductors offer spintronics.

Bibliography

[1] I. Zutic, J. Fabian, and S. Das Sarma, Rev. Mod. Phys. **76**, 323 (2004).

[2] A. V. Chumak, V. I. Vasyuchka, A. A. Serga, and B. Hillebrands, Nat. Phys. **11**, 453 (2015).

[3] J. Linder and J. W. A. Robinson, Nat. Phys. **11**, 307 (2015).

[4] A. I. Buzdin, Rev. Mod. Phys. **77**, 935 (2005).

[5] F. S. Bergeret, A. F. Volkov, and K. B. Efetov, Rev. Mod. Phys. **77**, 1321 (2005).

[6] Eschrig, M. Rep. Prog. Phys. **78**, 10 (2015).

[7] V. L. Ginzburg, Zh. Eksp. Teor. Fiz. **31**, 202 (1956) [Sov. Phys. JETP 4, 153 (1957)]; L. N. Bulaevski and V. L. Ginzburg, Sov. Phys. JETP **18**, 530 (1964).

[8] S. S. Saxena *et al.* ., Nature (London) **406**, 587 (2000).

[9] D. Aoki, A. Huxley, E. Ressouche, D. Braithwaite, J. Flouquet, J.-P. Brison, E. Lhotel, and C. Paulsen, Nature (London) **413**, 613 (2001).

[10] N. T. Huy, A. Gasparini, D. de Nijs, Y. Huang, J. Klaasse, T. Gortenmulder, A. de Visser, A. Hamann, T. Görlach, and H. Löhneysen, Phys. Rev. Lett. **99**, 067006 (2007).

[11] M. Eschrig, T. Löfwander, T. Champel, J. C. Cuevas, J. Kopu, and G. Schön, J. Low Temp. Phys. **147**, 457 (2007).

[12] Y. Tanaka, A. A. Golubov, S. Kashiwaya, and M. Ueda, Phys. Rev. Lett. **99**, 037005 (2007).

[13] F. S. Bergeret, A. F. Volkov, and K. B. Efetov, Phys. Rev. Lett. **86**, 4096 (2001).

[14] M. Eschrig, J. Kopu, J. C. Cuevas, Gerd Schön, Phys. Rev. Lett. **90**, 137003 (2003)

[15] R. S. Keizer, S. T. B. Goennenwein, T. M. Klapwijk, G. Miao, G. Xiao, and A. Gupta, Nature (London) **439**, 825 (2006).

[16] H. Z. Arham, T. S. Khaire, R. Loloee, W. P. Pratt, Jr., and N. O. Birge, Phys. Rev. B **80**, 174515 (2009).

[17] J.W. A. Robinson, J. D. S. Witt, and M. G. Blamire, Science **329**, 59 (2010).

[18] Trupti S. Khaire, Mazin A. Khasawneh, W. P. Pratt, Jr., and Norman O. Birge Phys. Rev. Lett. **104**, 137002 (2010).

[19] I. Sosnin, H. Cho, V. T. Petrashov, and A. F. Volkov, Phys. Rev. Lett. **96**, 157002 (2006).

[20] J .W. A. Robinson, F. Chiodi, G. B. Halasz, M. Egilmez, M. G. Blamire, Scientific Reports **2**, 699 (2012).

[21] M. S. Anwar, F. Czeschka, M. Hesselberth, M. Porcu, and J. Aarts, Phys. Rev. B **82**, 100501(R) (2010).

[22] D. Sprungmann, K. Westerholt, H. Zabel, M. Weides, and H. Kohlstedt, Phys. Rev. B **82**, 060505(R) (2010).

[23] Z. Pajovic, M. Bozovic, Z. Radovic, J. Cayssol, and A. Buzdin, Phys. Rev. B **74**, 184509 (2006).

[24] M. Houzet and A. I. Buzdin, Phys. Rev. B **76**, 060504(R) (2007).

[25] K. Halterman, P. H. Barsic, O. T. Valls, Phys. Rev Lett. **99**, 127002 (2007)

[26] M. Eschrig and T. Löfwander, Nature Physics **4**, 138-143 (2008)

[27] P. M. R. Brydon, D. Manske, M. Sigrist, J. Phys. Soc. Jpn. **77**, 103714 (2008); P. M. R. Brydon, W. Chen, Y. Asano, D. Manske Phys. Rev. B **88**, 054509 (2013)

[28] M. Alidoust, J. Linder, G. Rashedi, T. Yokoyama, A. Sudbø, Phys. Rev. B **81**, 014512 (2010)

[29] T. E. Baker, A. Richie-Halford, A. Bill, arXiv:1310.6580.

[30] Z. Shomali, M. Zareyan, W. Belzig, New Journal of Physics **13** (2011) 083033

[31] A. Cottet, Phys. Rev. Lett. **107**, 177001 (2011)

[32] A. I. Buzdin, A. S. MelâĂŹnikov, and N. G. Pugach, Phys. Rev. B **83**, 144515 (2011).

[33] I. B. Sperstad, J. Linder, A. Sudbø, Phys. Rev. B **78**, 104509 (2008)

[34] Ya. V. Fominov, A. F. Volkov, and K. B. Efetov, Phys. Rev. B **75**, 104509 (2007).

[35] G. Annunziata, M. Cuoco, C. Noce, A. Romano, and P. Gentile, Phys. Rev. B **80**, 012503 (2009); G. Annunziata *et al.* , Phys. Rev. B **83**, 060508(R) (2011).

[36] K. Halterman, O. T. Valls, P. H. Barsic, Phys. Rev. B **77**, 174511 (2008)

[37] F. Romeo and R. Citro, Phys. Rev. Lett. **111**, 226801 (2013)

[38] R. Grein, M. Eschrig, G. Metalidis, and G. Schön, Phys. Rev. Lett. **102**, 227005 (2009).

[39] Y. Asano, Y. Sawa, Y. Tanaka, and A. A. Golubov, Phys. Rev. B **76**, 224525 (2007)

[40] T. Yokoyama, Y. Tanaka, and A. A. Golubov, Phys. Rev. B **75**, 134510 (2007).

[41] J. Linder, M. Cuoco, A. Sudbø, Phys. Rev. B **81**, 174526 (2010)

[42] G. B. Halasz, J. W. A. Robinson, J. F. Annett, and M. G. Blamire, Phys. Rev. B **79**, 224505 (2009)

[43] I. V. Bobkova and A. M. Bobkov Phys. Rev. B **82**, 024515 (2010)

[44] I. V. Bobkova and A. M. Bobkov Phys. Rev. Lett. **108**, 197002 (2012)

[45] I. Margaris, V. Paltoglou, and N. Flytzanis, J. Phys.: Condens. Matter **22**, 445701 (2010)

[46] F. Sebastian Bergeret, A. Verso, and Anatoly F. Volkov, Phys. Rev. B **86**, 060506(R) (2012).

[47] J.-F. Liu and K. S. Chan, Phys. Rev. B **82**, 184533 (2010).

[48] J. C. Slonczewski, J. Magn. Magn. Mater. **159**, L1 (1996).

[49] L. Berger, Phys. Rev. B **54**, 9353 (1996).

[50] C. W. J. Beenakker and H. van Houten Phys. Rev. Lett. **66**, 3056 (1991); C. W. J. Beenakker Phys. Rev. Lett. **67**, 3836 (1991).

[51] X. Waintal and P. W. Brouwer, Phys. Rev. B **65**, 054407 (2002).

[52] E. Zhao and J. A. Sauls, Phys. Rev. B **78**, 174511 (2008)

[53] F. Konschelle and A. Buzdin, Phys. Rev. Lett. **102**, 017001 (2009).

[54] V. Braude and Ya. M. Blanter, Phys. Rev. Lett. **100**, 207001 (2008)

[55] J. Linder and T. Yokoyama, Phys. Rev. B **83**, 012501 (2011).

[56] P. D. Sacramento, L. C. Fernandes Silva, G. S. Nunes, M. A. N. Araujo, and V. R. Vieira, Phys. Rev. B **83**, 054403 (2011); P. D. Sacramento and M. A. N. Araujo, European Physical Journal B **76**, 251 (2010).

[57] S. Teber, C. Holmqvist, and M. FogelstrÃűm, Phys. Rev. B **81**, 174503 (2010); C. Holmqvist, S. Teber, and M. Fogelström, Phys. Rev. B **83**, 104521 (2011).

[58] L. D. Landau and E. M. Lifshitz, Pys. Z. Sowjet. **8**, 153 (1935)

[59] T. L. Gilbert, IEEE Trans. Magn. **40**, 3443 (2004)

[60] H. Sickinger, A. Lipman, M. Weides, R. G. Mints, H. Kohlstedt, D. Koelle, R. Kleiner, and E. Goldobin, Phys. Rev. Lett. **109**, 107002 (2012).

[61] A. Buzdin, Phys. Rev. B **72**, 100501(R) (2005).

[62] V. Braude and Yu. V. Nazarov, Phys. Rev. Lett. **98**, 077003 (2007)

[63] A. Buzdin, Phys. Rev. Lett. **101**, 107005 (2008)

[64] J. Linder, Y. Tanaka, T. Yokoyama, A. Sudbø, N. Nagaosa Phys. Rev. B **81**, 184525 (2010)

[65] J.-F. Liu and K. S. Chan, Phys. Rev. B **82**, 125305 (2010).

[66] E. Goldobin, D. Koelle, R. Kleiner, and R. G. Mints, Phys. Rev. Lett. **107**, 227001 (2011).

[67] M. Alidoust and J. Linder, Phys. Rev. B **87**, 060503(R) (2013)

[68] D. M. Heim, N. G. Pugach, M. Yu. Kupriyanov, E. Goldobin, D. Koelle, and R. Kleiner J. Phys.: Condens. Matter **25**, 215701 (2013)

[69] D. Feinberg and C. Balseiro, arXiv:1405.6889.

[70] T. Ortlepp, Ariando, O. Mielke, C. J. M. Verwijs, K. F. K. Foo, H. Rogalla, F. H. Uhlmann, and H. Hilgenkamp, Science **312**, 1495 (2006).

[71] A. K. Feofanov, V. A. Oboznov, V. V. Bolï£¡ginov, J. Lisenfeld, S. Poletto, V. V. Ryazanov, A. N. Rossolenko, M. Khabipov, D. Balashov, A. B. Zorin, P. N. Dmitriev, V. P. Koshelets, and A. V. Ustinov, Nat. Phys. **6**, 593 (2010).

[72] P.G. Gennes Superconductivity of Metals and Alloys (Benjamin, New York, 1966)

[73] G. E. Blonder, M. Tinkham, and T. M. Klapwijk, Phys. Rev. B **25**, 4515 (1982)

[74] N. N. Bogoliubov, JETP USSR **34**, 58 (1958); N. N. Bogoliubov, Nuovo Cimento **7**, 794-805 (1958); J. G. Valatin, Nuovo Cimento **7** , 843-857 (1958).

[75] V. V. Ryazanov, V. A. Oboznov, A. Yu. Rusanov, A. V. Veretennikov, A. A. Golubov, and J. Aarts Phys. Rev. Lett. **86**, 2427 (2001)

[76] A. A. Golubov, M. Yu. Kupriyanov, and E. Ilichev, Rev. Mod. Phys. **76**, 411 (2004

[77] F. Bergeret, A. Volkov, and K. Efetov, Phys. Rev. B **68**, 064513 (2003).

[78] N. L. Schryer and L. R.Walker, J. Appl. Phys. **45**, 5406 (1974).

[79] Y. Tserkovnyak, A. Brataas, G. E. W. Bauer, and B. I. Halperin, Rev. Mod. Phys. **77**, 1375 (2005).

[80] A. A. Jara, C. Safranski, I. N. Krivorotov, C.-T. Wu, A. N. Malmi-Kakkada, O. T. Valls, K. Halterman, arXiv:1404.2304

[81] C. Ishii, Progr. of Theor. Phys., 1970, **44**, 1525.

[82] 1 G. Lawes, G. Srinivasan, J. Phys. D: Appl. Phys. **44**, 243001 (2011).

[83] A. P. PyatakovÂăand A. K. Zvezdin, Phys.ÂăUsp.Âă**55**,Âă557 (2012).

[84] L. W. Martin *et al.* , J. Phys: Condens. Matter **20** 434220 (2008); H. Bea *et al.* , J. Phys: Condens. Matter **20** 434221 (2008).

[85] H. Schmid, Ferroelectrics **162**,Âă317 (1994).

[86] M. Gajek *et al.* , Nature Mater. **6**, 296 (2007).

[87] M. Bides *et al.* , Nature Mater. **7**, 425 (2008).

[88] G. Catalan *et al.* , Rev. Mod. Phys. **84**, 119 (2012).

[89] J. F. Scott, Science **315**, 954 (2007).

[90] L. D. Landau and E. M. Lifshitz. *Electrodynamics of Continuous Media* (Oxford: Pergamon Press, 1984).

[91] G. A. Smolenskii and I. Chupis, Sov. Phys. Usp. **25**, 475 (1982).

[92] V. G. BarâĂŹyakhtar V G, V. A. LâĂŹvov, and D. A. Yablonskii, JETP Lett. **37**Âă673 (1983).

[93] Y. J. Choic *et al.* , Phys Rev Lett. **105**, 097201 (2010).

[94] Y. H. Chu *et al.* , Nature Mater. **7**, 478 (2008)

[95] A. S. Logginov *et al.* , Appl. Phys. Lett. **93**, 182510 (2008)

[96] N. Lei *et al.* , Nature Comm. **4**, 1378 (2013).

[97] M. Mostovoy, Phys. Rev. Lett. **96**, 067601 (2006).

[98] F. Kagawa *et al.* , Phys. Rev. Lett. **102**, 057604 (2009).

[99] H.-B. Chen, Y.-H. Liu, Y.-Q. Li, J. Appl. Phys. **115**, 133913 (2014)

[100] J. Linder, Phys. Rev. B **90**, 041412(R) (2014).

[101] P. Yan, X. S. Wang, and X. R. Wang, Phys. Rev. Lett. **107**, 177207 (2011).

[102] A. Manchon *et al.* , arXiv:1401.0883.

[103] G. Tatara and H. Kohno, Phys. Rev. Lett. **92**, 086601 (2004); S. Zhang and Z. Li, Phys. Rev. Lett. **93**, 127204 (2004); A. Thiaville, Y. Nakatani, J. Miltat, and Y. Suzuki, Europhys. Lett. **69**, 990 (2005).

[104] J. Shibata *et al.* , J. Phys. D: Appl. Phys. **44**, 384004 (2011); J. Grollier *et al.* , C. R. Physique **12**, 399 (2011).

[105] J.-S. Kim *et al.* , Phys. Rev. B **85**, 174428 (2012).

[106] B. Van de Wiele *et al.* , Appl. Phys. Lett. **104**, 012401 (2014).

[107] V. G. BarâĂŹyakhtar,V. A. LâĂŹvov,D. A. Yablonskii JETP Lett. **37**, 673 (1983)

[108] A. Sparavigna, A. Strigazzi, A. Zvezdin, Phys. Rev. B **50**, 2953 (1994)

[109] Tedrow, P. M. & Meservey, R. Phys. Rev. Lett. **26**, 192-195 (1971).

[110] Tedrow, P. M. & Meservey, R. Phys. Rev. B **7**, 318-326 (1973).

[111] Tedrow, P. M. & Meservey, R. Phys. Rep. **238**, 173-243 (1994).

[112] Johnson, M. & Silsbee, R. H. Phys. Rev. Lett. **55**, 1790-1793 (1985).

[113] Li, B. *et al.* . Phys. Rev. Lett. **110**, 097001 (2013).

[114] Yang, H., Yang, S-H., Takahashi, S., Maekawa, S. & Parkin, S. S. P. Nature Mater. **9**, 586-593 (2010).

[115] Quay, C. H. L., Chevallier, D., Bena, C. & Aprili, M. Nature Phys. **9**, 84-88 (2013).

[116] Wakamura, T., Omori, Y., Niimi, Y., Takahashi, S., Fujimaki, A., Maekawa, S. & Otani, Y. Nature Materials **14**, 675âĂŞ678 (2015).

[117] Kolenda, S., Wolf, M. J., Beckmann, D. *arXiv:1509.05568.*

[118] Grein, R., Eschrig, M., Metalidis, G. & Schön, G. Phys. Rev. Lett. **102**, 227005 (2009).

[119] Moor, A., Volkov, A. & Efetov, K. B. *arXiv: 1508.06665.*

[120] Halterman, K., Valls, O. T. & Wu, C.-T. *arxiv::1506.05480.*

[121] Di Bernardo, A., Diesch, S., Gu, Y., Linder, J., Divitini, G., Ducato, C., Scheer, E., Blamire, M. G. & Robinson, J. W. A. Nat. Commun. **6**, 8053 (2015).

[122] Kalcheim, Y., Millo. O, Di Bernardo, A., Pal, A. & Robinson, J. W. A. Phys. Rev. B **92**, 060501(R) (2015).

[123] Bergeret, F.S. and Tokatly, I.V. Phys. Rev. Lett. **110**, 117003 (2013).

[124] Bergeret, F.S. and Tokatly, I.V. Phys. Rev. B **89**, 134517 (2014).

[125] G. Eilenberger, Z. Phys. **214**, 195 (1968).

[126] K. Usadel, Phys. Rev. Lett. **25**, 507 (1970)

[127] W. Belzig, F.K. Wilhelm, G. Schon, C. Bruder, and A.D. Zaikin, Superlattices and Microstructures **25**, 1251-1288 (1999)

[128] V. Chandrasekhar. *Proximity-Coupled Systems: Quasiclassical Theory of Superconductivity*. Book chapter in "Superconductivity"', edited by K. H. Benneman and J. B. Ketterson (2004).

[129] Y. Nazarov, Superlattices and Microstructures, **25**, 1221 (1999)

[130] M. Yu. Kupriyanov and V. F. Lukichev, JETP **67**, 1163 (1988).

[131] A. Millis, D. Rainer, and J. A. Sauls, Phys. Rev. B **38**, 4504 (1988).

[132] J. Linder, T. Yokoyama, and A. Sudbø, Phys. Rev. B **79**, 054523 (2009

[133] A. Cottet, D. Huertas-Hernando, W. Belzig, and Y. Nazarov, Phys. Rev. B **80**, 184511 (2009)

[134] Eschrig, M., Cottet. A, Belzig, W. & Linder, J. New J. Phys. **17**, 083037 (2015).

[135] N. Schopohl and K. Maki, Phys. Rev. B **52**, 490 (1995); A. Konstandin, J. Kopu, and M. Eschrig, Phys. Rev. B **72**, 140501(R) (2005)

[136] I. Gomperud and J. Linder, Phys. Rev. B **92**, 035416 (2015)

[137] Khaire, T. S., Pratt, W. P. Jr. & Birge, N. O. Phys. Rev. B **79**, 094523 (2009).

[138] Ruotolo, A., Bell. C. & Blamire, M. G. J. Appl. Phys. **96**, 512 (2004).

[139] Miron, I. M. *et al.* . Nature **476**, 189 (2011).

[140] Volkov, A. F. & Efetov, K. B. Phys. Rev. B **81**, 144522 (2010).

[141] Arjoranta, J. & Heikkilä, T. *arXiv:1507.02320*.

[142] Alidoust, M. and Halterman, K. New J. Phys. **17**, 033001 (2015).

[143] Jacobsen, S.H. and Linder, J. Giant triplet proximity effect in π-biased Josephson Junctions with spin-orbit coupling. Phys. Rev. B **92**, 024501 (2015).

[144] Jacobsen, S.H., Ouassou, J.A. and Linder, J. Phys. Rev. B **92**, 024510 (2015).

[145] Oboznov, V. A., Bol'ginov, V. V., Feofanov, A. K., Ryazanov, V. V. & Buzdin, A. I. Phys. Rev. Lett. **96**, 197003 (2006).

[146] Le Sueur, H. *et al.* . Phys. Rev. Lett. **100**, 197002 (2008).

[147] Slonczewski, J.C. J. Magn. Magn. Mater. **126**, 374 (1993).

[148] Slonczewski, J. C. J. Magn. Magn. Mater. **159**, L1-L7 (1996).

[149] Nogueira, S. F. & Benneman. Europhys. Lett. **67**, 620 (2004).

[150] In Figs. 4.2 and 4.4 we show the critical charge current and spin currents, where we take the critical currents to occur at a phase difference of $\phi = \pi/2$ between the superconductors. It is known that the critical charge current may deviate slightly from this phase difference near the transition points between the 0 and π ground states since higher order harmonics may become increasingly significant when the current is very small, but this is negligible for our scheme and the implications are discussed further in-text.

Appendix A

Calculation of Andreev levels

In order to solve the Bogoliubov-de Gennes equations we write the wavefunction in plane-wave form $\Psi(y) = e^{iky}\psi$. The wave vectors of electron- and hole-like quasiparticles inside the superconductor are:

$$k_S = \sqrt{2m(\mu \pm \sqrt{E^2 - \Delta^2})} \tag{A.1}$$

while for the homogeneous ferromagnets we have:

$$k_f^\sigma = \sqrt{2m(\mu \pm E + \sigma h)}. \tag{A.2}$$

Finally, in the domain wall case we find:

$$k_{DW}^\sigma = \sqrt{2m(\mu \pm E) + a^2 + \sigma 2\sqrt{2ma^2(\mu \pm E) + m^2h^2}} \tag{A.3}$$

where $a = \frac{\pi}{2l_{DW}}$. Defining $\alpha = \frac{h}{2\mu}$ and $\eta = \frac{a^2}{2m(\mu \pm E)}$, we find in the limit $E \ll \mu$ that $\eta = \frac{a^2}{k_F^2}$ and the wave vector for the domain wall becomes:

$$k_{DW}^\sigma = \sqrt{2m(\mu \pm E) + \eta^2 + \sigma 2\sqrt{\eta^2 + \alpha^2}} \tag{A.4}$$

During our calculation we use the approximation that $E \ll \mu$ and that α and η are small. For $\alpha \gg \eta$, the wavevector for the quasiparticles in the domain wall ferromagnet can be simplified further:

$$k_{DW}^\sigma = 2m\mu(1 + \sigma\alpha) \tag{A.5}$$

while for for $\alpha \ll \eta$

$$k_{DW}^\sigma = 2m\mu(1 + \sigma\eta) \tag{A.6}$$

For a ferromagnetic layer with arbitrary orientation of magnetization, we have:

$$\Psi_F(y) = \sum_{p=\pm} \left(t_{e,\uparrow}^\pm \begin{pmatrix} \cos(\frac{\theta}{2}) \\ \sin(\frac{\theta}{2})e^{i\chi} \\ 0 \\ 0 \end{pmatrix} e^{\pm ik_F^\uparrow y} + t_{e,\downarrow}^\pm \begin{pmatrix} -\sin(\frac{\theta}{2})e^{-i\chi} \\ \cos(\frac{\theta}{2}) \\ 0 \\ 0 \end{pmatrix} e^{\pm ik_F^\downarrow y} + \right. \tag{A.7}$$

$$\left. t_{h,\uparrow}^\pm \begin{pmatrix} 0 \\ 0 \\ \cos(\frac{\theta}{2}) \\ \sin(\frac{\theta}{2})e^{-i\chi} \end{pmatrix} e^{\pm(-ik_F^\uparrow y)} + t_{h,\downarrow}^\pm \begin{pmatrix} 0 \\ 0 \\ -\sin(\frac{\theta}{2})e^{i\chi} \\ \cos(\frac{\theta}{2}) \end{pmatrix} e^{\pm(-ik_F^\downarrow y)} \right)$$

where θ is the angle between the magnetization and the z-axis, χ is the angle between the magnetization and the x-axis in the $x-y$-plane, $\pm$ corresponds to the direction of the moving particles. For the domain wall layer, we first perform a unitary transformation $\hat{\mathcal{U}}$ of the Hamiltonian to remove the explicit spatial dependence of the exchange field due to the domain wall texture. This is achieved by rotating the system so that the local spin quantization axis is aligned with the local magnetization direction. Starting out with $\hat{H}\psi = \varepsilon\psi$, we rewrite it to $\hat{H}_{\mathrm{rot}}\Psi = \varepsilon\Psi$ where $\hat{H}_{\mathrm{rot}} = \hat{\mathcal{U}}\hat{H}\hat{\mathcal{U}}^{-1}$ and $\Psi = \hat{\mathcal{U}}\psi$. The new wavefunction Ψ may then be expressed as follows:

$$\Psi_{DW}(y) = \sum_{p=\pm}\left(t^{\pm}_{e,\uparrow}\begin{pmatrix}\phi_1^{\uparrow}\\ \pm\phi_2^{\uparrow}\\ 0\\ 0\end{pmatrix} e^{\pm ik^{\uparrow}_{DW}y} + t^{\pm}_{e,\downarrow}\begin{pmatrix}\pm\phi_2^{\downarrow}\\ \phi_1^{\downarrow}\\ 0\\ 0\end{pmatrix} e^{\pm ik^{\downarrow}_{DW}y} + \right. \tag{A.8}$$
$$\left. t^{\pm}_{h,\uparrow}\begin{pmatrix}0\\ 0\\ \phi_1^{\uparrow}\\ \pm\phi_2^{\uparrow}\end{pmatrix} e^{\pm(-ik^{\uparrow}_{DW}y)} + t^{\pm}_{h,\downarrow}\begin{pmatrix}0\\ 0\\ \pm\phi_2^{\downarrow}\\ \phi_1^{\downarrow}\end{pmatrix} e^{\pm(-ik^{\downarrow}_{DW}y)}\right)$$

where

$$\phi_1^{\sigma} = \sigma(\alpha + \eta^2\sqrt{\alpha^2+\sigma\eta^2}), \phi_2^{\sigma} = \sigma i\eta\sqrt{1+\eta^2+2\sqrt{\alpha^2+\eta^2}} \tag{A.9}$$

We may then revert to the original wavefunction ψ, which enters the boundary conditions, by doing the inverse transformation $\psi = \hat{U}^{-1}\Psi$. The coefficients $t^{\pm}_{e(h),\sigma}$ are associated with right- left-going ($\pm$) ELQ and HLQ propagating throught the ferromagnetic layers. The spin index $\sigma = \uparrow$ or $\downarrow$.
The wave functions must satisfy the boundary conditions of 1) continuity of the wave function at the boundary:

$$(\Psi_k - \Psi_l)|_{y=L_i} = 0 \tag{A.10}$$

and 2) discontinuity of the first derivative at the boundary:

$$\partial(\Psi_k - \Psi_l)|_{y=L_i} = \frac{2m}{\hbar}U\Psi|_{y=L_i} \tag{A.11}$$

where $L_i = 0$, L_1, L_2, L_3, indexes k and l are associated with corresponding index of the wave functions. We have defined the normalized barrier strength $Z = 2mU/(\hbar k_F)$. Note that in the domain wall case, extra terms $\partial_y\hat{\mathcal{U}}$ arise in the boundary conditions due to the unitary transformation of the wavefunction. From the boundary conditions, we can obtain all the scattering coefficients and set up a homogeneous system of linear equations, demanding that the determinant is equal to zero in order to have a non-trivial solution. The resulting characteristic equation is then solved for the energy which represents the Andreev Bound State (ABS). In the ABS-energy for the trilayered structure, the coefficient B before the anomalous $\sin\gamma$ term satisfies

$$B \propto \sin 2\beta_1 \sin 2\beta_2 \sin 2\beta_3 \tag{A.12}$$

whereas for the structure with spin-active interfaces

$$B \propto \sin^2 \beta. \tag{A.13}$$

In the scenario with a domain wall ferromagnet, there exists is no managable expression for B in the general case.

Appendix B

Methods for quasiclassical theory

We solved the Riccati parameterised Usadel equation with spin-orbit coupling [144] iteratively between the layers, using the NOTUR supercomputer facilities (Kongull). In the normal metal, spin-orbit coupling is included in the Usadel equation Eq. (4.65) by replacing the derivative with its covariant equivalent. We describe the normal-metal-ferromagnet interfaces via the spin-dependent boundary conditions

$$\begin{aligned} 2L_j\zeta_j\hat{g}_j\partial_z\hat{g}_j = [\hat{g}_j,\hat{g}_k] + 2L_j\zeta_j\hat{g}_j\text{ß}\left[\hat{\boldsymbol{A}}_z,\hat{g}_j\right] \\ + \sigma_j\tilde{G}_{MR}\left[\hat{g}_j,\left\{\hat{M},\hat{g}_k\right\}\right] + \sigma_j\text{ß}\tilde{G}_\theta\left[\hat{g}_j,\hat{M}\right], \end{aligned} \tag{B.1}$$

where $j,k = \{\text{left},\text{right}\}$, $j \neq k$ denotes the two sides of the interface and the orientation determines the sign $\sigma_{\text{right}} = 1$, $\sigma_{\text{left}} = -1$. The thin-film layering direction is taken to be in the z-direction, and $\tilde{G}_{MR}$ and $\tilde{G}_\theta$ denote the interfacial magnetoresistance and scattering phase shifts respectively. We chose $\zeta_j = 3$ for the transparency parameter of all interfaces. The spin-orbit coupling field $\hat{\boldsymbol{A}} = \text{diag}(\boldsymbol{A}, -\boldsymbol{A}^*)$, and we have considered the case $\boldsymbol{A} = (\beta\sigma_x - \alpha\sigma_y, \alpha\sigma_x - \beta\sigma_y, 0)$, where α,β are the Rashba and Dresselhaus coefficients respectively. The extrinsic spin-orbit scattering and spin-flip terms are given by

$$\begin{aligned} \hat{\sigma}_{so} &= -\frac{1}{8\tau_{so}}\sum_i \hat{\alpha}_i\hat{\rho}_3\hat{g}^R\hat{\rho}_3\hat{\alpha}_i, \\ \hat{\sigma}_{sf} &= -\frac{1}{8\tau_{sf}}\sum_i \hat{\alpha}_i\hat{g}^R\hat{\alpha}_i S_i, \end{aligned} \tag{B.2}$$

where τ_{so} and τ_{sf} are the mean scattering times, S_i is the spin expectation value and we have defined the matrix $\hat{\alpha}_i = \text{diag}(\sigma_i, \sigma_i^T)$. The general form of the retarded Green function is

$$\hat{g}^R = \begin{pmatrix} N(I+\gamma\tilde{\gamma}) & 2N\gamma \\ -2\tilde{N}\tilde{\gamma} & -\tilde{N}(I+\tilde{\gamma}\gamma) \end{pmatrix}, \tag{B.3}$$

with normalization matrices $N = (I-\gamma\tilde{\gamma})^{-1}$ and $\tilde{N} = (I-\tilde{\gamma}\gamma)^{-1}$ and identity matrix I. The $\tilde{\cdot}$ operation denotes complex conjugation and $\varepsilon \to (-\varepsilon)$. Regard-

ing the choice of junction parameter, one may consider a reasonable approximation of the normal-state density of states to be of the order $N_0 \sim 10^{22}/(\text{eV cm}^3)$, and the diffusion constant of CuNi to be[145] $D \sim 5$ cm^2/s.

Paper I

Spin supercurrent, magnetization dynamics, and φ-state in spin-textured Josephson junctions

Physical Review B **90**, 054504 (2014)

PHYSICAL REVIEW B **90**, 054504 (2014)

Spin supercurrent, magnetization dynamics, and φ-state in spin-textured Josephson junctions

Iryna Kulagina and Jacob Linder
Department of Physics, Norwegian University of Science and Technology, N-7491 Trondheim, Norway
(Received 16 June 2014; revised manuscript received 7 July 2014; published 7 August 2014)

The prospect of combining the dissipationless nature of superconducting currents with the spin polarization of magnetic materials is interesting with respect to exploring superconducting analogs of topics in spintronics. In order to accomplish this aim, it is pivotal to understand not only how such spin supercurrents can be created, but also how they interact dynamically with magnetization textures. In this paper, we investigate the appearance of a spin supercurrent and the resulting magnetization dynamics in a textured magnetic Josephson current by using three experimentally relevant models: (i) a superconductor|ferromagnet|superconductor (S|F|S) junction with spin-active interfaces, (ii) a $S|F_1|F_2|F_3|S$ Josephson junction with a ferromagnetic trilayer, and (iii) a Josephson junction containing a domain wall. In all of these cases, the supercurrent is spin polarized and exerts a spin-transfer torque on the ferromagnetic interlayers which causes magnetization dynamics. Using a scattering matrix formalism in the clean limit, we compute the Andreev bound states and resulting free energy of the system which in turn is used to solve the Landau-Lifshiftz-Gilbert equation. We compute both how the inhomogeneous magnetism influences the phase dependence of the charge supercurrent and the magnetization dynamics caused by the spin polarization of the supercurrent. Using a realistic experimental parameter set, we find that the spin supercurrent can induce magnetization switching that is controlled by the superconducting phase difference. Moreover, we demonstrate that the combined effect of chiral spin symmetry breaking of the system as a whole with interface scattering causes the systems above to act as phase batteries that may supply any superconducting phase difference φ in the ground state. Such a φ-junction is accompanied by an anomalous supercurrent appearing even at zero phase difference, and we demonstrate that the flow direction of this current is controlled by the chirality of the magnetization configuration.

DOI: 10.1103/PhysRevB.90.054504 PACS number(s): 74.50.+r, 74.45.+c, 74.78.Fk, 76.50.+g

I. INTRODUCTION

The synergistic effects of combining ferromagnetism and superconductivity, two seemingly disparate phenomena, have garnered much attention in recent years [1,2]. Investigations regarding the mutual interplay between these condensed phases may be traced back to the early work of Ginzburg [3] and it is by now established that ferromagnetic order not necessarily acts detrimentally toward superconductivity; the two may even coexist in a series of uranium-based heavy-fermion compounds such as UGe_2, UCoGe, and UIr [4–6]. Whereas such systems pose several challenges with regard to experimental investigations, e.g., due to requirements of very high pressures in some cases, the combined influence of FM and SC order can be studied in a more controllable fashion by tailoring hybrid structures with the desired properties.

The physical mechanism behind the unlikely alliance of magnetic and superconducting order is symmetry breaking combined with the Pauli exclusion principle [7]. As long as the Cooper pair wave function respects the correct antisymmetry property under an exchange of the particle coordinates for spin, space, and time, the Cooper pairs can in fact become spin polarized. Such an effect takes place in FM/SC structures since both the explicit translation symmetry breaking due to the interface and the presence of a band-splitting exchange field creates Cooper pairs with different symmetry properties than in the bulk superconductor [8]. The consequence of same-spin electrons constituting a Cooper pair is that they become insensitive to the paramagnetic limitation of internal or external magnetic fields, allowing such correlations to survive distances up to hundreds of nanometers inside a ferromagnet [9], even in extreme cases such as half-metallic compounds [10,11]. In such a scenario, the limiting factor of the penetration depth is not determined by the strength of the magnetic exchange field, but by other pair-breaking events such as spin-flip and inelastic scattering [12]. Experiments have unambiguously observed such long-ranged superconducting correlations arising in FM/SC structures that feature magnetic textures of some sort: this includes multilayered magnetic structures [13,14], domain wall or intrinsically textured ferromagnets [15,16], and interfaces with spin-active scattering and/or disorder [17,18]. A large amount of theoretical work has recently been devoted to the topic of spin-triplet correlations arising in S/F hybrid structures (see, e.g., [19–41]).

The existence of long-ranged spin-polarized superconducting correlations raises an interesting question: is it possible to utilize this to obtain a superconducting analog to central topics in spintronics such as domain wall motion and magnetization switching? It is well known that resistive (normal) spin-polarized currents play a central part in terms of obtaining magnetization dynamics in spintronics [42]. Spin-currents enable a transfer of angular momentum to the magnetic order parameter of a material via the effect of spin-transfer torque [43,44]. Since spin supercurrents also carry angular momentum, the same effect is possible in this context and a few previous works have investigated the possibility of magnetization dynamics in superconducting hybrid structures [45,46,48–51,56]. However, it remains unclear how the superconducting phase difference affects the dynamics via the Andreev bound-state spectrum. In this paper, we will consider three experimentally relevant types of FM/SC weak-link structures that all have in common that the region separating the superconductors is spin-textured. We will compute the spin-polarized supercurrent analytically, and demonstrate that

its spin torque can give rise to magnetization switching by solving the nonlinear Landau-Lifshitz-Gilbert [52] equation numerically. This constitutes a way to directly utilize the spin-polarized nature of the recently observed long-range triplet currents in order to dynamically alter magnetization textures. In addition to this, we will demonstrate that the magnetic structure in such Josephson junctions has a profound effect on the superconducting ground state itself. Whereas it is known that superconductor|ferromagnet|superconductor (S|F|S) junctions normally have a ground-state phase difference of 0 or π, it was very recently demonstrated experimentally that it is possible to construct a φ-state junction where the ground-state phase takes on any value between 0 and π [53]. Such a φ-state was originally proposed to occur in SFS junctions in [54] and subsequently studied in several works [55–62], offering the unique possibility to design phase batteries [63,65] with an arbitrary phase shift rather than only 0 or π which could be used to bias both classical and quantum circuits. We will compute the free-energy and belonging supercurrent-phase relation in inhomogeneous magnetic Josephson junctions and show that anomalous behavior arises in the form of a finite supercurrent even at zero phase difference. As will be shown, this is intimately linked with a chiral spin symmetry breaking and scattering at the interfaces of the structure and results in the possibility of a controllable φ-state by adjusting the magnetization vectors in the system.

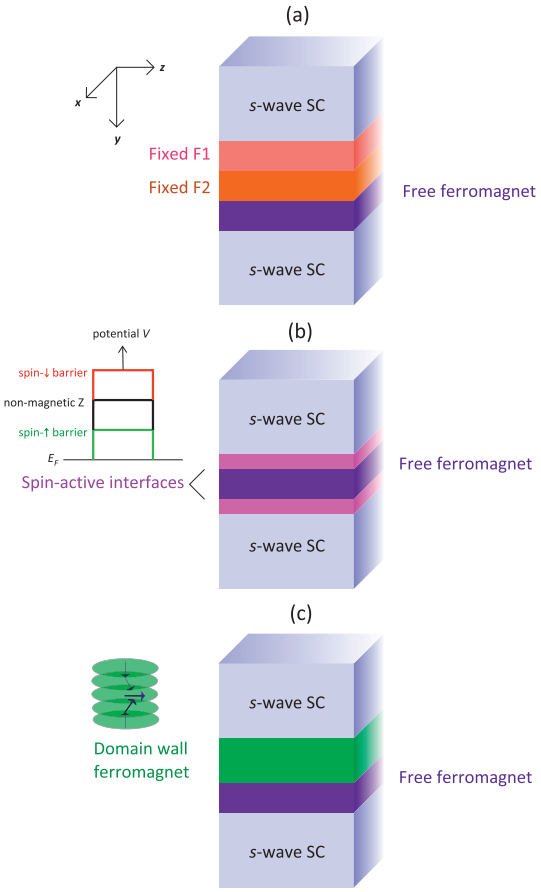

FIG. 1. (Color online) The three setups considered in this paper for magnetization dynamics induced by a spin-polarized supercurrent: (a) a trilayer S|F|S junction with noncollinear magnetization, (b) S|F|S junction with spin-active interfaces, and (c) S|DW|F|S junction where the supercurrent is polarized by a domain wall.

This paper is organized as follows. In Sec. II, we outline the theoretical framework used in our calculations of the spin supercurrent, Andreev levels, the magnetization dynamics, and the ground-state energy of the system under consideration (see Fig. 1). In essence, we are combining the mean-field Bogoliubov–de Gennes equations in a scattering state framework to compute the free energy from which all thermodynamic quantities may be obtained, and then extract the effective magnetic field in our theory which is used as input in the Landau-Lifshitz-Gilbert equation in order to obtain the magnetization dynamics. Additional details of the calculations are found in the Appendix. In Sec. III, we give a comprehensive treatment of the Andreev levels that arise and compute the spin-polarized supercurrent flowing in the system. We provide results for the current-phase relation and magnetization dynamics, and show how a φ-state may arise in noncollinear arrangements in addition to magnetization switching. We give a detailed discussion of our results in Sec. IV, in particular with regard to the experimental feasibility of our proposed setup and the regime of validity for the approximations made in our calculations. Finally, we summarize our findings in Sec. V.

II. THEORY

We consider a ballistic Josephson junction composed of one or more ferromagnetic layers sandwiched between two conventional s-wave superconducting electrodes. The entire structures is positioned along the y axis such that the interfaces lie in the x-z plane. We choose the origin $y = 0$ to be at the interface between the left superconducting layer and its proximate ferromagnetic. Assuming large superconducting banks with size $d \gg \xi_S$, these layers are characterized by their bulk superconducting gap Δ and the macroscopic phase difference across the junction, $\gamma = \gamma_R - \gamma_L$.

The ferromagnetic part of the junction depends on the specific model considered as shown in Fig. 1. We will treat three experimentally relevant model systems in order to illustrate the rich physics that arises due to the spin-polarized nature of the long-ranged superconducting correlations. In Fig. 1(a), we consider a multilayered ferromagnetic junction, similar to a recent experiment [14]. As predicted by Ref. [20], the Josephson current in such a structure should have a long-ranged contribution that depends on the relative orientation of the magnetization vectors in each of the ferromagnetic layers. To treat a general scenario, we consider an arbitrary direction of the magnetization in the free layer and fix the orientation in the two hard magnetic layers to the z and x axis, respectively. The three layers $j \in \{1,2,3\}$ are characterized by their thickness L_j and exchange field h_j, and we will also

consider the influence of interface resistance captured by an effective dimensionless parameter Z (see Appendix). As we will calculate below, the rich physics including supercurrent-induced magnetization reversal and the appearance of a φ ground state is intimately related to chiral symmetry breaking by the magnetization vectors $\boldsymbol{M}_j$ [35,39], characterized by a finite value of the chirality vector:

$$\boldsymbol{\chi} = \boldsymbol{M}_1 \cdot (\boldsymbol{M}_2 \times \boldsymbol{M}_3). \tag{1}$$

Next, we consider in Fig. 1(b) a free magnetic layer with low anisotropy where the interface region coupling to the superconductors is spin active. Such interfaces are known to give rise to spin mixing and spin rotation [22], which considerably alters the superconducting proximity effect. We consider a situation where the barrier moments lie in the x-z plane with the parallel, perpendicular, and antiparallel alignments given by $\phi_L = \phi_R = 0$; $\phi_L = 0$ and $\phi_R = \pi/2$; and $\phi_L = 0$ and $\phi_R = \pi$, respectively. The spin-active interfaces are characterized by barriers [37]

$$U = [\hat{1} - \rho_m \cos(\phi)(\tau_0 \otimes \sigma_3) - \rho_m \sin(\phi)(\tau_0 \otimes \sigma_1)]. \tag{2}$$

One of our results is that breaking chiral spin symmetry is not a sufficient condition to generate an anomalous zero-phase difference supercurrent. Instead, the scattering taking place at the interfaces separating the various regions will be shown to play a pivotal part in this. Finally, we include the effect of a domain wall by considering in Fig. 1(c) a setup where the ferromagnetic region consists of a domain wall and a free magnetic layer. The domain wall is taken to be of Bloch type, thus rotating around the y axis with a characteristic length scale of λ. This particular choice of domain wall is not essential to the resulting physics, and the results we obtain are qualitatively unchanged for other types of magnetization textures. The structure of the domain wall is described by a vector $\boldsymbol{f}$ proportional to the magnetization vector [66]. In order to obtain analytical results, we use the following form:

$$\boldsymbol{f}(y) = \begin{cases} [\sin\left(\frac{\pi y}{l_{\rm dw}}\right), 0, \cos\left(\frac{\pi y}{l_{\rm dw}}\right)], & \text{if} \quad 0 < y < l_{\rm dw}, \\ 0, & \text{otherwise.} \end{cases} \tag{3}$$

The starting point for all scenarios described above is the mean-field Bogoliubov–de Gennes equations [68] describing quasiparticle propagation in these structures. Due to the noncollinear magnetization textures, one must consider the full spin⊗particle-hole space and use a four-component wave function $\Psi = (u_\uparrow, u_\downarrow, v_\uparrow, v_\downarrow)^T$:

$$\begin{pmatrix} \hat{H}_0(y) & \hat{\Delta}(y) \\ -\hat{\Delta}^\dagger(y) & -\hat{H}_0^{\,T}(y) \end{pmatrix} \Psi(y) = E\Psi(y), \tag{4}$$

where $\hat{\Delta}(y) = i\sigma_2\Delta(y)$ and the single-particle Hamiltonian is

$$\hat{H}_0(x) = \left[-\frac{\nabla}{2m} - \mu(y)\right]\hat{1} - h\boldsymbol{f}(y)\cdot\boldsymbol{\sigma}, \tag{5}$$

where m is effective mass of quasiparticles, μ is chemical potential, and $\boldsymbol{\sigma}$ is the Pauli matrix spin vector. The quasiparticle energy E is measured relative the chemical potential which in the low-temperature limit considered here equals the Fermi energy. The eigenstates Ψ may be constructed once the magnetization texture $\boldsymbol{f}(y)$ is specified (see Fig. 1). In each case, the free layer magnetization is allowed to take arbitrary directions. This enables a study of the supercurrent-induced magnetization dynamics on the magnetic order parameter of this layer. We also mention that the scattering states in the domain wall region treated in case (c) may be obtained by employing a unitary transformation of the Hamiltonian which rotates the spin basis to follow the magnetization texture. This also alters the boundary conditions to the superconducting regions. All of these calculational details are left for the Appendix.

Using the framework sketched above, one may compute the allowed energy levels that exist in the Josephson junctions. These Andreev levels ε will depend on the junction geometry, the $U(1)$ superconducting phase gradient, and the magnetization texture. With them in hand, both the free energy $\mathcal{F}$ and the charge supercurrent I are obtained via [67]

$$\mathcal{F}(\gamma) = -\frac{1}{\beta}\sum_j \ln(1 + e^{-\beta\varepsilon_j}), \quad I(\gamma) = \frac{2e}{\hbar}\sum_i f(\varepsilon_i)\frac{\partial\varepsilon_i}{\partial\gamma}, \tag{6}$$

where $f(\varepsilon)$ is Fermi-Dirac distribution function and $\beta = 1/k_BT$. The fact that the supercurrent is spin polarized due to the long-range triplet proximity effect and flows under equilibrium conditions directly implies that the exchange interaction between the ferromagnets will be altered by the superconducting phase difference γ. In fact, there is an interesting codependence between the phase difference γ and the noncollinearity of the magnetization vectors regarding the supercurrent I and the equilibrium magnetic torque τ as first noted by Waintal and Brouwer [45]. Considering for simplicity two monodomain ferromagnets with a relative angle θ between the magnetization vectors, it follows from $I = \frac{2e}{\hbar}\frac{\partial\mathcal{F}}{\partial\gamma}$ and $\tau = \frac{\partial\mathcal{F}}{\partial\theta}$ that

$$\frac{\partial I}{\partial\theta} = \frac{2e}{\hbar}\frac{\partial\tau}{\partial\gamma}. \tag{7}$$

The above equation is simple, yet it conveys a powerful message: if the supercurrent is sensitive to the magnetization orientation, then the torque exerted on the magnetic order parameters is sensitive to the superconducting phase difference. This is the core principle which enables the supercurrent-induced magnetization dynamics in inhomogeneous S|F|S junctions. The induced superconducting correlations are long-ranged since they become spin-polarized and thus avoid picking up a finite center-of-mass momentum which acts pair-breaking. In turn, their spin-polarized nature makes them sensitive to the magnetization texture in the junction such that a mutual interplay is enabled between the supercurrent and the magnetization.

Having obtained the free energy of the system from the Andreev levels, one may also compute the effective field $\boldsymbol{H}_{\rm eff}$ that couples to the magnetic order parameter:

$$\boldsymbol{H}_{\rm eff} = -\frac{1}{V}\frac{\partial\mathcal{F}}{\partial\boldsymbol{M}}. \tag{8}$$

The effective field is used to describe the supercurrent-induced magnetization dynamics in the free layer (purple region in

Fig. 1) by solving the Landau-Lifshitz-Gilbert equation [52]:

$$\frac{\partial \boldsymbol{M}}{\partial t} = -\zeta \boldsymbol{M} \times \boldsymbol{H}_{\text{eff}} + \alpha \boldsymbol{M} \times \frac{\partial \boldsymbol{M}}{\partial t}, \tag{9}$$

where ζ is the gyromagnetic ratio and α is the Gilbert damping constant. As long as the effective field is not fully aligned with the magnetization, it will exert a torque on it which induces magnetization dynamics. We are considering a monodomain macrospin model for the soft ferromagnetic layer, such that there is no contribution from the spin stiffness term $\sim \frac{\partial^2 \boldsymbol{M}}{\partial y^2}$. However, we include the influence of magnetic anisotropy with additional terms $\pm K_j M_j^2$, $j \in \{x,y,z\}$ in the free energy where K_j are the anisotropy constants and the $\pm$ sign determines the hard and easy axes of magnetization.

III. RESULTS

We will now proceed to present our results for the Andreev bound-state (ABS) spectrum, the system's free energy, the current-phase relation, and the ensuing magnetization dynamics via spin supercurrents. We treat each of the three proposed systems in Fig. 1 separately. In each subsection, we start by considering the analytical expression for the ABS energy. Obtaining this quantity serves as the foundation for the computation of both the total free energy of the system and the equilibrium supercurrent, as given by Eq. (6). The technical procedure for doing so consists of three steps. First, we obtain the eigenstate wave functions that solve the BdG equations in each region (see Appendix for details). From these wave functions, the appropriate scattering states involving particle- and hole-like excitations are constructed with belonging probability coefficients. The energies ε that allow for a nontrivial solution of the scattering coefficients are obtained by matching the wave functions at each interface region using appropriate boundary conditions and setting up a system of linear equations of the type $\hat{A}\mathbf{x} = \mathbf{b}$ where $\mathbf{x}$ contains the scattering coefficients. Solving the characteristic equation $\det\hat{A} = 0$ allows one to identify the ABS solutions for ε. The boundary conditions require some special care for the systems under consideration in the present paper; i.e., they are modified from conventional boundary conditions both for setup (b) and (c) in Fig. 1.

A. Trilayered S|F|F|F|S structure

The magnetizations in the first two layers F_1 and F_2 are assumed to be fixed via strong anisotropy energies along the $\hat{z}$ and $\hat{x}$ directions, respectively. In F_3, we allow for an arbitrary magnetization direction in order to explore the effect of spin-supercurrent-induced magnetization dynamics. This material should then consist of a much softer ferromagnet than F_1 and F_2. For a completely arbitrary parameter set, the analytical expression for the ABS energy is overwhelming. However, physical insight can be obtained in experimentally relevant limiting cases. In the quasiclassical regime of a rather weak ferromagnet $h/\mu \ll 1$, one finds that

$$\varepsilon_j = \Delta_0 \sqrt{1 - \mathcal{A}\cos\gamma + \mathcal{B}Z^3(h_y/h)\sin\gamma - \mathcal{C} \pm \sqrt{\mathcal{D}(\gamma)}}, \tag{10}$$

where the coefficients $\mathcal{A},\mathcal{B},\mathcal{C}$ are independent of the phase difference γ. Instead, they are functions of the junction parameters such as length L, barrier Z, and exchange field h. It should be noted that Eq. (10) is valid for arbitrary interface transparency Z. We provide some additional details for the coefficients in Eq. (10) in the Appendix. The quantity $\mathcal{D}(\gamma)$ is a rather large expression which depends on γ; the essential property of this quantity is nevertheless that

$$\left.\frac{\partial \mathcal{D}(\gamma)}{\partial \gamma}\right|_{\gamma=0} \propto \mathcal{B}Z^3(h_y/h). \tag{11}$$

We prove now that it follows from the above properties of the Andreev level that there will be a finite supercurrent at zero phase difference. This finding is then independent of the specific details of the coefficients introduced above.

The presence of an anomalous current is seen to be contingent on two factors: (1) the presence of scattering barriers and (2) $h_y \neq 0$ in the free F layer. The absence of either of these causes the supercurrent to revert to conventional behavior. We comment first on the role of the scattering barriers. In Eq. (10), it was assumed that the scattering barrier Z was the same for the interfaces between the ferromagnetic regions whereas the S/F interface was taken to be completely transparent. By allowing for different barrier values, which will be the case in general since the value of Z depends on the specific materials connected, one finds that the term providing the anomalous current reads $\frac{1}{2}\mathcal{B}Z_1Z_2(Z_1+Z_2)h_y\sin\gamma$. Here, Z_1 is the barrier between the F_1/F_2 interface whereas Z_2 is the barrier between the F_2/F_3 interface. This demonstrates that in the short-junction regime where the Andreev bound states carry the current, barriers at both ferromagnetic interfaces are required in order to produce the anomalous current: setting either Z_1 or Z_2 to zero cancels the $\sin\gamma$ term in Eq. (10). We will later establish a connection between this observation and the results for the domain wall junction to be considered in a section below.

Second, the fact that the anomalous supercurrent only appears when $h_y \neq 0$ means that the presence of an explicitly broken chiral spin symmetry the system is a necessary criterium. Interestingly, we find that direction of the current is actually controlled by the specific chirality, i.e., the sign of h_y. A consequence of this is that the magnetization direction then acts as a 0-π switch as it controls the direction of the supercurrent, which offers a way of exerting dynamical control over a superflow of spins. In a somewhat different multilayer setup where the magnetization vectors were all in-plane (and thus without any anomalous supercurrent), the direction of the magnetization rotation was also found to influence the sign of the supercurrent in Ref. [64]. The precise quantitative behavior of our system depends also on the following parameters: the interface barrier, the magnetic anisotropy constant, and the length of ferromagnetic layers. For convenience, we introduce the normalized and dimensionless variables $\beta_i = \frac{k_F L_i h}{2\mu}$, where the index i denotes the ferromagnetic layer under consideration. Throughout this work, we set $k_F L = 2\pi n$, where n is an integer. The presence of ferromagnetism introduces additional phase shifts for the Andreev bound states as they propagate through the system.

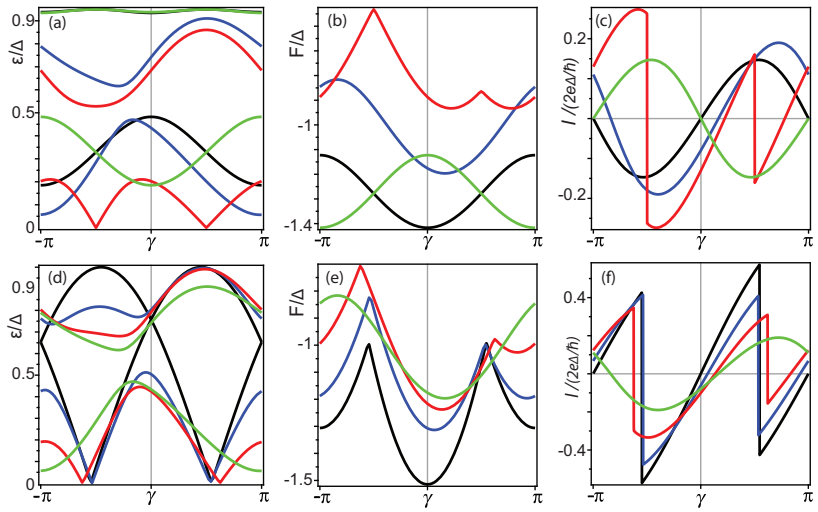

FIG. 2. (Color online) (a), (d) Andreev bound-state energies as a function of superconducting phase difference γ. (b), (e) Free energy of the system as a function of γ and (c), (f) supercurrent-phase relation for our trilayered S|F|F|F|S structure. In all plots, we have set $\beta_1 = \beta_2 = \pi/3$. In (a), (b), (c), we fix the barrier at $Z = 2$ and investigate the effect of different values of β_3 (proportional to both exchange field h and width L of the free ferromagnetic layer): $\beta_3 = 0$ (black), $15\pi/100$ (blue), $25\pi/100$ (red), $50\pi/100$ (green). For (d), (e), (f), we fix $\beta_3 = 15\pi/100$ and investigate the effect of a varying barrier potential: $Z = 0$ (black), 1 (blue), 1.5 (red), 2 (green).

In Fig. 2, we plot the ABS energy [(a), (d)], the free energy [(b), (e)], and the Josephson current [(c), (f)] as function of the phase difference. We fixed $\beta_1 = \beta_2 = \pi/3$ and considered several values for β_3 and Z. The magnetization in the free layer has been set to $\mathbf{m} \parallel \hat{y}$ in order to demonstrate the appearance and consequences of the anomalous supercurrent. To give the reader a better idea about which values these correspond to in an experimental setup, we note that for a weakly polarized ferromagnet with $h/\mu = 0.02$ (exchange field of around 30 meV), $\beta = \pi/3$ corresponds to a length of 15 nm. In Fig. 2, we consider in (a)–(c) the effect of varying the width or exchange field of the free ferromagnetic layer, captured in the parameter β_3. We consider here a weakly transparent interface $Z = 2$. In (d)–(f), we instead fix β_3 and consider the influence of having different barrier potentials Z. The panels for the ABS energies clearly display that the current is spin-polarized as their spin-degeneracy is completely removed in the present system. One important feature is that the effect of increasing Z on the spectrum is that the maxima and minima are shifted away from a phase difference $\gamma = 0$ and $\gamma = \pi$. The fact that the derivative of the ABS energy with respect to γ does not vanish at these points implies that there will be a finite current even in the absence of any superconducting phase difference. This will be referred to as an *anomalous supercurrent*. We observe that there is no anomalous supercurrent when $Z = 0$, as seen also in Eq. (10).

The presence of an anomalous supercurrent is intimately related to an unusual property for the quantum ground state of the system, which is illustrated in the plots for the free energy in Figs. 2(b) and 2(e). The global minimum of F is seen to not necessarily occur at the conventional 0 and π states for the phase difference; in fact, for weakly transparent interfaces it deviates strongly from these values and occurs at an intermediate phase $\in [0,\pi]$. This is a manifestation of a so-called φ-junction. In the right column of Fig. 2, we plot the supercurrent-phase relation for various choices of the length and exchange field for the free ferromagnetic layer as well as different values of the interface transparency. When a φ-junction is realized, we have $I(\gamma = 0) \neq 0$ and an anomalous current is present. Its magnitude is strongly dependent on $\beta_3 \propto hL$ and Z, and is seen to reach up to 50% of the critical Josephson current (for $\beta_3 = \pi/4$ in the figure under consideration).

Having considered the equilibrium properties of the magnetically textured trilayer-Josephson junction, we now wish to address whether magnetization dynamics will be generated when a spin-polarized supercurrent flowing through the system. In particular, we will consider whether and how the presence of the aforementioned anomalous supercurrent alters the dynamics of the free ferromagnetic layer. To explore this, we solve the Landau-Lifshitz-Gilbert (LLG) equation numerically without any approximation for the ABS energies, i.e., valid for arbitrary parameter values. The main ingredient which makes this possible is the effective field, which contains both the contribution from anisotropy terms and the ABS energies. It may be written as

$$\mathbf{H}_{\text{eff}} = \frac{2}{|M_0|}(K_e \boldsymbol{m}_i - K_h \boldsymbol{m}_j) - \frac{1}{V|M_0|}\frac{\partial \mathcal{F}}{\partial \boldsymbol{m}}, \qquad (12)$$

where $K_{e(h)}$ is the easy (hard) axis anisotropy constant while $\mathcal{F}$ is the contribution to the free energy from the ABS energies [see Eq. (6)] and $i(j)$ can be x or y or z in accordance with in which direction is easy (hard) axis. We comment specifically on the regime of validity for our approach that consists of

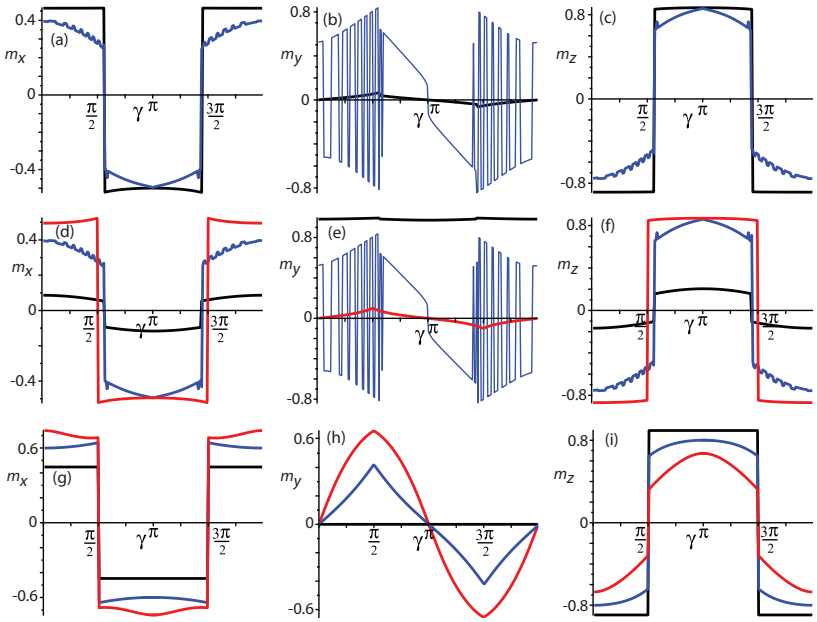

FIG. 3. (Color online) Stable magnetization state as a function of superconducting phase difference γ for $t \to \infty$ when $\mathbf{m}_3(t=0) \parallel \hat{y}$ initially. The components of the magnetization are given in the left (m_x), middle (m_y), and right (m_z) columns. For all panels, we fix $\beta_1 = \beta_2 = \pi/3$. (a)–(c) We set $\beta_3 = 5\pi/100$, $Z = 0.5$, and consider different values of the anisotropy constant: $K = 10^4$ J/m^3 (black line), 10^5 (blue line). (d)–(f) We set $Z = 0.5$, $K = 10^5$, and consider different values of the β_3 parameter: $\beta_3 = \pi/100$ (black), $5\pi/100$ (blue), $25\pi/100$ (red). (g)–(i) We set $\beta_3 = 25\pi/100$, $K = 10^5$, and consider different values of the barrier transparency: $Z = 0$ (black), 1 (blue), 2 (red).

combining a scattering matrix approach in equilibrium with the time-dependent LLG equation in Sec. IV. For now, we simply state that this framework is justified when the magnetization dynamics is sufficiently slow compared to the rate at which the system relaxes to an equilibrium state [69], and is commonly used in the literature. In our numerical simulations, we will set $\beta_1 = \beta_2 = \pi/3$, $\Delta = 10^{-22}$ J, $\mu_0 = 10^{-6}$ H/m, and $|M_0| = 10^5$ A/m. The Gilbert damping parameter is set to $\alpha = 0.02$.

Before discussing the obtained results, it should be noted that the time dynamics of the magnetic order parameter in the free F layer depends on the relative magnitude of the anisotropy and ABS energy terms in the effective field $\mathbf{H}_{\text{eff}}$. Depending on the parameters of the system, one of these will dominate or they will be of similar magnitude and compete. We will take the cross-sectional area of the junction to be $1\ \mu\text{m} \times 1\ \mu\text{m}$ and consider a width of 10 nm for the free layer. With a lattice constant of $a = 0.1$ nm and estimating the number of transverse modes as $N/V = 10^{28}$ m^{-3}, we find that for $K \leqslant 10^3$ J/m^3 the ABS term dominates whereas for $K \geqslant 10^5$ J/m^3 the anisotropy governs the dynamics. In order to limit the parameter space, we will consider only a high to moderate interface transparency ($Z \leqslant 2$) and a junction length of the free F layer satisfying $\beta_3 \leqslant 25\pi/100$. These values are representative for a set of experimentally attainable interface transparencies ranging from high to low as well as different values for the exchange field of the free ferromagnetic layer, ranging from weakly to moderately polarized. In each case, we solve the LLG equation numerically and identify the stable state that arises when $t \to \infty$ and its dependence on the superconducting phase difference. The initial condition for the magnetization of the free layer is taken to be along its easy anisotropy axis. We discuss the experimental realization of this setup in more detail in Sec. IV.

First, consider the case with anisotropy along the $\hat{y}$ direction shown in Fig. 3. We plot the stable state ($t \to \infty$) for each of the magnetization components and investigate the effect of varying the anisotropy strength K (top row), the combined effect of exchange field and width of the ferromagnetic layer $\beta_3 \propto hL$ (middle row), and the interface barrier transparency Z (bottom row). Several observations can be made. Whereas the qualitative behavior of the m_x (left column) and m_z (right column) components are equivalent, displaying a symmetry around $\gamma = \pi$, the m_y (middle column) component displays different behavior. For some parameter values, we observe very fast oscillations in terms of the value of the stable state as a function of the superconducting phase difference. Remarkably, this is a direct result of the presence of an anomalous supercurrent in the system. To see this, consider the LLG equation for a stable, time-independent magnetization:

$$\mathbf{m} \times \mathbf{H}_{\text{eff}} = 0, \tag{13}$$

where $\mathbf{H}_{\text{eff}}$ contains a contribution from both the anisotropy and ABS energies. From the definition of the effective field,

one can show that the components of it satisfy

$$(\mathbf{H}_{\text{eff}})^i \propto \sum_k C(\varepsilon_k)\frac{\partial \varepsilon_k}{\partial h_i}. \tag{14}$$

Now, the partial derivative of the ABS energy depends strongly on which component of the field one considers. For instance, one finds $\frac{\partial \varepsilon_k}{\partial h_y} \propto \sin\gamma$ (odd function of the phase difference) whereas $\frac{\partial \varepsilon_k}{\partial h_z}$ is mainly determined by $\cos\gamma$ (even function of the phase difference). In turn, these properties also determine the symmetries of $(\mathbf{H}_{\text{eff}})_i$ with respect to γ. This observation is essential as it explains the qualitative behavior of the magnetization dynamics in Fig. 3. Let us write out the stable state condition componentwise where we explicitly separate the contribution from anisotropy and ABS energies:

$$\begin{aligned} m_y H^z_{\text{ABS}} - m_z H^y_{\text{ABS}} - K m_y m_z &= 0, \\ m_x H^z_{\text{ABS}} - m_z H^x_{\text{ABS}} &= 0, \\ m_x H^y_{\text{ABS}} - m_y H^x_{\text{ABS}} + K m_x m_y &= 0. \end{aligned} \tag{15}$$

There are now three possible scenarios: (1) the anisotropy term dominates, (2) the ABS energy term dominates, or (3) the contribution from both of these are comparable. When the anisotropy term dominates the effective field, one would expect that the magnetization does not deviate much from its original configuration (along the easy axis). This is seen in panel (e) for the black line. When the anisotropy term is small compared to H_{ABS}, we can neglect the terms $\propto K$ in Eq. (15) which allows us to conclude the following: since H^y_{ABS} is close to antisymmetric in γ whereas H^z_{ABS} is close to symmetric, the first and third line dictate that m_y must be close to antisymmetric in γ whereas m_x and m_z must be close to symmetric. This is again consistent with Fig. 3. Therefore, we may conclude that it is the appearance of the anomalous supercurrent (which is proportional to the $\sin\gamma$ term in the effective field) that is responsible for the qualitatively different behavior of m_y compared to the other components. Finally, the oscillatory behavior of m_y may be understood as a competition between the anisotropy and the ABS contribution to the effective field. Whereas dominating K permits a symmetric m_y with respect to the phase difference γ while dominating ABS contribution gives an antisymmetric m_y, the two terms compete when they are of comparable magnitude and give rise to a stable state for m_y which displays symmetry in a certain range of γ and otherwise antisymmetry. Having established the influence of the superconducting phase difference on the magnetization dynamics, the plots moreover show that magnetization switching is possible. For instance, panel (l) shows that depending on the phase difference γ, the stable magnetization state is almost fully aligned with either the $+\hat{z}$ or the $-\hat{z}$ direction.

Consider next the case where we change the initial magnetization configuration of the free ferromagnetic layer to be along the $\hat{x}$ or $\hat{z}$ direction. The results are shown in Fig. 4.

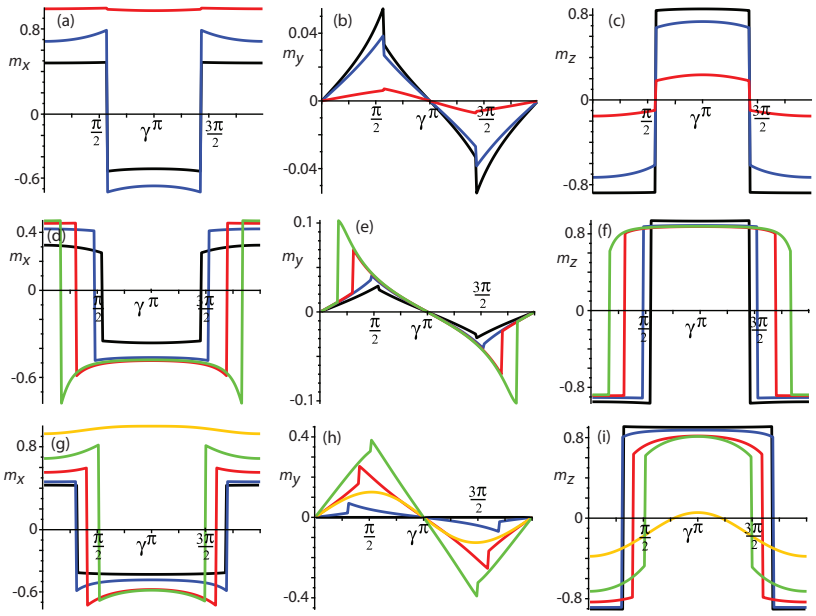

FIG. 4. (Color online) Stable magnetization state as a function of superconducting phase difference γ for $t \to \infty$ when $\mathbf{m}_3 \parallel \hat{y}$ initially. The components of the magnetization are given in the left (m_x), middle (m_y), and right (m_z) columns. For all panels, we fix $\beta_1 = \beta_2 = \pi/3$. (a)–(c) $\mathbf{m}_3(t=0) \parallel \hat{x}$ as initial condition with $\beta_3 = \pi/100$ and $Z = 0.5$. We consider several values of the anisotropy constant: $K = 10^3$ J/m^3 (black line), 10^4 (blue line), 10^5 (red line). (d)–(f) $\mathbf{m}_3(t=0) \parallel \hat{z}$ as initial condition with $Z = 0.5$ and $K = 10^4$ J/m^3. We here consider different values of the β_3 parameter: $\beta_3 = \pi/100$ (black), $15\pi/100$ (blue), $25\pi/100$ (red). (g)–(i) $\mathbf{m}_3(t=0) \parallel \hat{z}$ as initial condition with $\beta_3 = 15\pi/100$ and $K = 10^4$ J/m^3. We consider several choices for the barrier transparency: $Z = 0$ (black), 0.5 (blue), 1 (red), 1.5 (green), 3 (yellow).

The corresponding equation governing the stable state now changes compared to Eq. (15) since the anisotropy contribution will now *always* appear in the second line. As a result, one concludes that regardless of the strength of the anisotropy and regardless of whether the initial configuration is along $\hat{x}$ or $\hat{z}$, the m_y component will always be close to antisymmetric in γ, as seen in Fig. 4.

Let us also comment specifically on the role played by the interface barrier potential Z and the parameter $\beta_3 \propto hL$ in terms of how they influence the magnetization dynamics. A common feature for both Figs. 3 and 4 is that the m_y component grows with increasing barrier Z. This should be seen in conjunction with that the magnitude of the anomalous supercurrent also increases with Z (up to $Z \simeq 2$), as shown in Fig. 2. In effect, the anomalous supercurrent increases in magnitude with Z and is seen to have a feedback effect on the magnetization in terms of enhancing the magnitude of m_y. With regard to the role of β_3, its main role is seen to oppose the effect of the anisotropy. As β_3 increases, the influence of the ABS contribution to the effective field becomes more dominant as evidenced by the emergent antisymmetric m_y dependence on γ.

B. S|F|S junction with spin-active interface zones

We proceed to consider the structure shown in Fig. 1(b): an SFS junction where the interfaces are spin-active. More specifically, we allow (as before) for an arbitrary magnetization direction in the free ferromagnetic layer whereas the interface regions are modeled via Eq. (2) in the perpendicular configuration in order to allow for the possibility of spin chirality breaking with the interface moments and the bulk moment all pointing along different axes. In the quasiclassical regime of a sufficiently weak ferromagnet, we find the following analytical expression for the ABS energy:

$$\varepsilon_j = \Delta_0\sqrt{1 - \mathcal{A}\cos\gamma - \mathcal{B}(h_y/h)Z^2\rho_m^2\alpha\sin\gamma - \mathcal{C} \pm \sqrt{\mathcal{D}(\gamma)}}, \tag{16}$$

where the coefficients $\mathcal{A},\mathcal{B},\mathcal{C}$ are independent of the phase difference γ. The quantity $\mathcal{D}(\gamma)$ is a rather large expression which depends on γ; the essential property of this quantity is nevertheless that

$$\left.\frac{\partial\mathcal{D}(\gamma)}{\partial\gamma}\right|_{\gamma=0} \propto \mathcal{B}(h_y/h)Z^2\rho_m^2\alpha. \tag{17}$$

Similarly to the trilayer structure the $\sin(\gamma)$ contribution is only present when $h_y \neq 0$ and is accompanied by an anomalous supercurrent. The effect increases with the strength of the interface barrier Z and its existence is actually contingent on a nonzero Z. Therefore, the same conclusion as for the trilayer structure holds here: chiral spin-symmetry breaking is not a sufficient criterion for the appearance of an anomalous supercurrent; it also requires scattering at the interfaces.

In Fig. 5, we provide a plot for the ABS spectrum, free energy, and supercurrent-phase relation for the system with spin-active interfaces. In this structure, there is a new parameter compared to the trilayer case, namely the ratio between the magnetic and nonmagnetic part of the barrier ρ_m. In what follows, we set $\rho_m = 0.5$. Considering first the ABS spectrum, we see that the shift of the extremal values away from 0 and π are very small when the conditions for a nonzero anomalous supercurrent are present (finite Z and h_y). In fact, the free energy plots are very close to describing the usual

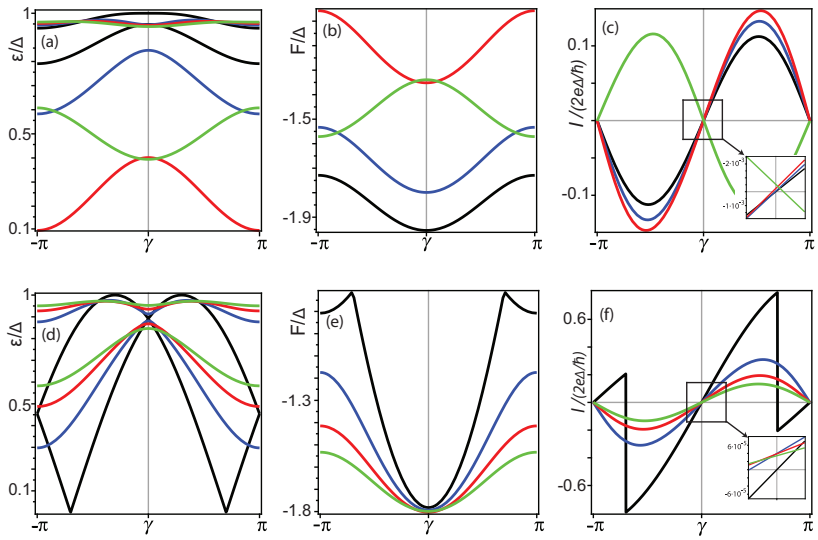

FIG. 5. (Color online) (a), (d) Andreev bound-state energies as a function of superconducting phase difference γ. (b), (e) Free energy of the system as a function of γ and (c), (f) supercurrent-phase relation for our spin-active SFS structure. In (a), (b), (c), we fix the barrier at $Z = 2$ and investigate the effect of different values of β (proportional to both exchange field h and width L of the free ferromagnetic layer): $\beta = 0$ (black), $15\pi/100$ (blue), $25\pi/100$ (red), $50\pi/100$ (green). For (d), (e), (f), we fix $\beta = 15\pi/100$ and investigate the effect of a varying barrier potential: $Z = 0$ (black), 1 (blue), 1.5 (red), 2 (green).

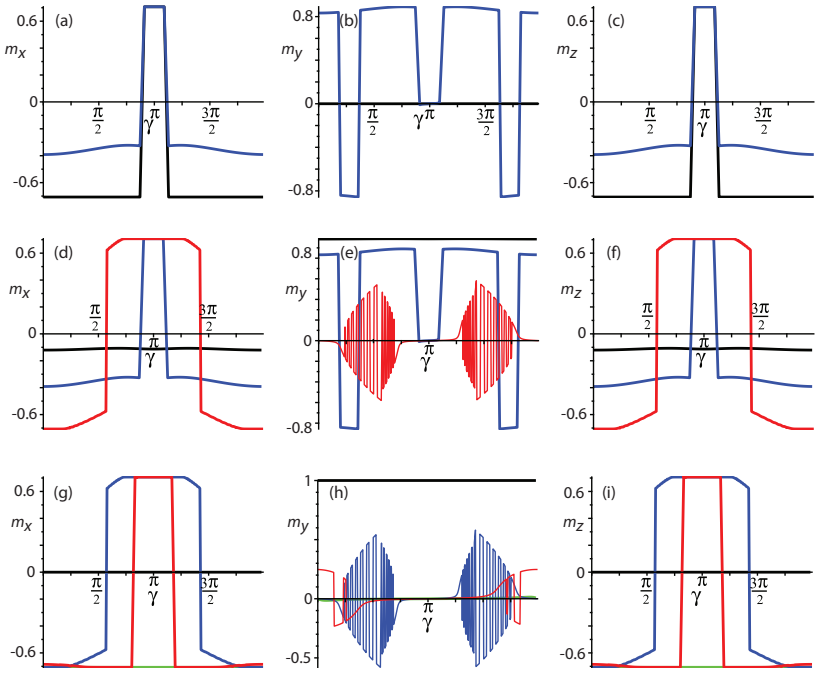

FIG. 6. (Color online) Stable magnetization state as a function of superconducting phase difference γ for $t \to \infty$ when $\mathbf{m}_3(t=0) \parallel \hat{y}$ initially. The components of the magnetization are given in the left (m_x), middle (m_y), and right (m_z) columns. In all panels, we fix $\rho_m = 0.5$. (a)–(c) We fix $\beta = 15\pi/100$, $Z = 0.5$, and consider several values of the anisotropy constant: $K = 10^4$ J/m^3 (black line), 10^5 (blue line). (d)–(f) We fix $Z = 0.5$, $K = 10^5$, and consider several values of the β parameter: $\beta = 5\pi/100$ (black), $15\pi/100$ (blue), $25\pi/100$ (red). (g)–(i) We fix $\beta = 25\pi/100$, $K = 10^5$, and consider several values of the interface transparency: $Z = 0$ (black), 0.5 (blue), 1 (red), 2 (green).

0-π transitions. However, the zoom-in in the right column of Fig. 5 demonstrates that there is a small but finite value of the supercurrent at $\gamma = 0$, which is equivalent to saying that the junction is in a φ-state. Both the present and the trilayer system can then in principle act as phase batteries supplying whichever phase difference that may be desirable as its ground state.

For the magnetization dynamics, we consider in this section only the case where the initial configuration is along the $\hat{y}$ axis since this gives the qualitatively most interesting behavior (see Fig. 6). Using the $\hat{x}$ and $\hat{z}$ directions as the free layer initial state provides similar results to those in the previous section. One key difference is nevertheless that unlike the trilayer case, there is no magnetization dynamics whatsoever in the present scenario when $Z = 0$. The reason is that for perfectly transparent interfaces, the junction is equivalent to a homogeneous SFS junction and there is no spin-transfer torque due to misaligned magnetic moments. Moreover, we see that for all parameter choices we have $m_x(t \to \infty) = m_z(t \to \infty)$. This stems from the fact that the influence of both spin-active interfaces is equivalent in magnitude so that the induced x and z components of the bulk magnetization take the same values. The qualitative behavior of the stable-state magnetization $m_y(t \to \infty)$ is determined by the relative contribution of the anisotropy term and the ABS energies, and a similar analysis to that for the trilayer case holds here as well. With increasing $\beta \propto hL$, the influence of the anisotropy term decreases.

C. Domain wall S|F|S junction

The final structure under consideration in this work is one where the magnetic weak link connecting the superconductors consists of two layers: a magnetic domain wall ferromagnet and, as before, a free ferromagnetic layer. The domain wall is modeled via Eq. (3). In the quasiclassical regime $h \ll \mu$, we obtain the expression

$$\varepsilon_j = \Delta_0 \sqrt{1 - \mathcal{A}\cos\gamma - \mathcal{B} \pm \sqrt{(\mathcal{A}\cos\gamma)^2 + \mathcal{C}\cos\gamma + \mathcal{D}}}, \tag{18}$$

where all coefficients $\mathcal{A}, \mathcal{B}, \mathcal{C}$, and $\mathcal{D}$ are independent of γ and instead depend on all the other parameters in the junction. In obtaining Eq. (18), we considered the limit $\eta \ll 1$ and $\alpha_{\rm dw} \gg \eta$ where

$$\alpha_{\rm dw} = h_{\rm dw}/2\mu, \quad \eta = a^2/k_F^2, \quad a = \pi/2l_{\rm dw}. \tag{19}$$

To understand what this limit means physically, we note that it is equivalent to stating that the domain wall width $l_{\rm dw}$ far exceeds a typical lattice spacing constant as it should. From this expression, it is clear that the ground-state energy will always occur at $\gamma = 0$ or $\gamma = \pi$, in contrast to the two previously analyzed configurations. The $\sin\gamma$ term responsible for the anomalous supercurrent and φ-junction is absent. For this reason, we do not include any results for the magnetization dynamics of this system. We instead show graphically in Fig. 7

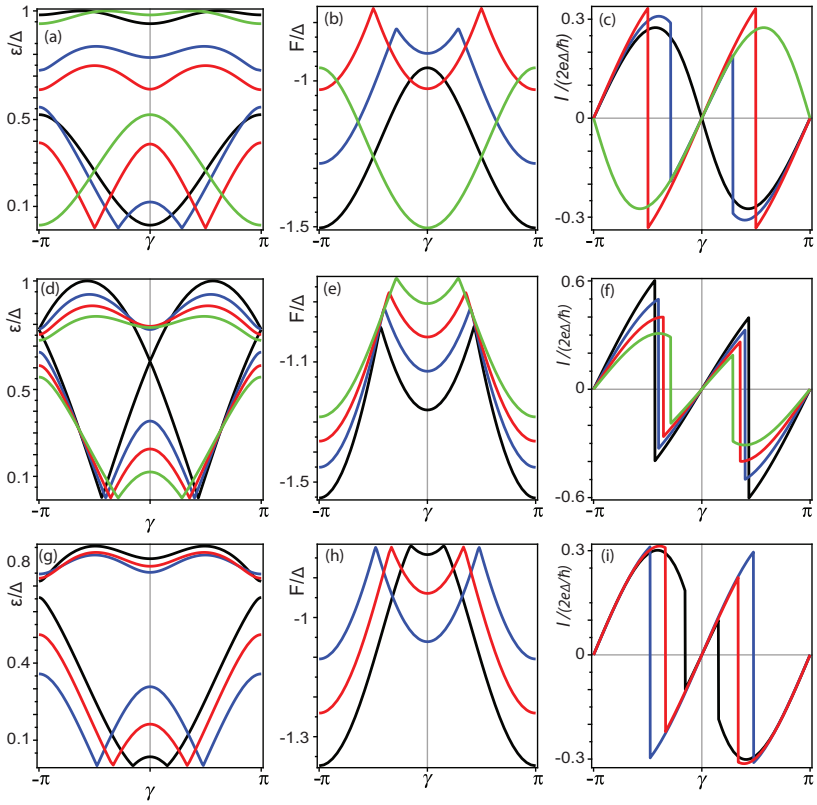

FIG. 7. (Color online) (a), (d), (g) Andreev bound-state energies as a function of superconducting phase difference γ. (b), (e), (h) Free energy of the system as a function of γ and (c), (f), (j) supercurrent-phase relation for our S/DW/F/S structure. In (a), (b), (c), we set $Z = 2$, $\eta = 10^{-4}$ and investigate the effect of different values of the β_2 parameter: $\beta_2 = 0$ (black), $15\pi/100$ (blue), $25\pi/100$ (red), $50\pi/100$ (green). In (d), (e), (f), we set $\beta_2 = 15\pi/100$, $\eta = 10^{-4}$ and investigate the effect of the magnitude of the barrier transparency: $Z = 0$ (black), 1 (blue), 1.5 (red), 2 (green). Finally, for (g), (h), (i), we set $Z = 2$, $\beta_2 = 15\pi/100$ and investigate the effect of the domain wall width: $\eta = 10^{-4}$ (black), 8×10^{-3} (blue), 5×10^{-3} (red).

the ABS energies [(a), (d), (g)], the free energy of the system [(b), (e), (h)], and the supercurrent-phase relation [(c), (f), (j)]; all are shown for various parameter choices. The fact that the anomalous supercurrent is absent is an important observation, because it demonstrates that chiral spin-symmetry breaking (or alternatively, non-coplanar magnetization vectors) alone is insufficient to induce such a term. In fact, the finding that the term causing a φ-junction is absent in the present case of a domain wall is consistent with our findings for the trilayer junction above. There, it was shown that if either interface barrier between the ferromagnetic layers was absent, the anomalous supercurrent vanishes. Such a scenario is similar to the present case, since two misaligned ferromagnetic regions without any interface scattering barrier can be thought of as a simplified domain wall.

IV. DISCUSSION

We discuss here some issues which are relevant for the approximations made in our model as well as how to realize experimentally the proposed setups. First of all, the variation of the magnetization dynamics on the superconducting phase difference can be probed in several ways. In our treatment, we have considered a phase-biased Josephson junction with a fixed superconducting phase rather than a fixed current bias. In the latter case, the superconducting phase would vary together with the magnetization dynamics since the supercurrent-phase relation is sensitive to the exact magnetization configuration. Instead, by phase-biasing the junction via a loop geometry and a minute external field corresponding to a flux quantum (which has no effect on the magnetization dynamics), the current is allowed to vary as the magnetization dynamics takes place while the phase remains fixed. Another approach would be to study a phase-driven junction with a voltage bias as done, e.g., in [47,49].

For the computation of the magnetization dynamics, we used as initial condition that the magnetization of the free layer was along the easy axis anisotropy. In general, however, the magnetization configuration that solves the static LLG equation in equilibrium is not necessarily with the free layer

along the easy axis. This is due to the presence of the effective field stemming from the ABS energies that exist in the junction. We have attempted to find a general analytical solution for the orientation of the free layer which solves $\mathbf{m} \times \mathbf{H}_{\text{eff}} = 0$ when including all terms in the free energy, but the resulting expressions were too cumbersome to be of any use. The initial condition used in the numerical simulations is nevertheless feasible to realize experimentally, simply by applying an external field along the anisotropy axis to artificially enhance it so that the free layer $\mathbf{m}$ is fixed along that direction. By then turning off the field, the resulting magnetization due to the Andreev bound states and the change in superconducting phase difference may then be observed. It is important to underline that the supercurrent-induced magnetization dynamics studied in this paper is a nonequilibrium effect even when the SC phase difference is kept constant. The reason is that the system is initially prepared in a magnetization configuration which is not the ground state of the system so that there is a finite torque acting on the free layer which eventually goes to zero as the system relaxes into a stable state for $t \to \infty$.

In the situation considered in the majority of previous literature on magnetic Josephson junctions, the magnetization is considered fixed and thus already being in its ground state (e.g., due to strong anisotropy fixing). One then assumes that there is no feedback on the magnetization from the Josephson current, and so one only needs to minimize the superconducting part of the free energy with respect to the phase difference: the magnetic part is already assumed to be minimized. If one instead, as we have done, allows for the Andreev bound states and (thus supercurrent) to have a considerable influence on the free energy on equal footing as the anisotropy, the superconducting correlations will alter the favorable orientation of the magnetization. The free energy should then be minimized both with respect to the magnetization orientation and the superconducting phase difference.

Let us also comment specifically on our technical treatment of how the Andreev-bound state contribution to the free energy gives rise to an effective field that enters the LLG equation. Defining the effective field $\mathbf{H}_{\text{eff}}$ as the functional derivative of the magnetic order parameter evaluated at its instantaneous configuration requires that the magnetization dynamics be slow compared to relaxation processes in the system. In other words, the derived free energy may be treated as time-dependent if the system approximately equilibriates in pace with the change in magnetization. A lag between the magnetization dynamics $\mathbf{m}(t)$ and degrees of freedom that are coupled to it may be interpreted as a dissipation of energy and in turn captured by the Gilbert-damping parameter that we have accounted for [69]. For a driven superconducting phase where the phase difference is $\gamma(t) = \omega_J t + \gamma_0$, the above criterium is satisfied when $\omega_J \ll k_B T_c$ [47] so that the phase is treated as a time-dependent perturbation.

It is worthwhile to point out that the diffusive limit of transport is usually the experimentally most relevant one. Our motivation for performing the calculations in the ballistic regime was primarily for the sake of analytical transparency: using the BdG equations, we have obtained an analytical expression for the Andreev bound-state energies from which one can directly infer the required conditions of the appearance of the anomalous supercurrent. In the diffusive limit, one would have to use the quasiclassical Usadel equations. For the types of structures that we have considered with multilayers, an analytical solution might be possible but probably not in a particularly illuminating form. In fact, a previous work [20] that considered a trilayer SFS junction using the quasiclassical formalism was unable to identify the appearance of the φ-state using an analytical approach, presumably due to all the simplifications that are required for this purpose. This suggests that a calculation in the full proximity effect regime, where only a numerical approach is viable, would be required in the diffusive limit in order to correctly obtain the predicted effects. Whereas this is certainly interesting, it lies outside the scope of our work. Having stated this, we think it is reasonable to expect that our results will be qualitatively valid for the diffusive limit as well for the following two reasons: (i) The fundamental mechanism for the generation of an anomalous supercurrent and φ-state relies on the breaking of a chiral spin symmetry combined with the presence of interface scattering. None of these effects pertain uniquely to the ballistic limit of transport, and hence one would expect that the same physics would transpire in the diffusive limit given the same conditions as in our paper. (ii) In the regime of moderate to low interface transparency, the supercurrent-phase relation is close to sinusoidal and the higher harmonics (which typically are much more pronounced in the ballistic limit) are suppressed. In this way, our system becomes more comparable to the diffusive case where it is known that the first harmonic is the most important contribution. Quantitatively, there may certainly be some differences between the diffusive and ballistic treatments, but we do not expect any dramatic alterations of the underlying physics for the reasons mentioned above.

Finally, in order for the magnetization vectors to be misaligned as in, e.g., the trilayer case, it is necessary to reduce the exchange coupling between the layers. This can be achieved by inserting a normal metal spacer between the F regions. We have omitted this layer in our calculations since it would merely complicate the analytical expressions without introducing any new physics. It should be noted that spacer thicknesses as small as 4 nm are sufficient to experimentally allow for misaligned magnetization vectors in superconducting hybrid structures, as very recently reported in [70].

V. CONCLUSION

In conclusion, we have investigated the spin and charge transport in several models of magnetically textured Josephson junctions. We have made predictions for the ABS energy spectrum, the free energy and its phase dependence, and the supercurrent-phase relation. Moreover, we have considered the magnetization dynamics induced by the presence of a triplet spin supercurrent in these systems and computed how the stable-state magnetization $\mathbf{m}(t \to \infty)$ is controlled by the superconducting phase difference. A key finding is that the presence of an anomalous supercurrent $\propto \cos\gamma$, which results in a φ-state, strongly influences the resulting magnetization dynamics and gives rise to symmetry properties of the stable state which may be understood by analyzing the resulting effective field $\mathbf{H}_{\text{eff}}$. Moreover, we demonstrated that chiral spin symmetry breaking is insufficient to generate such an

anomalous supercurrent: the presence of scattering barriers separating different magnetic regions plays an instrumental role in creating this effect. Our results may provide a basis for future investigations of how controllable magnetization dynamics can be obtained with spin supercurrents that are tuned via the superconducting phase difference.

ACKNOWLEDGMENTS

The authors thank J. W. A. Robinson, K. Halterman, and D. Kulagin for very useful discussions. I.K. and J.L. were supported by the Research Council of Norway, Grant No. 205591/F20 (FRINAT).

APPENDIX: CALCULATION OF ANDREEV LEVELS

In order to solve the Bogoliubov–de Gennes equations we write the wave function in plane-wave form $\Psi(y) = e^{iky}\psi$. The wave vectors of electron- and hole-like quasiparticles (ELQs and HLQs, respectively) inside the superconductor are

$$k_S = \sqrt{2m(\mu \pm \sqrt{E^2 - \Delta^2})}, \tag{A1}$$

while for the homogeneous ferromagnets we have

$$k_f^\sigma = \sqrt{2m(\mu \pm E + \sigma h)}. \tag{A2}$$

Finally, in the domain wall case we find

$$k_{\mathrm{DW}}^\sigma = \sqrt{2m(\mu \pm E) + a^2 + \sigma 2\sqrt{2ma^2(\mu \pm E) + m^2h^2}}, \tag{A3}$$

where $a = \frac{\pi}{2l_{\mathrm{DW}}}$. Defining $\alpha = \frac{h}{2\mu}$ and $\eta = \frac{a^2}{2m(\mu \pm E)}$, we find in the limit $E \ll \mu$ that $\eta = \frac{a^2}{k_F^2}$ and the wave vector for the domain wall becomes

$$k_{\mathrm{DW}}^\sigma = \sqrt{2m(\mu \pm E) + \eta^2 + \sigma 2\sqrt{\eta^2 + \alpha^2}}. \tag{A4}$$

During our calculation we use the approximation that $E \ll \mu$ and that α and η are small. For $\alpha \gg \eta$, the wave vector for the quasiparticles in the domain wall ferromagnet can be simplified further:

$$k_{\mathrm{DW}}^\sigma = 2m\mu(1 + \sigma\alpha) \tag{A5}$$

while for for $\alpha \ll \eta$

$$k_{\mathrm{DW}}^\sigma = 2m\mu(1 + \sigma\eta). \tag{A6}$$

For a ferromagnetic layer with arbitrary orientation of magnetization, we have

$$\begin{aligned}\Psi_F(y) = \sum_{p=\pm}\Bigg[& t_{e,\uparrow}^{\pm}\begin{pmatrix}\cos\left(\frac{\theta}{2}\right)\\ \sin\left(\frac{\theta}{2}\right)e^{i\chi}\\ 0\\ 0\end{pmatrix}e^{\pm ik_F^{\uparrow}y} + t_{e,\downarrow}^{\pm}\begin{pmatrix}-\sin\left(\frac{\theta}{2}\right)e^{-i\chi}\\ \cos\left(\frac{\theta}{2}\right)\\ 0\\ 0\end{pmatrix}e^{\pm ik_F^{\downarrow}y}\\ & + t_{h,\uparrow}^{\pm}\begin{pmatrix}0\\ 0\\ \cos\left(\frac{\theta}{2}\right)\\ \sin\left(\frac{\theta}{2}\right)e^{-i\chi}\end{pmatrix}e^{\pm(-ik_F^{\uparrow}y)} + t_{h,\downarrow}^{\pm}\begin{pmatrix}0\\ 0\\ -\sin\left(\frac{\theta}{2}\right)e^{i\chi}\\ \cos\left(\frac{\theta}{2}\right)\end{pmatrix}e^{\pm(-ik_F^{\downarrow}y)}\Bigg],\end{aligned} \tag{A7}$$

where θ is the angle between the magnetization and the z axis, χ is the angle between the magnetization and the x axis in the x-y plane, and $\pm$ corresponds to the direction of the moving particles. For the domain wall layer, we first perform a unitary transformation $\hat{\mathcal{U}}$ of the Hamiltonian to remove the explicit spatial dependence of the exchange field due to the domain wall texture. This is achieved by rotating the system so that the local spin quantization axis is aligned with the local magnetization direction. Starting out with $\hat{H}\psi = \varepsilon\psi$, we rewrite it to $\hat{H}_{\mathrm{rot}}\Psi = \varepsilon\Psi$ where $\hat{H}_{\mathrm{rot}} = \hat{\mathcal{U}}\hat{H}\hat{\mathcal{U}}^{-1}$ and $\Psi = \hat{\mathcal{U}}\psi$. The new wave function Ψ may then be expressed as follows:

$$\Psi_{\mathrm{DW}}(y) = \sum_{p=\pm}\left[t_{e,\uparrow}^{\pm}\begin{pmatrix}\phi_1^{\uparrow}\\ \pm\phi_2^{\uparrow}\\ 0\\ 0\end{pmatrix}e^{\pm ik_{\mathrm{DW}}^{\uparrow}y} + t_{e,\downarrow}^{\pm}\begin{pmatrix}\pm\phi_2^{\downarrow}\\ \phi_1^{\downarrow}\\ 0\\ 0\end{pmatrix}e^{\pm ik_{\mathrm{DW}}^{\downarrow}y} + t_{h,\uparrow}^{\pm}\begin{pmatrix}0\\ 0\\ \phi_1^{\uparrow}\\ \pm\phi_2^{\uparrow}\end{pmatrix}e^{\pm(-ik_{\mathrm{DW}}^{\uparrow}y)} + t_{h,\downarrow}^{\pm}\begin{pmatrix}0\\ 0\\ \pm\phi_2^{\downarrow}\\ \phi_1^{\downarrow}\end{pmatrix}e^{\pm(-ik_{\mathrm{DW}}^{\downarrow}y)}\right], \tag{A8}$$

where

$$\phi_1^\sigma = \sigma(\alpha + \eta^2\sqrt{\alpha^2 + \sigma\eta^2}), \quad \phi_2^\sigma = \sigma i\eta\sqrt{1 + \eta^2 + 2\sqrt{\alpha^2 + \eta^2}}. \tag{A9}$$

We may then revert to the original wave function ψ, which enters the boundary conditions, by doing the inverse transformation $\psi = \hat{U}^{-1}\Psi$. The coefficients $t^{\pm}_{e(h),\sigma}$ are associated with right-going or left-going ($\pm$) ELQs and HLQs propagating through the ferromagnetic layers. The spin index $\sigma = \uparrow$ or $\downarrow$.

The wave functions must satisfy the boundary conditions of (1) continuity of the wave function at the boundary,

$$(\Psi_k - \Psi_l)|_{y=L_i} = 0, \tag{A10}$$

and (2) discontinuity of the first derivative at the boundary,

$$\partial(\Psi_k - \Psi_l)|_{y=L_i} = \frac{2m}{\hbar} U\Psi|_{y=L_i}, \tag{A11}$$

where $L_i = 0$, L_1, L_2, L_3, and indexes k and l are associated with corresponding index of the wave functions. We have defined the normalized barrier strength $Z = 2mU/(\hbar k_F)$. Note that in the domain wall case, extra terms $\partial_y \hat{\mathcal{U}}$ arise in the boundary conditions due to the unitary transformation of the wave function. From the boundary conditions, we can obtain all the scattering coefficients and set up a homogeneous system of linear equations, demanding that the determinant be equal to zero in order to have a nontrivial solution. The resulting characteristic equation is then solved for the energy which represents the Andreev bound state (ABS). In the ABS energy for the trilayered structure, the coefficient B before the anomalous $\sin\gamma$ term satisfies

$$B \propto \sin 2\beta_1 \sin 2\beta_2 \sin 2\beta_3, \tag{A12}$$

whereas for the structure with spin-active interfaces

$$B \propto \sin^2 \beta. \tag{A13}$$

In the scenario with a domain wall ferromagnet, there exists no manageable expression for B in the general case.

[1] A. I. Buzdin, Rev. Mod. Phys. **77**, 935 (2005).

[2] F. S. Bergeret, A. F. Volkov, and K. B. Efetov, Rev. Mod. Phys. **77**, 1321 (2005).

[3] V. L. Ginzburg, Zh. Eksp. Teor. Fiz. **31**, 202 (1956) [Sov. Phys. JETP **4**, 153 (1957)]; L. N. Bulaevski and V. L. Ginzburg, Sov. Phys. JETP **18**, 530 (1964).

[4] S. S. Saxena *et al.*, Nature (London) **406**, 587 (2000).

[5] D. Aoki, A. Huxley, E. Ressouche, D. Braithwaite, J. Flouquet, J.-P. Brison, E. Lhotel, and C. Paulsen, Nature (London) **413**, 613 (2001).

[6] N. T. Huy, A. Gasparini, D. de Nijs, Y. Huang, J. Klaasse, T. Gortenmulder, A. de Visser, A. Hamann, T. Görlach, and H. Löhneysen, Phys. Rev. Lett. **99**, 067006 (2007).

[7] M. Eschrig, T. Löfwander, T. Champel, J. C. Cuevas, J. Kopu, and G. Schön, J. Low Temp. Phys. **147**, 457 (2007).

[8] Y. Tanaka, A. A. Golubov, S. Kashiwaya, and M. Ueda, Phys. Rev. Lett. **99**, 037005 (2007).

[9] F. S. Bergeret, A. F. Volkov, and K. B. Efetov, Phys. Rev. Lett. **86**, 4096 (2001).

[10] M. Eschrig, J. Kopu, J. C. Cuevas, and Gerd Schön, Phys. Rev. Lett. **90**, 137003 (2003).

[11] R. S. Keizer, S. T. B. Goennenwein, T. M. Klapwijk, G. Miao, G. Xiao, and A. Gupta, Nature (London) **439**, 825 (2006).

[12] H. Z. Arham, T. S. Khaire, R. Loloee, W. P. Pratt, Jr., and N. O. Birge, Phys. Rev. B **80**, 174515 (2009).

[13] J. W. A. Robinson, J. D. S. Witt, and M. G. Blamire, Science **329**, 59 (2010).

[14] Trupti S. Khaire, Mazin A. Khasawneh, W. P. Pratt, Jr., and Norman O. Birge, Phys. Rev. Lett. **104**, 137002 (2010).

[15] I. Sosnin, H. Cho, V. T. Petrashov, and A. F. Volkov, Phys. Rev. Lett. **96**, 157002 (2006).

[16] J.W. A. Robinson, F. Chiodi, G. B. Halasz, M. Egilmez, and M. G. Blamire, Sci. Rep. **2**, 699 (2012).

[17] M. S. Anwar, F. Czeschka, M. Hesselberth, M. Porcu, and J. Aarts, Phys. Rev. B **82**, 100501(R) (2010).

[18] D. Sprungmann, K. Westerholt, H. Zabel, M. Weides, and H. Kohlstedt, Phys. Rev. B **82**, 060505(R) (2010).

[19] Z. Pajovic, M. Bozovic, Z. Radovic, J. Cayssol, and A. Buzdin, Phys. Rev. B **74**, 184509 (2006).

[20] M. Houzet and A. I. Buzdin, Phys. Rev. B **76**, 060504(R) (2007).

[21] K. Halterman, P. H. Barsic, and O. T. Valls, Phys. Rev. Lett. **99**, 127002 (2007).

[22] M. Eschrig and T. Löfwander, Nat. Phys. **4**, 138 (2008).

[23] P. M. R. Brydon, D. Manske, and M. Sigrist, J. Phys. Soc. Jpn. **77**, 103714 (2008); P. M. R. Brydon, W. Chen, Y. Asano, and D. Manske, Phys. Rev. B **88**, 054509 (2013).

[24] M. Alidoust, J. Linder, G. Rashedi, T. Yokoyama, and A. Sudbø, Phys. Rev. B **81**, 014512 (2010).

[25] T. E. Baker, A. Richie-Halford, and A. Bill, arXiv:1310.6580.

[26] Z. Shomali, M. Zareyan, and W. Belzig, New J. Phys. **13**, 083033 (2011).

[27] A. Cottet, Phys. Rev. Lett. **107**, 177001 (2011).

[28] A. I. Buzdin, A. S. Melnikov, and N. G. Pugach, Phys. Rev. B **83**, 144515 (2011).

[29] I. B. Sperstad, J. Linder, and A. Sudbø, Phys. Rev. B **78**, 104509 (2008).

[30] Ya. V. Fominov, A. F. Volkov, and K. B. Efetov, Phys. Rev. B **75**, 104509 (2007).

[31] G. Annunziata, M. Cuoco, C. Noce, A. Romano, and P. Gentile, Phys. Rev. B **80**, 012503 (2009); G. Annunziata, M. Cuoco, C. Noce, A. Sudbø, and J. Linder, *ibid.* **83**, 060508(R) (2011).

[32] K. Halterman, O. T. Valls, and P. H. Barsic, Phys. Rev. B **77**, 174511 (2008).

[33] F. Romeo and R. Citro, Phys. Rev. Lett. **111**, 226801 (2013).

[34] R. Grein, M. Eschrig, G. Metalidis, and G. Schön, Phys. Rev. Lett. **102**, 227005 (2009).

[35] Y. Asano, Y. Sawa, Y. Tanaka, and A. A. Golubov, Phys. Rev. B **76**, 224525 (2007).
[36] T. Yokoyama, Y. Tanaka, and A. A. Golubov, Phys. Rev. B **75**, 134510 (2007).
[37] J. Linder, M. Cuoco, and A. Sudbø, Phys. Rev. B **81**, 174526 (2010).
[38] G. B. Halász, J. W. A. Robinson, J. F. Annett, and M. G. Blamire, Phys. Rev. B **79**, 224505 (2009).
[39] I. Margaris, V. Paltoglou, and N. Flytzanis, J. Phys.: Condens. Matter **22**, 445701 (2010).
[40] F. S. Bergeret, A. Verso, and A. F. Volkov, Phys. Rev. B **86**, 060506(R) (2012).
[41] J.-F. Liu and K. S. Chan, Phys. Rev. B **82**, 184533 (2010).
[42] I. Žutić, J. Fabian, and S. Das Sarma, Rev. Mod. Phys. **76**, 323 (2004).
[43] J. C. Slonczewski, J. Magn. Magn. Mater. **159**, L1 (1996).
[44] L. Berger, Phys. Rev. B **54**, 9353 (1996).
[45] X. Waintal and P. W. Brouwer, Phys. Rev. B **65**, 054407 (2002).
[46] E. Zhao and J. A. Sauls, Phys. Rev. B **78**, 174511 (2008).
[47] F. Konschelle and A. Buzdin, Phys. Rev. Lett. **102**, 017001 (2009).
[48] V. Braude and Ya. M. Blanter, Phys. Rev. Lett. **100**, 207001 (2008).
[49] J. Linder and T. Yokoyama, Phys. Rev. B **83**, 012501 (2011).
[50] P. D. Sacramento, L. C. Fernandes Silva, G. S. Nunes, M. A. N. Araujo, and V. R. Vieira, Phys. Rev. B **83**, 054403 (2011); P. D. Sacramento and M. A. N. Araujo, Eur. Phys. J. B **76**, 251 (2010).
[51] S. Teber, C. Holmqvist, and M. Fogelström, Phys. Rev. B **81**, 174503 (2010); C. Holmqvist, S. Teber, and M. Fogelström, *ibid.* **83**, 104521 (2011).
[52] L. D. Landau and E. M. Lifshitz, Phys. Z. Sowjetunion **8**, 153 (1935); T. L. Gilbert, IEEE Trans. Magn. **40**, 3443 (2004).
[53] H. Sickinger, A. Lipman, M. Weides, R. G. Mints, H. Kohlstedt, D. Koelle, R. Kleiner, and E. Goldobin, Phys. Rev. Lett. **109**, 107002 (2012).
[54] A. Buzdin, Phys. Rev. B **72**, 100501(R) (2005).
[55] V. Braude and Yu. V. Nazarov, Phys. Rev. Lett. **98**, 077003 (2007).
[56] A. Buzdin, Phys. Rev. Lett. **101**, 107005 (2008).
[57] J. Linder, Y. Tanaka, T. Yokoyama, A. Sudbø, and N. Nagaosa, Phys. Rev. B **81**, 184525 (2010).
[58] J.-F. Liu and K. S. Chan, Phys. Rev. B **82**, 125305 (2010).
[59] E. Goldobin, D. Koelle, R. Kleiner, and R. G. Mints, Phys. Rev. Lett. **107**, 227001 (2011).
[60] M. Alidoust and J. Linder, Phys. Rev. B **87**, 060503(R) (2013).
[61] D. M. Heim, N. G. Pugach, M. Yu. Kupriyanov, E. Goldobin, D. Koelle, and R. Kleiner, J. Phys.: Condens. Matter **25**, 215701 (2013).
[62] D. Feinberg and C. Balseiro, arXiv:1405.6889.
[63] T. Ortlepp, Ariando, O. Mielke, C. J. M. Verwijs, K. F. K. Foo, H. Rogalla, F. H. Uhlmann, and H. Hilgenkamp, Science **312**, 1495 (2006).
[64] F. S. Bergeret, A. F. Volkov, and K. B. Efetov, Phys. Rev. B **68**, 064513 (2003).
[65] A. K. Feofanov, V. A. Oboznov, V. V. Bolginov, J. Lisenfeld, S. Poletto, V. V. Ryazanov, A. N. Rossolenko, M. Khabipov, D. Balashov, A. B. Zorin, P. N. Dmitriev, V. P. Koshelets, and A. V. Ustinov, Nat. Phys. **6**, 593 (2010).
[66] N. L. Schryer and L. R. Walker, J. Appl. Phys. **45**, 5406 (1974).
[67] C. W. J. Beenakker, Phys. Rev. Lett. **67**, 3836 (1991); C. W. J. Beenakker and H. van Houten, *ibid.* **66**, 3056 (1991).
[68] P. G. de Gennes, *Superconductivity of Metal and Alloys* (W. A. Benjamin, Inc., New York, 1966).
[69] Y. Tserkovnyak, A. Brataas, G. E. W. Bauer, and B. I. Halperin, Rev. Mod. Phys. **77**, 1375 (2005).
[70] A. A. Jara, C. Safranski, I. N. Krivorotov, C.-T. Wu, A. N. Malmi-Kakkada, O. T. Valls, and K. Halterman, Phys. Rev. B **89**, 184502 (2014).

Paper II

Electric-field control over spin-wave and current induced domain wall motion and magnonic torques in multiferroics

Submitted to Physical Review Letters (arXiv:1411.3327)

Electric-Field Control over Spin-Wave and Current Induced Domain Wall Motion and Magnonic Torques in Multiferroics

Iryna Kulagina and Jacob Linder
Department of Physics, Norwegian University of Science and Technology, N-7491 Trondheim, Norway
(Dated: November 12, 2014)

We discover that the way spin-waves exert magnetic torques in multiferroic materials can cause not only domain wall motion, but also magnetization dynamics for homogeneous magnetization textures. Interestingly, the domain wall motion can be controlled via purely electrical means with the spin-waves being generated by an ac electric field $\boldsymbol{E}$ while the direction of the wall motion also is sensitive to an applied dc $\boldsymbol{E}$ field. Moreover, we determine the interaction between spin-transfer torque from an electric current and a magnetic domain wall in multiferroics and show that the Walker breakdown threshold scales with the magnitude of a perpendicular electric field, offering a way to control the properties of domain wall propagation via electric gating.

Over the last decade, there has been a surge of interest in multiferroic materials [1–3] which displays simultaneously ferromagnetic/antiferromagnetic, ferroelectric, and/or ferroelastic order [4]. Besides the obvious allure of this multifunctionality from a practical viewpoint, such as usage for the purpose of magnetic random access memories [5, 6], the magnetoelectric cross-coupling between these orders is interesting from a fundamental physics perspective [7–13].

It is known that a wide variety of multiferroic materials host textured magnetic order parameter profiles [2] such as domain walls. Domain walls may be thought of as topological defects which interface different regions of a material and exhibit properties that differ from the ones in the homogeneous domains. Controlling the transport of magnetic domain wall structures is currently an active field of research [25] in spintronics as it offers an interesting way to transfer information in a non-volatile manner. In the context of multiferroics, inhomogeneous magnetic distributions $\boldsymbol{M}$ such as domain walls may induce an electric polarization $\boldsymbol{P}$ which opens up the possibility to influence magnetic domain walls via electric fields $\boldsymbol{E}$ [11]. Indeed, it has been experimentally shown that it is possible to manipulate magnetic domain wall structures via an external $\boldsymbol{E}$ field [14]. Magnetoelectric coupling has also been demonstrated to provide strain-controlled domain wall motion [15].

However, an analytical framework and understanding of how domain wall motion takes place in multiferroics when exposed to central driving forces in spintronics such as spin-polarized currents or spin-waves remains largely unexplored [17, 18]. In this paper, we answer the question: how does magnetic domain walls in multiferroics respond to the spin-transfer torque induced by electric currents and spin-waves?

We find that spin-waves generated in multiferroic materials are capable not only of causing domain wall motion, but even inducing torques on homogeneous magnetization textures. This is different from conventional homogeneous ferromagnets where no such spin-wave torque exists. Moreover, we find that the domain wall motion can be controlled fully electrically since the spin-waves may be generated by an ac $\boldsymbol{E}$ field while the velocity of the wall also is found to depend on the application of a constant dc $\boldsymbol{E}$ field. Again, this is different compared to the magnonic torque induced by spin-waves on domain walls in conventional ferromagnets where the wall moves toward the spin-wave source [20]. Finally, we show that the effect of a domain wall becoming distorted once exceeding a critical velocity, known as Walker breakdown, can be delayed by electric gating on magnetic domain walls in multiferroics under the influence of a current-induced spin-transfer torque.

Let us start by establishing the theoretical framework to be used in this work. To account for inhomogeneous magnetic textures the free energy under consideration includes the exchange interaction $F_{\text{exc}} = \int \mathrm{d}\boldsymbol{r} \frac{J}{2}(\nabla \boldsymbol{m})^2$ and anisotropy energy $F_{\text{an}} = \int \mathrm{d}\boldsymbol{r}(-\frac{K}{2}m_z^2 + \frac{K_\perp}{2}m_x^2)$, where the Zeeman-coupling due to an external magnetic field may also be included via $F_Z = -\int \mathrm{d}\boldsymbol{r}(\boldsymbol{M}\cdot\boldsymbol{B}_{\text{ext}})$. Above, J is the exchange coefficient while $\boldsymbol{M} = M_0\boldsymbol{m}$ is the magnetization with M_0 as its magnitude, $K > 0$ and $K_\perp > 0$ are constant of anisotropy for the easy and hard axis, while $\boldsymbol{B}_{\text{ext}}$ is the external magnetic field. Since the system under consideration is not a conventional ferromagnet, but rather a multiferroic, we must include the cross-coupling term between the electrical and magnetic degrees of freedom $F_P = -\int \mathrm{d}\boldsymbol{r}\boldsymbol{E}\cdot\boldsymbol{P}$ where the polarization induced by the magnetic texture is given by [16] (considering a cubic lattice symmetry for concreteness) $\boldsymbol{P} = \gamma_0[\boldsymbol{M}(\nabla\cdot\boldsymbol{M}) - (\boldsymbol{M}\cdot\nabla)\boldsymbol{M}]$. The magnitude of the magnetoelectric coupling coefficient is denoted γ_0.

The total free energy is then represented by $F = F_{\text{exc}} + F_{\text{an}} + F_Z + F_P$ and we make use of the Landau-Lifshitz-Gilbert equation (LLG) [23] to investigate the dynamics of a domain wall in this multiferroic system. We will in this work consider both the influence of spin-waves induced torques and current-induced torques, commencing with the latter. In this case, the standard phenomenological equation of motion used to describe the spin-transfer torque effect of an electric current is (in normalized form):

$$\frac{\partial \boldsymbol{m}}{\partial t} = -\boldsymbol{m}\times\boldsymbol{H}_{\text{eff}} + \alpha\boldsymbol{m}\times\frac{\partial \boldsymbol{m}}{\partial t} - u\frac{\partial \boldsymbol{m}}{\partial c} + \beta u\boldsymbol{m}\times\frac{\partial \boldsymbol{m}}{\partial c} \quad (1)$$

where α is the Gilbert damping constant, u is proportional to the current density, while β is the non-adiabatic term whose origin, although subject to some controversy, mostly is believed to be spin-relaxation processes that cause the itinerant electron spins constituting the current to not follow the do-

main wall profile fully adiabatically [22]. Although the magnetization is allowed to take any direction, we consider only variation along one spatial dimension (denoted c above) in order to provide analytical results. In what follows, we will consider time t in the unit of $(\gamma\mu_0 M_0)^{-1}$ where μ_0 is the vacuum permeability, γ is the gyromagnetic ratio, and use normalized length in the unit of $(J/M_0^2\mu_0)^{1/2}$. Finally, we express the current density parameter u in the unit of $\gamma\sqrt{J\mu_0}$, the free energy F and anisotropy constants K and $K_\perp$in the unit of $M_0^2\mu_0$, E in unit of $\gamma M_0\mu_0\sqrt{J\mu_0}$, and the magnetoelectric coupling constant γ_0 in the unit of $(\gamma M_0^2\mu_0)^{-1}$.

A key observation is that not all types of magnetic textures will provide a net magnetoelectric polarization $\boldsymbol{P}$: a net component of the magnetization along the direction of spatial variation v is required, thus ruling out Bloch walls. For this reason, we will focus here on Neel (NDW) and head-to-head domain walls (HDW). To be concrete, we choose easy-axis of magnetic anisotropy along the z direction and the hard axis along x direction (see Fig. for the schematic setup). Before we can explore the dynamics of multiferroic domain walls, one has to check whether an applied electric field alters the static domain wall profile itself. Some care must be exercised here, since we find that the validity of the usual Walker solution [24] for the domain wall profile depends on the orientation of the electric field relative the hard axis of anisotropy. For instance, the Walker profile is not valid for the NDW and HDW when the $\boldsymbol{E}$ field is applied along the hard-axis direction. Thus, we consider the electrical field as $\boldsymbol{E} = (0, 0, E_z)$ for NDW and $\boldsymbol{E} = (0, E_y, 0)$ for HDW. Due to our chocie for the coordinate axes, we can conventially write the normalized magnetization in the same way for both types of domain walls: $\boldsymbol{m} = (\sin(\theta)\cos(\phi), \sin(\theta)\sin(\phi), \sigma\cos(\theta))$, where $\theta(c) = 2\arctan[\exp^{(c-\chi)/\lambda}]$ where $c = y$ and $c = z$ for NDW and HDW correspondingly, λ is the DW width, χ is the position of the DW center, and the topological charge of the domain wall is σ. The azimuthal angle for the static Walker profile $\phi = \pm\pi/2$ for both our geometries and we assume that $K \gg K_\perp$ to justify the description of the domain wall as a solitonic object described only by the degrees of freedom associated with its center position and tilt angle [25].

The equation of motion for the center-coordinate $\chi(t)$ and the angle $\phi(t)$ is for the NDW

$$\alpha\sigma\dot{\chi} + \lambda\dot{\phi} = -\sigma\beta u + \lambda B_z \text{ and } \sigma\dot{\chi} - \alpha\lambda\dot{\phi} = -\sigma u - \frac{1}{2}\lambda K_\perp \sin(2\phi) + \sigma\lambda\pi\gamma_0 E_y\cos(\phi). \quad (2)$$

For the HDW, we have

$$\alpha\sigma\dot{\chi} + \lambda\dot{\phi} = -\sigma\beta u,\ \sigma\dot{\chi} - \alpha\lambda\dot{\phi} = -\sigma u - \frac{1}{2}\lambda K_\perp\sin(2\phi) - \frac{B_y}{\pi}\cos(\phi) + 2\sigma\lambda\pi\gamma_0 E_z\cos(\phi). \quad (3)$$

The behaviour of the domain wall is different in two regimes which separated by the Walker breakdown, defined by $\partial_t\phi \neq 0$. In the regime where there is no Walker breakdown, the following equations must be satisfied for NDW $\frac{u}{\varkappa_\perp} = \sin(2\phi) + b_{\text{NDW}} - \epsilon\cos(\phi)$ and for HDW $\frac{u}{\varkappa_\perp} = \sin(2\phi) + (b_{\text{HDW}} + \epsilon)\cos(\phi)$ where $\varkappa_\perp = \frac{\sigma\alpha\lambda K_\perp}{2(\beta-\alpha)}$, $b = B/B_0$, $\epsilon = E/E_0$, $E_0 = \frac{\sigma K_\perp}{4\pi\gamma_0}$, $B_{0,\text{HDW}} = \frac{\pi\lambda K_\perp}{2}$, $B_{0,\text{NDW}} = \frac{\alpha K_\perp}{2}$ This allows us to determine a quantity of central practical importance, namely the critical current density u_c at which Walker breakdown takes place. We find:

$$u_{\text{HDW},c} = \varkappa_\perp[b + \sqrt{2}f(\epsilon)/32],\ u_{\text{NDW},c} = \sqrt{2}\varkappa_\perp f(\epsilon')/32,$$
$$f(x) = (3x + \sqrt{x^2+32})[16 - x^2 + x\sqrt{x^2+32}]^{1/2} \quad (4)$$

where $\epsilon^{'} = b + \epsilon$. From this, the maximum domain wall velocity $V_{\text{DW},c}$ that is attainable before deformation sets in is computed via $V_{\text{DW},c} = -\beta u_c/\alpha$. The corresponding angles ϕ corresponding to the constant tilt angle of the DW are $\phi_{WB} = -\arcsin(\frac{1}{8}(\epsilon - \sqrt{\epsilon^2+32}))$ and $\phi_{WB} = \pi - \arcsin(\frac{1}{8}(\epsilon^{'} - \sqrt{(\epsilon^{'})^2+32}))$ for NDW and HDW, respectively. We here included the presence of a magnetic field for generality, and in the limit without any spin-transfer torque effect our expressions are consistent with Ref. [18]. Setting $B = 0$ in order to focus on the spin-transfer torque effect, it is seen from the above equations that the critical current in both the NDW and HDW case is the same and increases with E. This could be of practical importance since it offers a way to delay Walker breakdown induced by electric current, and increase the velocity of the domain wall transport, via a gate voltage. In Fig. 2, we plot the maximum domain wall velocity as a function of the applied electric field.

We now turn our attention to the question of how spin-waves interact dynamically with both homogeneous magne-

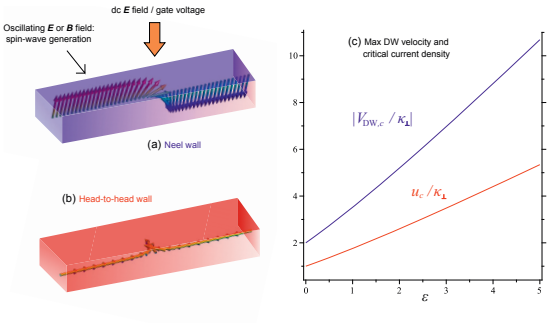

FIG. 1: (Color online) Schematic setup considered in this work. We consider two types of domain walls in multiferroics which give rise to a net electric polarization due to the magnetoelectric effect: (a) Neel and (b) head-to-head domain walls. An ac $\boldsymbol{E}$ or $\boldsymbol{B}$ field is applied transversely to the structure in order to generate spin-waves locally, which then propagate through the system and interact with the domain wall. We also allow for the possibility of a dc $\boldsymbol{E}$ field (gate voltage) applied across the top and bottom of the structure. In (c), we show how the maximum domain wall velocity attainable before Walker breakdown $V_{\text{DW},c}$ and the critical current density u_c scales with the applied normalized electric field ε. We have chosen parameters $\alpha = 0.01$ and $\beta = 0.02$.

tization textures and domain wall structures in multiferroic materials. As it turns out, these two situations are inseparable and must be considered together. The reason for this is that we find that *spin-waves induce a torque even on a homogeneous magnetization due to the magnetoelectric coupling*. To illustrate this effect analytically, consider a thin-film ferromagnet with propagating magnons where the magnetization lies in-plane (say, xz-plane). Writing out the effective field explicitly, we then have:

$$\begin{aligned}\boldsymbol{H}_{\text{eff}} &= J\partial_z^2\boldsymbol{m} + Km_x\hat{\boldsymbol{x}} + 2\gamma_0\partial_z m_z(E_x\hat{\boldsymbol{x}} + E_y\hat{\boldsymbol{y}}) \\ &\quad - 2\gamma_0\hat{\boldsymbol{z}}(E_x\partial_z m_x + E_y\partial_z m_y). \end{aligned} \tag{5}$$

To describe spin-wave propagation and its influence on the magnetic order parameter, we write the total normalized magnetization as $\boldsymbol{m} = (\sigma_0, \delta m_y + s_y, \delta m_z + s_z)$ where $\sigma_0 = \pm 1$ describes the equilibrium macrospin orientation, taking into account the possibility of ordering along both $\pm\hat{x}$ for the sake of generality. Moreover, δm_j and s_j describe the change in the magnetic order parameter and the spin-wave excitations, respectively, and are assumed to be small compared to σ_0 which allows for a perturbation treatment. With the above effective field, we insert $\boldsymbol{m}$ into the LLG equation and average over one spin-wave oscillation period. Discarding higher order terms, we are left with the following equations:

$$\begin{aligned} J\partial_z^2 m_z &= H_k m_z + \gamma_0 E_y \partial_z m_y + \gamma_0\sigma_0 E_x\langle s_z\partial_z s_z\rangle, \\ J\partial_z m_y &= H_k m_y + \gamma_0 E_y \partial_z m_z + \gamma_0\sigma_0 E_x\langle s_y\partial_z s_z\rangle. \end{aligned} \tag{6}$$

We also obtain a set of equations for the spin-wave amplitudes s_j to leading order:

$$\begin{aligned} \sigma_0\partial_t s_y + \alpha\partial_t s_z &= \gamma J\partial_z^2 s_z - \gamma s_z H_k + \gamma\gamma_0 E_y\partial_z s_y, \\ \sigma_0\partial_t s_z - \alpha\partial_t s_y &= -\gamma A\partial_z^2 s_y + \gamma s_y H_k - \gamma\gamma_0 E_y\partial_z s_z. \end{aligned} \tag{7}$$

The underlying assumption here is that the spin waves vary on a much shorter time scale than the magnetization texture, as is reasonable. Consider first the case with an electric field only along the $\hat{\mathbf{x}}$-direction of the film, such that $E_y = 0$. Remarkably, the above equations then become formally equivalent to the equations of motion for spin-waves and subsequent change in magnetization due to the torque from the spin-waves as occurring in both topological insulators [19] and ferromagnets with Dzyaloshinskii-Moryia interaction [21]. We may thus immediately conclude that there is a *spin-wave induced magnetoelectric torque* acting even homogeneous magnetization textures in multiferroic materials. This effect vanishes completely if one sets the magnetoelectric coupling γ_0 to zero. What is more, however, the present case appears to offer additional physics compared to the aforementioned scenarios: if we allow for an out-of-plane component for the electric field, $E_y \neq 0$, an extra term proportional to $\partial_z s_j$ and $\partial_z \delta m_j$ appear in Eqs. (6) and (7). This term influences the magnonic torque and offers an additional way to control it which differs from the influence of the in-plane electric field component. The influence of the new term $\propto E_y$ complicates the analytical solution, and so we choose to proceed via a numerical route in order to also investigate the influence of magnons on inhomogeneous spin-textures in multiferroics.

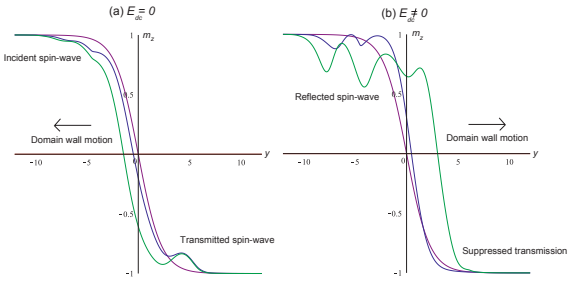

FIG. 2: (Color online) Plot of spin-wave induced domain wall motion via a transverse AC electric field E_{ac}. The normalized parameters used are $\omega = 0.75, K = 0.2, K_\perp = 0.01, E_{\text{ac}}\gamma_0 = 5, \alpha = 0.01$. In (a), there is no gate voltage field E_{dc} and we present snapshots of the instantaneous domain wall profile at normalized times $t = 0$ (static profile, purple line), $t = 22$, and $t = 47$. In (b), we set $E_{\text{dc}}\gamma_0 = 2$ and consider times $t = 0, 15, 21$.

We are now in a position to determine how spin-waves interact with a domain wall texture, which thus also requires their interaction with the homogeneous part of the domains to be taken into account according to the above results. This is different from previous works on magnon-induced domain wall motion in ferromagnets [20], where no such homogeneous torque is present. We have thus solved the full LLG equation without any perturbative approximations where the initial profile at $t = 0$ consists of a magnetic domain wall center around $z = 0$. Anti-reflection boundary conditions were implemented near the edges of the system in order to remove spin-wave backscattering, modelled by allowing the Gilbert damping α to rise rapidly very close to the edges. As a consistency check against previous works, we verified that spin-wave generation via an ac external magnetic field $\boldsymbol{B}(t)$, applied locally in a small region of one of the domains, induced motion in the opposite direction of the magnon flow.

Turning now to the present multiferroic system, we now demonstrate that the presence of the magnetoelectric coupling in the effective field offers a new result compared to previous work on spin-wave induced domain wall motion. Since a gradient in the magnetization couples to the electric field, one could envision that not only an ac magnetic field could drive spin-wave induced domain wall motion, but that the same could take place via an *ac electric field*. An important aspect of realizing such an effect is that the electric field would have to be applied in a region where there was a magnetization gradient, in effect not too deep inside the domains with fixed magnetization direction. To determine if electric-field induced domain wall motion via magnons is possible, we applied an ac electric field $\boldsymbol{E}(t)$ locally near the domain wall region and the result is shown in Fig. 2(a) (see figure caption for parameters used). As seen, the spin-waves emanating from this procedure indeed trigger domain wall motion and thus demonstrates the possibility to achiev electric control over magnon-induced

magnetization texture transport. Remarkably, we find that even the direction of motion of the domain wall can be controlled by applying an additional constant gate-field: whereas the domain wall moves towards the spin-wave source without any such dc field, it moves away from the domain wall in its presence. This finding suggests that the magnetoelectric coupling alters the effective potential felt by the spin-waves as they propagate through the domain wall, causing it to deviate from the reflectionless potential which is experienced by spin-waves in conventional ferromagnets with a belonging phase shift after passing through the wall [20]. In fact, the physical mechanism behind this effect is suggested by closer inspection of the curves in Fig. 2. When $E_{\rm dc} = 0$, the spin-waves pass through the domain wall and the wall moves toward the spin-wave source due to conservation of angular momentum. However, when $E_{\rm dc} \neq 0$, it is seen that no spin-waves emanate on the other side of the domain wall: instead, they are reflected and the domain wall moves *away* from the spin-wave source due to a transfer of linear momentum p. In this way, the direction of the domain wall motion is controllable by a gate voltage effect.

We have investigated the interaction between the spin-waves and the domain wall over a range of magnitudes for $E_{\rm dc}$ and find that it alters the amount of spin-wave reflection: Fig. 2(b) shows a scenario where the reflection is almost complete. An analytical description of this effect has proven elusive to us so far, due to the complicating factor of the spin-wave torque acting even on the homogeneous domains of the magnetization profile, although this is work in progress. We note that linear-momentum transfer of spin-waves to domain walls in ferromagnets have also been investigated in Ref. [26], and been shown to be possible at special resonance frequencies of the applied dc $\boldsymbol{B}$ field. In our treatment of the current-induced case, the dominant effect of the applied current is the spin-transfer torque effect described by the two last terms in Eq. (1) and not the associated electric field along the structure which accompanies such a current, an approximation which should be better the higher conductivity the multiferroic is (in order to reduce the required voltage-drop, and thus field $\boldsymbol{E}$, that generates the current). Candidate materials for the effects predicted in this work include epitaxial iron garnet films, which when grown on (210) and (110) gadolinium-gallium garnet substrates generates a Neel component of the domain wall structure due to anisotropy and hence activates the magnetoelectric coupling [14]. We also note that very recently, domain wall motion via electric field was observed in a hybrid multiferroic consisting of ferromagnetic-ferroelectric heterostructure [27].

Concluding, we have here demonstrated that domain wall motion in multiferroic materials hosts a wealth of interesting effects which are distinct from conventional ferromagnets in terms of its response to spin-wave and current-induced torques, including the possibility to control the direction of the domain wall motion via a gate voltage, and hope that these findings may stimulate further investigations.

Acknowledgments. This work was supported by the Research Council of Norway, Grant No. 205591/F20 (FRINAT) and Grant No. 216700.

[1] 1 G. Lawes, G. Srinivasan, J. Phys. D: Appl. Phys. **44**, 243001 (2011).
[2] A. P. Pyatakovand A. K. Zvezdin, Phys.Usp.**55**,557 (2012).
[3] L. W. Martin *et al.*, J. Phys: Condens. Matter **20** 434220 (2008); H. Bea *et al.*, J. Phys: Condens. Matter **20** 434221 (2008).
[4] H. Schmid, Ferroelectrics **162**,317 (1994).
[5] M. Gajek *et al.*, Nature Mater. **6**, 296 (2007).
[6] M. Bides *et al.*, Nature Mater. **7**, 425 (2008).
[7] G. Catalan *et al.*, Rev. Mod. Phys. **84**, 119 (2012).
[8] J. F. Scott, Science **315**, 954 (2007).
[9] L. D. Landau and E. M. Lifshitz. *Electrodynamics of Continuous Media* (Oxford: Pergamon Press, 1984).
[10] G. A. Smolenskii and I. Chupis, Sov. Phys. Usp. **25**, 475 (1982).
[11] V. G. Baryakhtar V G, V. A. Lvov, and D. A. Yablonskii, JETP Lett. **37**673 (1983).
[12] Y. J. Choic *et al.*, Phys Rev Lett. **105**, 097201 (2010).
[13] Y. H. Chu *et al.*, Nature Mater. **7**, 478 (2008)
[14] A. S. Logginov *et al.*, Appl. Phys. Lett. **93**, 182510 (2008)
[15] N. Lei *et al.*, Nature Comm. **4**, 1378 (2013).
[16] M. Mostovoy, Phys. Rev. Lett. **96**, 067601 (2006).
[17] F. Kagawa *et al.*, Phys. Rev. Lett. **102**, 057604 (2009).
[18] H.-B. Chen, Y.-H. Liu, Y.-Q. Li, J. Appl. Phys. **115**, 133913 (2014)
[19] J. Linder, Phys. Rev. B **90**, 041412(R) (2014).
[20] P. Yan, X. S. Wang, and X. R. Wang, Phys. Rev. Lett. **107**, 177207 (2011).
[21] A. Manchon *et al.*, arXiv:1401.0883.
[22] G. Tatara and H. Kohno, Phys. Rev. Lett. **92**, 086601 (2004); S. Zhang and Z. Li, Phys. Rev. Lett. **93**, 127204 (2004); A. Thiaville, Y. Nakatani, J. Miltat, and Y. Suzuki, Europhys. Lett. **69**, 990 (2005).
[23] L. D. Landau and E. M. Lifshitz, Phys. Z. Sowjetunion **8**, 153 (1935); T. L. Gilbert, IEEE Trans. Magn. **40**, 3443 (2004).
[24] N. L. Schryer and L. R. Walker, J. Appl. Phys. **45**, 5406 (1974).
[25] J. Shibata *et al.*, J. Phys. D: Appl. Phys. **44**, 384004 (2011); J. Grollier *et al.*, C. R. Physique **12**, 399 (2011).
[26] J.-S. Kim *et al.*, Phys. Rev. B **85**, 174428 (2012).
[27] B. Van de Wiele *et al.*, Appl. Phys. Lett. **104**, 012401 (2014).

Paper III

Controlling superconducting spin-flow with spin-flip immunity using a single homogeneous ferromagnetic layer

Submitted to Physical Review Letters (arXiv:1510.02488)

Controlling superconducting spin flow with spin-flip immunity using a single homogeneous ferromagnet

Sol H. Jacobsen, Iryna Kulagina, and Jacob Linder

Department of Physics, Norwegian University of Science and Technology, N-7491 Trondheim, Norway

Spin transport via electrons is typically plagued by Joule heating and short decay lengths due to spin-flip scattering. It is known that dissipationless spin currents can arise when using conventional superconducting contacts, yet this has only been experimentally demonstrated when using intricate magnetically inhomogeneous multilayers, or in extreme cases such as half-metals with interfacial magnetic disorder. Moreover, it is unknown how such spin supercurrents decay in the presence of spin-flip scattering. Here, we present a method for generating a spin supercurrent by using only a single homogeneous magnetic element. Remarkably, the spin supercurrent generated in this way does not decay spatially, in stark contrast to normal spin currents that remain polarized only up to the spin relaxation length. We also expose the existence of a superconductivity-mediated torque even without magnetic inhomogeneities, showing that the different components of the spin supercurrent polarization respond fundamentally differently to a change in the superconducting phase difference. This establishes a mechanism for tuning dissipationless spin and charge flow separately, and confirms the advantage that superconductors can offer in spintronics.

Current research in spintronics is attracting much attention, in large part due to the pivotal role that the quantum spin degree of freedom plays in an increasingly wide class of physical systems, ranging from ultracold atoms at the micro-Kelvin temperature scale to topological insulators at room-temperature. Spin transport in superconductors[1–3], which historically predated spin transport experiments in non-superconducting materials[4], have recently re-emerged as a potential avenue for enhancing and discovering new phenomena in spintronics. Recent results are encouraging, with experiments demonstrating not only infinite magnetoresistance[5], but also strongly enhanced quasiparticle spin lifetimes[6], spin relaxation lengths[7], spin Hall effects[8], and thermoelectric currents[9] compared with non-superconducting structures.

Creating and manipulating spin-flow is the central feature of superconducting spintronics[10,11]. It is known that in the presence of magnetically inhomogeneous structures, such as multilayers or ferromagnets with intrinsic textures such as domain walls, spin-polarized Cooper pairs can emerge[12] which thus carry not only charge but also spin supercurrents[13–17]. Experimentally, it has been demonstrated[18–21] that a dissipationless charge-current can flow through strong ferromagnets over distances far exceeding the penetration depth of conventional superconducting order into magnetic materials. This occurs precisely due to the creation of triplet Cooper pairs which are spin-polarized and thus insensitive to the pair-breaking effect of a magnetic Zeeman-field. In fact, triplet Cooper pairs were newly experimentally observed inside a conventional superconductor[22,23]. In very recent developments, it has been shown that intrinsic spin-orbit coupling offers an alternative avenue for generating the long-range (LR) triplet component[24,25]. In that case the appearance of the LR component depends on the relationship between the spin-orbit coupling and the exchange field, with the LR triplet defined as having its spin aligned with the exchange field. This is in contrast to the short-ranged (SR) triplet component which has its spin perpendicular to the field, and is thus vulnerable to pair-breaking in the same way as conventional singlet Cooper pairs. As we will show below, these recent developments will have profound consequences for the generation of spin supercurrents in spintronics.

To date, structures with magnetic inhomogeneities such as multiple magnetic layers have been required to create long-ranged spin-supercurrents[18–21]. This can be experimentally challenging for several reasons, primarily because it is far from trivial to exert control over the individual layers of magnetically inhomogeneous structures, and can be complicated yet further if the magnetic layer has intrinsic texture (such as the spiral order in Ho). Here we will show that it is possible to create a spin-polarized supercurrent using just *one single homogeneous magnetic element*, which eliminates the experimental complexities and heralds a new era for harnessing the dissipationless spin-flow of superconductors in spintronics. In addition to this reduction of complexity in producing a spin supercurrent, we show that this spin supercurrent does not decay even in the presence of spin-flip processes, *e.g.* via magnetic impurities or spin-orbit impurity scattering. This spin-flip immunity is fundamentally different from spin currents in non-superconducting structures which remain polarized for the duration of the spin relaxation time. Finally, we show that the spin polarization components of the supercurrent respond qualitatively differently to a change in the superconducting phase difference ϕ. The surprising consequence of this is that the dissipationless charge flow and spin flow can be tuned separately. In particular, both the magnitude and the polarization direction of the spin flow is controlled via the superconducting phase, offering an entirely new way to control spin transport.

Spin supercurrent with a single homogeneous ferromagnet

Consider the thin-film heterostructure depicted in Fig. **1**, which shows a Josephson junction of conventional s-wave superconductive sources with normal and ferromagnetic elements typically utilized in proximity effect experiments. We will now show that a long-ranged spin supercurrent is sustained in the junction even when only a single homogeneous ferromagnet is used. The key to achieving this is to deposit a very thin layer of a heavy normal metal such as gold or platinum at the superconducting interfaces. Recent experiments in the context of magnetization switching have shown that such interfaces will produce strong Rashba spin-orbit coupling due to the high atomic number of the metal and the interfacially broken inversion symmetry[26]. The magnetic element consists of a ferromagnetic alloy which has both an in- and out-of-plane component, achievable by using *e.g.* PdNi or CuNi, which can both feature out-of-plane magnetocrystalline anisotropy in thin-films[27,28]. It is clear, therefore, that no magnetic inhomogeneities are required, and the ferromagnet does not need to feature any intrinsic spin-orbit coupling. This is in contrast to previous works that have considered long-ranged currents in either magnetically textured junctions (see *e.g.* Refs. 13,29,30) or intrinsically spin-orbit coupled ferromagnets[24,31,32], where spin is not a conserved quantity, with several magnetic layers[25]. In our setup, only a single homogeneous ferromagnet is required because the heavy normal metals supply the spin-orbit coupling, significantly reducing the

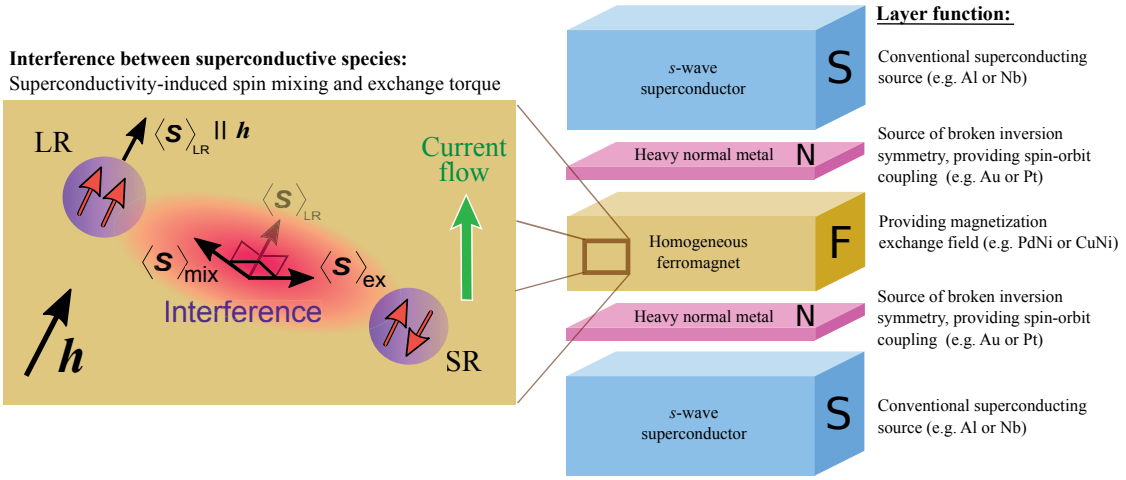

FIG. 1: **Proposed experimental setup and interference mechanism**. Schematic illustration of the thin-film superconducting junction within which a spin supercurrent is generated, which does not decay even in the presence of spin-flip scattering. There are two experimentally feasible ways to construct the thin-film such that the spin supercurrent appears. In the case where only Rashba spin-orbit coupling is present in the heavy-metal layers, the homogeneous ferromagnet is chosen to have out-of-plane magnetocrystalline anisotropy, such as the commonly available PdNi or CuNi[27,28]. In combination with the shape-anisotropy of the thin-film geometry, the exchange field within the ferromagnet will then have both an in-plane and out-of-plane component. If both Rashba and Dresselhaus spin-orbit coupling is present in the normal layers, *e.g.* by using a two-dimensional electron gas such as GaAs, the ferromagnet only needs an in-plane component. In both cases, this induces an interference effect between the long-ranged and short-ranged Cooper pairs, which results in a spin mixing term and an exchange torque, which acts on the magnetization and is present even in the absence of a charge current.

previously required level of junction complexity in order to host a spin supercurrent. Furthermore, as an alternative experimental scenario, it is possible to use a ferromagnet with a purely in-plane exchange field by employing normal layers that contain both Rashba and Dresselhaus coupling. Examples include crystals that lack an inversion structure and two-dimensional electron gases such as gallium arsenide. In this case, the singlet-triplet conversion is greatly enhanced[33,34], resulting in stronger supercurrents (see Fig. **2**).

The spin-supercurrent $\boldsymbol{I}_S$ may be computed via the quasiclassical Green function $\check{g}$ according to the formula[14]:

$$\boldsymbol{I}_S = I_{S_0} \int_{-\infty}^{\infty} \mathrm{d}\varepsilon \mathrm{Tr}\{\hat{\rho}_3 \hat{\boldsymbol{\tau}} (\check{g}\partial_z \check{g})^K\}. \quad (1)$$

Here, we have defined $\hat{\boldsymbol{\tau}} = \mathrm{diag}(\boldsymbol{m}\cdot\boldsymbol{\sigma}, \boldsymbol{m}\cdot\boldsymbol{\sigma}^*)$, where $\boldsymbol{m}$ is the desired polarization-direction of the spin supercurrent and $\boldsymbol{\sigma}$ is the vector of Pauli matrices, ε denotes the quasiparticle energy and K the Keldysh component of the Green function. $I_{S_0} = N_0\hbar D A\Delta/8L_F$, where N_0 is the normal-state density of states at the Fermi level, D the diffusion constant and A the interfacial contact area. The integral in Eq. (1) is dimensionless since the energies have been normalized to the bulk superconducting gap Δ and lengths normalized to the ferromagnet length L_F. The matrix $\hat{\rho}_3 = \mathrm{diag}(1,1,-1,-1)$. To find the Keldysh component we use the equilibrium relation

$$(\check{g}\partial_z\check{g})^K = [\hat{g}^R\partial_z\hat{g}^R + (\hat{\rho}_3\hat{g}^R\partial_z\hat{g}^R\hat{\rho}_3)^\dagger]\tanh(\beta\varepsilon/2), \quad (2)$$

where R and A denote the retarded and advanced components of $\check{g}$ respectively and $\beta = 1/k_BT$ is the inverse temperature with k_B being the Boltzmann constant. We find $\hat{g}^R$ by solving the Usadel equation for the system shown in Fig. **1** both analytically in the weak proximity effect and numerically in the full proximity effect regime using the NOTUR supercomputer cluster (Kongull); see Methods for further details. We can then compute the spin supercurrent from Eq. (1), and the charge supercurrent $\boldsymbol{I}_Q$ can be obtained from the same formula by removing $\hat{\boldsymbol{\tau}}$ from the trace and taking $I_{S_0} \to 2I_{S_0}e/\hbar = I_{Q_0}$, where e is the electronic charge.

The critical charge supercurrent $\boldsymbol{I}_Q^C$, obtained at a phase-difference[41] $\phi = \pi/2$, is shown in Fig. **2a**, demonstrating that it becomes long-ranged even if there is no magnetic inhomogeneity and only a single ferromagnet is used. The physical mechanism behind this effect is that the spin-orbit coupling present in the thin, heavy normal metal layers rotates the triplet Cooper pairs due to an anisotropic spin relaxation[25]. The spin-orbit coupling is described by α and β, being respectively the Rashba and Dresselhaus coefficients. These are normalised to the superconducting gap Δ and length of normal metal L_N in such a way that with a niobium superconductor of gap $\Delta \approx 3$ meV, $\alpha = 0.5/L_N$ corresponds to a Rashba parameter of the order 3×10^{-12} eV m. It is clear from Fig. **2a** that the critical current decays rapidly in the absence of spin-orbit coupling ($\alpha = \beta = 0$), and that this decay is strongly suppressed by the inclusion of spin-orbit coupling (note the log scale).

To model the ferromagnet, we assumed an exchange field $\boldsymbol{h} = h(0, \cos\theta, \sin\theta)$, with a strength $h/\Delta = 50$ and a canting of $\theta = 0.3\pi$ between the in- and out-of-plane components. The supercurrent exists for any orientation of the exchange field $\theta \in (0, \pi/2)$ and we will later discuss the precise dependence on the canting angle θ. We choose $\tilde{G}_{MR} = 0.2$ for the normalized interfacial magnetoresistance term and $\tilde{G}_\theta = 1$ for the interfacial scattering phase shift on both sides[35]. In this case, and with a typical superconducting coherence length of $\xi_S = 25$ nm, the LR component dominates for ferromagnets of length L_F greater than $\sim$ 10 nm, causing the critical current $\boldsymbol{I}_Q^C$ to decay slowly despite the presence of an ex-

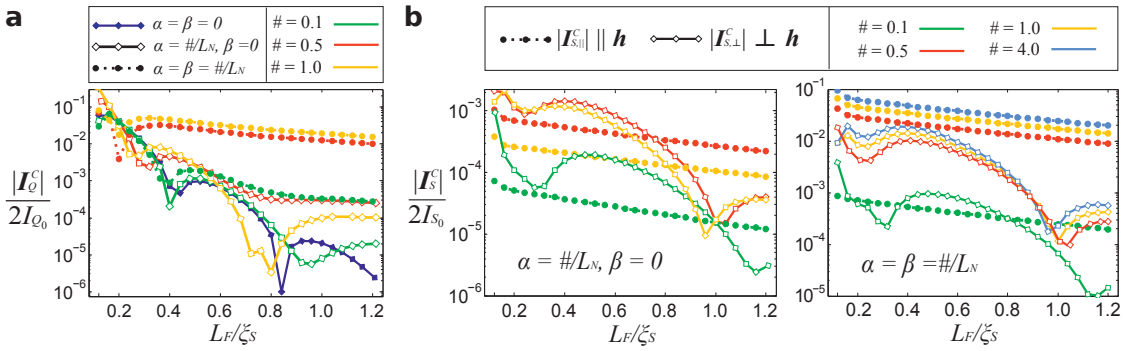

FIG. 2: **Charge and spin supercurrent vs. length**. The magnitude of the critical charge current $\boldsymbol{I}_Q^C$ (**a**) and the components of the critical spin current $\boldsymbol{I}_S^C$ (**b**) in the ferromagnet as a function of the length of the layer L_F is shown on a logarithmic scale. In the presence of spin-orbit coupling, the current becomes long-ranged as it makes a transition from an exponential decay with superimposed oscillations to a much slower decay with respect to L_F. For long ferromagnetic junctions, it is clear that the charge current is almost entirely due to the long-range component. Including both Rashba and Dresselhaus coupling results in a substantial enhancement of the critical charge currents compared with pure Rashba coupling. We assume bulk superconductivity in the superconductors, an exchange field $\boldsymbol{h} = 50\Delta(0, \cos\theta, \sin\theta)$ with $\theta = 0.3\pi$, and a normal metal layer length of $L_N/\xi_S = 0.08$. The spin-orbit coupling parameters are normalised to the superconducting gap and length of normal metal in such a way that with a niobium superconductor with gap $\Delta \approx 3$ meV and coherence length $\xi_S = 25$ nm, $\alpha = 0.5/L_N$ corresponds to Rashba coupling of the order 3×10^{-12} eV m.

change field $h \gg \Delta$, remaining orders of magnitude larger than the SR component for increasingly long ferromagnets. In this scheme, the associated current densities for a sample length $L_F \sim 10$ nm will be of the order $|j_Q^C| \sim 10^3$ A/cm^2 without spin-orbit coupling, and 1-2 orders higher with its inclusion (see Methods for details). This corresponds well with charge current densities measured in the experiment of Ref. 36, which also used a CuNi alloy as the ferromagnet. For stronger exchange fields, the LR component will dominate for even shorter junctions, but the overall current magnitude will be suppressed. The supercurrent carried by the LR Cooper pairs can be significantly enhanced by including Dresselhaus coupling, as can be seen from the dotted line in Fig. **2a**, in which case the achievable critical charge current is much greater than with Rashba coupling alone.

We now turn to the spin supercurrent. Without spin-orbit coupling, no spin-current flows in the junction since there exists no mechanism for converting from the SR to the LR component. In order to demonstrate the physical origin of the dissipationless spin current and its different polarization components, it is useful to first decompose the triplet correlations in the system into their long-ranged and short-ranged contribution: $\boldsymbol{f} = \boldsymbol{f}_{\rm LR} + \boldsymbol{f}_{\rm SR}$. To take an explicit example, consider the case with pure Rashba coupling and an exchange field $\boldsymbol{h} = (0, h_y, h_z)$. In that case, we may write the general expressions:

$$\begin{aligned} \boldsymbol{f}_{\rm LR} &= (f_x, -fh_z/h, fh_y/h), \\ \boldsymbol{f}_{\rm SR} &= (0, f'h_y, f'h_z)/h, \end{aligned} \tag{3}$$

so that $\boldsymbol{f}_{\rm LR} \cdot \boldsymbol{h} = 0$ when $\boldsymbol{f}_{\rm SR} \parallel \boldsymbol{h}$. Now, the spin expectation vector of a triplet Cooper pair is obtained by $\langle \boldsymbol{S} \rangle = \mathrm{i}\boldsymbol{f} \times \boldsymbol{f}^*$. Inserting the long-ranged state $\boldsymbol{f}_{\rm LR}$, one obtains $\langle \boldsymbol{S} \rangle_{\rm LR} = 2\mathrm{Im}\{f^* f_x\}(h_y \hat{\boldsymbol{y}} + h_z \hat{\boldsymbol{z}})/h$. This means that the spin of the LR Cooper pairs points along the exchange field, as expected. Similarly, one finds that $\langle \boldsymbol{S} \rangle_{\rm SR} = 0$ for the SR Cooper pairs. However, there exists an additional contribution. The spin expectation vector of the total proximity-induced superconducting state may be written

$$\begin{aligned} \langle \boldsymbol{S} \rangle_{\rm tot} &= \mathrm{i}(\boldsymbol{f}_{\rm LR} + \boldsymbol{f}_{\rm SR}) \times (\boldsymbol{f}_{\rm LR}^* + \boldsymbol{f}_{\rm SR}^*) \\ &= \langle \boldsymbol{S} \rangle_{\rm LR} + \langle \boldsymbol{S} \rangle_{\rm SR} + (\mathrm{i}\boldsymbol{f}_{\rm LR} \times \boldsymbol{f}_{\rm SR}^* + \mathrm{h.c.}). \end{aligned} \tag{4}$$

It follows that there exists a novel *interference term* $\langle \boldsymbol{S} \rangle_{\rm int} = \mathrm{i}\boldsymbol{f}_{\rm LR} \times \boldsymbol{f}_{\rm SR}^* + \mathrm{h.c.}$ between the LR and SR Cooper pairs, which upon insertion of $\boldsymbol{f}_{\rm LR}$ and $\boldsymbol{f}_{\rm SR}$ is found to contain two terms, $\langle \boldsymbol{S} \rangle_{\rm int} = \langle \boldsymbol{S} \rangle_{\rm ex} + \langle \boldsymbol{S} \rangle_{\rm mix}$, where

$$\langle \boldsymbol{S} \rangle_{\rm ex} = 2\mathrm{Im}\{(f')^* f\}\hat{\boldsymbol{x}}, \tag{5}$$

$$\langle \boldsymbol{S} \rangle_{\rm mix} = 2\mathrm{Im}\{(f')^* f_x\}(\hat{\boldsymbol{y}} h_z - \hat{\boldsymbol{z}} h_y)/h. \tag{6}$$

The *exchange* term $\langle \boldsymbol{S} \rangle_{\rm ex}$ of Eq. (5) is independent of the direction of the field $\boldsymbol{h}$. In contrast, the second term changes its spin-polarization direction as $\boldsymbol{h}$ is altered. We will explain the physical meaning of each of these terms in the section below. Before doing so, we briefly discuss how the spin-polarization of the critical current depends on the length of the ferromagnet. This is shown for the critical spin supercurrent in Fig. **2b**, displaying both the component parallel with the exchange field $\boldsymbol{I}_{S,\parallel}^C \parallel \boldsymbol{h}$ and the magnitude of the perpendicular components, $|\boldsymbol{I}_{S,\perp}^C| = (\boldsymbol{I}_{S,\rm ex}^2 + \boldsymbol{I}_{S,\rm mix}^2)^{1/2}$. It is clear that the polarization of the spin supercurrent along the magnetization direction has a qualitatively different behavior with the length of the system compared with the polarization perpendicular to the exchange field, which oscillates within its typical exponential decay. The reason for this is that the perpendicular component appears due to the interference between the LR and SR Cooper pairs, and thus is limited by the penetration depth of the short-ranged superconducting correlations. Note that there is a non-monotonic relationship between the maximal supercurrents and the magnitude of the spin-orbit coupling, in the same way as there exists a non-monotonic relation between the density of states and spin-orbit coupling in a ferromagnet[33].

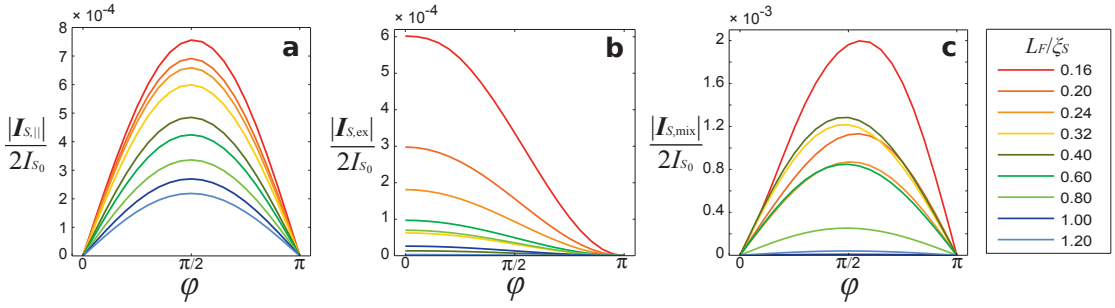

FIG. 3: **Controlling spin flow and polarization via superconducting phase difference**. The dependence of the spin supercurrent on the phase difference ϕ between the superconductors of the junction illustrated in Fig. 1 is shown. The component parallel to the exchange field $\boldsymbol{h} = h(0, \cos\theta, \sin\theta)$ is given in **a**, the component perpendicular to the field polarized in the x-direction in **b** and the perpendicular component along $(0, \sin(\theta), -\cos(\theta))$ in **c**. The spin-orbit coupling is chosen to be of pure Rashba type with $\alpha = 0.5/L_N$, and the parameters used are otherwise the same as in Fig. **2**. Results with both Rashba and Dresselhaus coupling are qualitatively similar, with consistently higher current magnitudes.

Controlling spin polarization with the superconducting phase

By analyzing the dependence of the spin supercurrent on the phase difference between the superconductors, it becomes clear that there is another fundamental difference between the parallel and perpendicular components. We will prove that *(i)* there exists a superconductivity-mediated exchange interaction in the system, even in the absence of any charge supercurrent and magnetic inhomogeneities, which acts with a torque on the magnetic order parameter and that *(ii)* both the magnitude and polarization direction of the spin supercurrent can be tuned via the superconducting phase difference.

The phase-dependence of the component of the spin supercurrent parallel to the exchange field, $\boldsymbol{I}_{S,\parallel}$, is plotted in Fig. **3a**, and shows the expected first-order sinusoidal dependence on the phase difference ϕ. This is physically reasonable since this component of the spin supercurrent is carried exclusively by the LR Cooper pairs which are polarized along the exchange field. When considering the perpendicular components of the spin supercurrent, however, the analysis in the preceding section showed that there exists two contributions $\boldsymbol{I}_{S,\text{ex}}$ and $\boldsymbol{I}_{S,\text{mix}}$ that originate from a novel interference between the LR and SR Cooper pairs. In order to unveil the physical meaning of these terms, we plot the variation of these with ϕ in Figs. **3b** and **c**. It is seen that these polarization components exhibit a fundamentally different response to the superconducting phase difference: $\boldsymbol{I}_{S,\text{ex}}$ is invariant under time-reversal $\phi \to (-\phi)$ and finite even in the absence of any phase difference $\phi = 0$ where no net charge current flows, whereas $\boldsymbol{I}_{S,\text{mix}}$ is antisymmetric under time-reversal. In effect, there exists a pure spin supercurrent flow without any charge current contamination in the system, even in the *absence* of any magnetic inhomogeneities or half-metallicity.

Based on these observations, we offer the following interpretation of our findings. The polarization component of the spin supercurrent $\parallel \boldsymbol{h}$ is understood simply as the polarization of the LR Cooper pairs that carry the long-ranged charge current and thus obeys the same type of current-phase relation as the charge current itself, vanishing both at $\phi = 0$ and $\phi = \pi$. The interference between the SR and LR Cooper pairs now provides the spin supercurrent components with distinct physical origins. The term $\boldsymbol{I}_{S,\text{mix}}$ represents the spin polarization that arises due to interference between LR and SR pairs carrying charge current, and is thus qualitatively similar to the charge current itself, with a $\sin\phi$ profile. In contrast, the term $\boldsymbol{I}_{S,\text{ex}}$ represents something more exotic: *it is a superconductivity-induced exchange torque acting on the magnetization, which is present even in the absence of any charge current*. From its numerical evaluation, we find that it may be written as $|\boldsymbol{I}_{S,\text{ex}}| = \mathcal{J}_1 + \mathcal{J}_2 \cos\phi$, with the constants $\{\mathcal{J}_1, \mathcal{J}_2\}$ depending on system-specific details such as the strength of the exchange field h, the length of the ferromagnet L_F and the strength of spin-orbit coupling α. This means that the exchange spin supercurrent is invariant under $\phi \to (-\phi)$ and that it has a term that is independent of the superconducting phase difference. The physical origin of this term is the following. Due to the proximity effect, both LR and SR superconducting correlations are induced in the ferromagnet in the presence of the inversion-symmetry breaking normal metal layers. The interference between these correlations create, according to Eq. (5), a net spin moment. Since this moment is misaligned with $\boldsymbol{h}$, it acts with a torque on the magnetic order parameter $\boldsymbol{h}$, attempting to rotate it so that the net torque vanishes. The presence of magnetic anisotropy in the system could be expected to attempt to counteract this torque. Importantly, this effect is present even without any net charge flow ($\phi = 0$) and exists with just a single, homogeneous ferromagnet. This is evident by comparing Figs. **3b** and **c**, where the different polarization components of the spin supercurrent are plotted against the superconducting phase difference. This result shows that the magnitude and polarization direction of a dissipationless spin current can both be tuned exclusively via the superconducting phase difference, which is a surprising finding that offers a new way to control spin flow. The superconducting phase difference may itself be set in the conventional way via current-bias, or by applying an external magnetic flux in a loop-geometry[37]. We underline that this superconductivity-mediated exchange interaction is very different from exchange interactions in *e.g.* conventional spin-valves with two ferromagnets, where a deviation from the parallel or antiparallel configuration produces a net equilibrium spin current that tries to align the magnetizations via a spin-torque[38–40]. In contrast, here such a torque exists even with a single, homogeneous ferromagnet due to a unique interference effect between long-ranged and short-ranged triplet Cooper pairs.

It is clear from Fig. **3** that the maximal spin-current polarized along the exchange field is achieved around $\phi = \pi/2$, corresponding well with the definition of the critical spin current[41], taken to be the spin polarization of the critical charge current. These simulations were run for a canting angle of $\theta = 0.3\pi$, and since this angle is in large part determined by material and geometry constraints it is

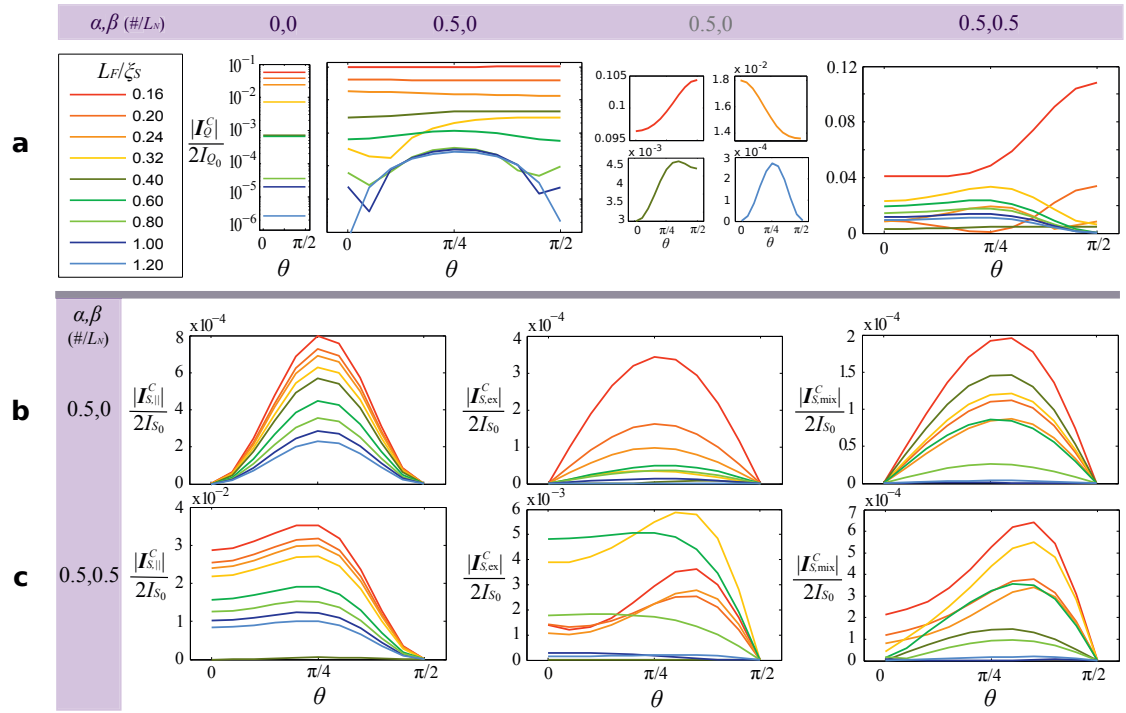

FIG. 4: **Charge- and spin-current vs. canting angle**. The effect of the canting angle θ between the in- and out-of-plane components of the exchange field $\boldsymbol{h} = 50\Delta(0, \cos\theta, \sin\theta)$ is shown for the charge current in **a**, and for the spin-current components in **b** and **c**. Without spin-orbit coupling, the charge current does not depend on the magnetization orientation, and there is zero spin-current. With Rashba spin-orbit coupling we see a significant enhancement in the charge current, with a canting profile stabilising towards a sinusoidal maximum at $\theta = \pi/4$ for increasingly large ferromagnets as the long-ranged triplet component become dominant. The parallel component of the spin-current monotonically decreases with ferromagnet length, while the perpendicular components are sensitive to the 0-π transition in the ground state. The inclusion of Dresselhaus spin-orbit coupling yields a dramatic increase in both charge- and spin-current, and it is evident that purely in-plane magnetization ($\theta = 0$) is sufficient to generate the long-range component.

instructive to consider the effect of the canting angle on the results. This is shown in Fig. **4**, and demonstrates that the long-ranged component of the charge current favours a canting angle of $\theta = \pi/4$, visible at longer sample lengths. It is also clear that the inclusion of both Rashba and Dresselhaus spin-orbit coupling allows the long-ranged component to be generated with a purely in-plane exchange field[24,25].

Spin-flip immunity

Upon analysing the spin supercurrent in the above structure, one discovers an additional feature which pertains uniquely to currents generated by superconductors. Unlike conventional spin-polarized currents, we find that a spin *super*current does not decay due to either spin-orbit impurity scattering or spin-flip scattering caused by magnetic impurities. This result has immediate implications for the usage of superconductors in spintronics, since it means that spin-flow created in this way is preserved even in regions with strong spin-flip scattering. We emphasize that this stands in complete contrast to conventional spin-currents, which have a decay length dictated by the amount of spin-flip scattering present.

Here we provide a general proof that the spin supercurrent is conserved both in normal metal and ferromagnetic systems, even in the presence of spin-orbit impurity scattering and isotropic spin-flip scattering from magnetic impurities. Using the relation between the Keldysh, retarded and advanced components of the Green function which holds at equilibrium (Eq. (2)), the Usadel equation may be written

$$D\partial_z \mathrm{Tr}\{\hat{\rho}_3\hat{\tau}_j\hat{g}^R\partial_z\hat{g}^R\} + \mathrm{iTr}\{\hat{\rho}_3\hat{\tau}_j[\hat{\Sigma},\hat{g}^R]\} = 0, \qquad (7)$$

where we have defined $\hat{\Sigma} = \varepsilon\hat{\rho}_3 + \hat{M} - \hat{\sigma}_{\mathrm{so}} - \hat{\sigma}_{\mathrm{sf}}$, and $\hat{\tau}_j$ denotes the polarization-direction of interest. $\hat{M} = \mathrm{diag}(\boldsymbol{h}\cdot\boldsymbol{\sigma}, (\boldsymbol{h}\cdot\boldsymbol{\sigma})^*)$, where $\boldsymbol{h}$ is the magnetization exchange field, whereas the spin-orbit and magnetic impurity spin-flip self-energies have been included via the terms $\hat{\sigma}_{\mathrm{so}}$ and $\hat{\sigma}_{\mathrm{sf}}$ (see Methods for details). For any matrix $\hat{X}$ one has $\mathrm{Tr}\{\hat{X}^\dagger\} = (\mathrm{Tr}\{\hat{X}\})^*$, from which it follows that if $\mathrm{Tr}\{\hat{\rho}_3\hat{\tau}_j[\hat{\Sigma},\hat{g}^R]\} = 0$, then the spin supercurrent will be conserved. By inserting the most general expression for the quasiclassical retarded Green function $\hat{g}^R$ [given in Eq. (10)], direct evaluation shows that the above trace is always zero in the absence of an exchange field despite the presence of spin-flip scattering. In the presence of an exchange field, the same holds for the spin supercurrent $\boldsymbol{I}_{S,\parallel}$ polarized along the magnetization and remains true even if the exchange field

is spatially inhomogeneous. It is remarkable that a spin supercurrent, controllable via the superconducting phase difference, has no decay even if both spin-orbit and magnetic impurities are present in the sample.

In conclusion, we have shown three major results: (i) a long-ranged spin supercurrent can be created without any magnetic inhomogeneities, (ii) the spin polarization components of the current can be tuned separately via the superconducting phase difference, and (iii) spin supercurrents created in this way do not decay even in the presence of spin-flip scattering, *i.e.* they display spin-flip immunity. We have proposed that this may be observed experimentally in a Josephson junction consisting of conventional s-wave superconductors (*e.g.* Al or Nb) with very thin layers of a heavy normal metal (*e.g.* Pt or Au) and a single homogeneous ferromagnet with magnetocrystalline out-of-plane anisotropy (*e.g.* PdNi or CuNi). We would like to note that no "exotic" materials, such as unconventional superconductors or noncentrosymmetric ferromagnets, are required – the effects predicted in this work appear by combining conventional superconductors and metals, which should make experimental verification of our results readily achievable. Our results confirm the significant and immediate advantage that superconductors offer spintronics.

Methods

We solved the Riccati parameterised Usadel equation with spin-orbit coupling[34] iteratively between the layers, using the NOTUR supercomputer facilities (Kongull). In the normal metal, spin-orbit coupling is included in the Usadel equation Eq. (7) by replacing the derivative with its covariant equivalent. We describe the normal-metal-ferromagnet interfaces via the spin-dependent boundary conditions

$$2L_j\zeta_j\hat{g}_j\partial_z\hat{g}_j = [\hat{g}_j,\hat{g}_k] + 2L_j\zeta_j\hat{g}_j\mathrm{i}\left[\hat{\boldsymbol{A}}_z,\hat{g}_j\right] + \sigma_j\tilde{G}_{MR}\left[\hat{g}_j,\left\{\hat{M},\hat{g}_k\right\}\right] + \sigma_j\mathrm{i}\tilde{G}_\theta\left[\hat{g}_j,\hat{M}\right], \tag{8}$$

where $j,k=\{\text{left},\text{right}\}$, $j\neq k$ denotes the two sides of the interface and the orientation determines the sign $\sigma_{\text{right}}=1$, $\sigma_{\text{left}}=-1$. The thin-film layering direction is taken to be in the z-direction, and $\tilde{G}_{MR}$ and $\tilde{G}_\theta$ denote the interfacial magnetoresistance and scattering phase shifts respectively. We chose $\zeta_j=3$ for the transparency parameter of all interfaces. The spin-orbit coupling field $\hat{\boldsymbol{A}}=\mathrm{diag}(\boldsymbol{A},-\boldsymbol{A}^*)$, and we have considered the case $\boldsymbol{A}=(\beta\sigma_x-\alpha\sigma_y,\alpha\sigma_x-\beta\sigma_y,0)$, where α,β are the Rashba and Dresselhaus coefficients respectively. The extrinsic spin-orbit scattering and spin-flip terms are given by

$$\hat{\sigma}_{so}=-\frac{1}{8\tau_{so}}\sum_i\hat{\alpha}_i\hat{\rho}_3\hat{g}^R\hat{\rho}_3\hat{\alpha}_i,$$
$$\hat{\sigma}_{sf}=-\frac{1}{8\tau_{sf}}\sum_i\hat{\alpha}_i\hat{g}^R\hat{\alpha}_iS_i, \tag{9}$$

where τ_{so} and τ_{sf} are the mean scattering times, S_i is the spin expectation value and we have defined the matrix $\hat{\alpha}_i=\mathrm{diag}(\sigma_i,\sigma_i^T)$. The general form of the retarded Green function is

$$\hat{g}^R=\begin{pmatrix}N(I+\gamma\tilde{\gamma}) & 2N\gamma\\ -2\tilde{N}\tilde{\gamma} & -\tilde{N}(I+\tilde{\gamma}\gamma)\end{pmatrix}, \tag{10}$$

with normalization matrices $N=(I-\gamma\tilde{\gamma})^{-1}$ and $\tilde{N}=(I-\tilde{\gamma}\gamma)^{-1}$ and identity matrix I. The $\tilde{\cdot}$ operation denotes complex conjugation and $\varepsilon\to(-\varepsilon)$. Regarding the choice of junction parameter, one may consider a reasonable approximation of the normal-state density of states to be of the order $N_0\sim 10^{22}/(\text{eV cm}^3)$, and the diffusion constant of CuNi to be[36] $D\sim 5$ cm^2/s.

[1] Tedrow, P. M. & Meservey, R. Spin-dependent tunneling into ferromagnetic nickel. Phys. Rev. Lett. **26**, 192-195 (1971).

[2] Tedrow, P. M. & Meservey, R. Spin polarization of electrons tunneling from films of Fe, Co, Ni, and Gd. *Phys. Rev. B* **7**, 318-326 (1973).

[3] Tedrow, P. M. & Meservey, R. Spin-polarized electron tunneling. *Phys. Rep.* **238**, 173-243 (1994).

[4] Johnson, M. & Silsbee, R. H. Interfacial charge-spin coupling: Injection and detection of spin magnetization in metals. *Phys. Rev. Lett.* **55**, 1790-1793 (1985).

[5] Li, B. *et al.*, Superconducting spin switch with infinite magnetoresistance induced by an internal exchange field. *Phys. Rev. Lett.* **110**, 097001 (2013).

[6] Yang, H., Yang, S-H., Takahashi, S., Maekawa, S. & Parkin, S. S. P. Extremely long quasiparticle spin lifetimes in superconducting aluminium using MgO tunnel spin injectors. *Nature Mater.* **9**, 586-593 (2010).

[7] Quay, C. H. L., Chevallier, D., Bena, C. & Aprili, M. Spin imbalance and spin-charge separation in a mesoscopic superconductor. *Nature Phys.* **9**, 84-88 (2013).

[8] Wakamura, T., Omori, Y., Niimi, Y., Takahashi, S., Fujimaki, A., Maekawa, S. & Otani, Y. Quasiparticle-mediated spin Hall effect in a superconductor. *Nature Materials* **14**, 675678 (2015).

[9] Kolenda, S., Wolf, M. J., Beckmann, D. Observation of thermoelectric currents in high-field superconductor-ferromagnet tunnel junctions. *arXiv:1509.05568*.

[10] Linder, J. and Robinson, J.W.A. Superconducting spintronics. *Nat. Phys.* **11**, 307 (2015).

[11] Eschrig, M. Spin-polarized supercurrents for spintronics: a review of current progress. *Rep. Prog. Phys.* **78**, 10 (2015).

[12] Bergeret, F. S., Volkov, A. F. & Efetov, K. B. Long-Range Proximity Effects in Superconductor-Ferromagnet Structures. *Phys. Rev. Lett.* **86**, 4096 (2001).

[13] Grein, R., Eschrig, M., Metalidis, G. & Schön, G. Spin-Dependent Cooper Pair Phase and Pure Spin Supercurrents in Strongly Polarized Ferromagnets. *Phys. Rev. Lett.* **102**, 227005 (2009).

[14] Alidoust, M., Linder, J., Rashedi, G., Yokoyama, T. & Sudbø, A. Spin-polarized Josephson current in superconductor/ferromagnet/superconductor junctions with inhomogeneous magnetization. *Phys. Rev. B* **81**, 014512 (2010).

[15] Shomali, Z., Zareyan, M. & Belzig, W. Spin supercurrent in Josephson contacts with noncollinear ferromagnets. *New J. Phys.* **13**, 083033 (2011) .

[16] Moor, A., Volkov, A. & Efetov, K. B. Nematic versus ferromagnetic spin filtering of triplet Cooper pairs in superconducting spin-

tronics. *arXiv: 1508.06665*.

[17] Halterman, K., Valls, O. T. & Wu, C.-T. Charge and spin currents in ferromagnetic Josephson junctions. *arxiv::1506.05480*.

[18] Khaire, S. T., Khasawneh, M., Pratt,W. P. Jr & Birge, N. O. Observation of spin-triplet superconductivity in Co-based Josephson junctions. *Phys. Rev. Lett.* **104**, 137002 (2010).

[19] Robinson, J.W. A.,Witt, J. D. S. & Blamire, M. G. Controlled injection of spin-triplet supercurrents into a strong ferromagnet. *Science* **329**, 59-61 (2010).

[20] Anwar, M. S., Czeschka, F., Hesselberth, M., Porcu, M. & Aarts, J. Long-range supercurrents through half-metallic ferromagnetic CrO2. *Phys. Rev. B* **82**, 100501(R) (2010).

[21] Keizer, R. S. et al. A spin triplet supercurrent through the half-metallic ferromagnet CrO2. *Nature* **439**, 825-827 (2006).

[22] Di Bernardo, A., Diesch, S., Gu, Y., Linder, J., Divitini, G., Ducato, C., Scheer, E., Blamire, M. G. & Robinson, J. W. A. Signature of Magnetic-Dependent Gapless Odd frequency States at Superconductor/Ferromagnet Interfaces. *Nat. Commun.* **6**, 8053 (2015).

[23] Kalcheim, Y., Millo. O, Di Bernardo, A., Pal, A. & Robinson, J. W. A. Inverse proximity effect at superconductor-ferromagnet interfaces: Evidence for induced triplet pairing in the superconductor. *Phys. Rev. B* **92**, 060501(R) (2015).

[24] Bergeret, F.S. and Tokatly, I.V. Singlet-triplet conversion and the long-range proximity effect in superconductor-ferromagnet structures with generic spin dependent fields. *Phys. Rev. Lett.* **110**, 117003 (2013).

[25] Bergeret, F.S. and Tokatly, I.V. Spin-orbit coupling as a source of long-range triplet proximity effect in superconductor-ferromagnet hybrid structures. *Phys. Rev. B* **89**, 134517 (2014).

[26] Miron, I. M. *et al.*. Perpendicular switching of a single ferromagnetic layer induced by in-plane current injection. *Nature* **476**, 189 (2011).

[27] Khaire, T. S., Pratt, W. P. Jr. & Birge, N. O. Critical current behavior in Josephson junctions with the weak ferromagnet PdNi. *Phys. Rev. B* **79**, 094523 (2009).

[28] Ruotolo, A., Bell. C. & Blamire, M. G. Perpendicular magnetic anisotropy and structural properties of NiCu/Cu multilayers. *J. Appl. Phys.* **96**, 512 (2004).

[29] Houzet, M. & Buzdin, A. I. Long range triplet Josephson effect through a ferromagnetic trilayer. *Phys. Rev. B* **76**, 060504(R) (2007).

[30] Volkov, A. F. & Efetov, K. B. Odd spin-triplet superconductivity in a multilayered superconductor-ferromagnet Josephson junction. *Phys. Rev. B* **81**, 144522 (2010).

[31] Arjoranta, J. & Heikkilä, T. Intrinsic spin-orbit interaction in diffusive normal wire Josephson weak links: supercurrent and density of states. *arXiv:1507.02320*.

[32] Alidoust, M. and Halterman, K. Spontaneous Edge Accumulation of Spin Currents in Finite-Size Two-Dimensional Diffusive Spin-Orbit Coupled SFS Heterostructures *New J. Phys.* **17**, 033001 (2015).

[33] Jacobsen, S.H. and Linder, J. Giant triplet proximity effect in π-biased Josephson Junctions with spin-orbit coupling. *Phys. Rev. B* **92**, 024501 (2015).

[34] Jacobsen, S.H., Ouassou, J.A. and Linder, J. Critical temperature and tunneling spectroscopy of superconductor-ferromagnet hybrids with intrinsic Rashba-Dresselhaus spin-orbit coupling. *Phys. Rev. B* **92**, 024510 (2015).

[35] Eschrig, M., Cottet. A, Belzig, W. & Linder, J. General boundary conditions for quasiclassical theory of superconductivity in the diffusive limit: application to strongly spin-polarized systems. *New J. Phys.* **17**, 083037 (2015).

[36] Oboznov, V. A., Bol'ginov, V. V., Feofanov, A. K., Ryazanov, V. V. & Buzdin, A. I. Thickness Dependence of the Josephson Ground States of Superconductor-Ferromagnet-Superconductor Junctions. *Phys. Rev. Lett.* **96**, 197003 (2006).

[37] Le Sueur, H. *et al.*Phase Controlled Superconducting Proximity Effect Probed by Tunneling Spectroscopy. *Phys. Rev. Lett.* **100**, 197002 (2008).

[38] Slonczewski, J.C. Mechanism of interlayer exchange in magnetic multilayers. *J. Magn. Magn. Mater.* **126**, 374 (1993).

[39] Slonczewski, J.C. Current-driven excitation of magnetic multilayers. *J. Magn. Magn. Mater.* **159**, L1-L7 (1996).

[40] Nogueira, S. F. & Benneman, K.-H. Spin Josephson effect in ferromagnet/ferromagnet tunnel junctions. *Europhys. Lett.* **67**, 620 (2004).

[41] In Figs. **2** and **4** we show the critical charge current and spin currents, where we take the critical currents to occur at a phase difference of $\phi = \pi/2$ between the superconductors. It is known that the critical charge current may deviate slightly from this phase difference near the transition points between the 0 and π ground states since higher order harmonics may become increasingly significant when the current is very small, but this is negligible for our scheme and the implications are discussed further in-text.

Acknowledgments

We thank J.A. Ouassou for useful discussions on computational aspects as well as N. Banerjee, J. Moodera, A. Di Bernardo, and J. W. A. Robinson for helpful comments. We acknowledge funding via the "Outstanding Academic Fellows" programme at NTNU, the COST Action MP-1201 and the Research Council of Norway Grant numbers 205591, 216700, and 240806.

Author contributions

S.H.J. performed the full proximity analysis and prepared the figures. I.K. carried out initial investigations in the weak proximity limit. J.L. had the idea and supervised the project. All authors analyzed the results and contributed to writing the manuscript.

Competing financial interests

The authors declare no competing financial interests.